



## **Design and Development of a Microfluidic Amperometric Immunosensor for the Quantitative Detection of 2,6-dichlorobenzamide (BAM) Herbicide Residue in Ground Water**

**Uthuppu, Basil; Aamand, Jens; Jakobsen, Mogens Havsteen; Jørgensen, Claus**

*Publication date:*  
2012

*Document Version*  
Publisher's PDF, also known as Version of record

[Link back to DTU Orbit](#)

*Citation (APA):*

Uthuppu, B., Aamand, J., Jakobsen, M. H., & Jørgensen, C. (2012). Design and Development of a Microfluidic Amperometric Immunosensor for the Quantitative Detection of 2,6-dichlorobenzamide (BAM) Herbicide Residue in Ground Water. Kgs. Lyngby: Technical University of Denmark (DTU).

## **DTU Library** Technical Information Center of Denmark

---

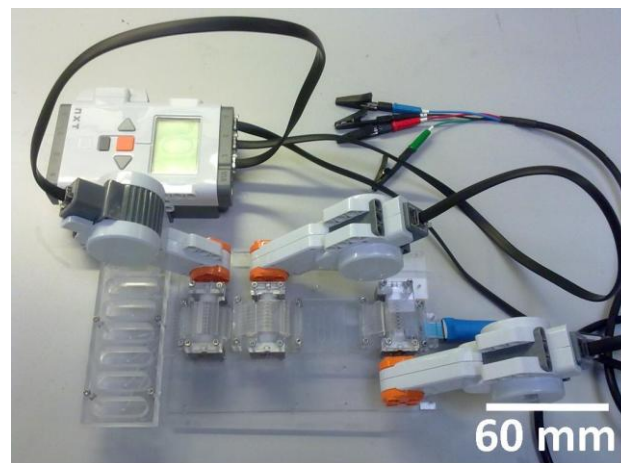
### **General rights**

Copyright and moral rights for the publications made accessible in the public portal are retained by the authors and/or other copyright owners and it is a condition of accessing publications that users recognise and abide by the legal requirements associated with these rights.

- Users may download and print one copy of any publication from the public portal for the purpose of private study or research.
- You may not further distribute the material or use it for any profit-making activity or commercial gain
- You may freely distribute the URL identifying the publication in the public portal

If you believe that this document breaches copyright please contact us providing details, and we will remove access to the work immediately and investigate your claim.

Design and Development of a Microfluidic  
Amperometric Immunosensor for the Quantitative  
Detection of 2,6- dichlorobenzamide (BAM)  
Herbicide Residue in Ground Water



Ph.D. Thesis

Basil Uthuppu

Surface Engineering Group  
DTU Nanotech

Department of Micro- and Nanotechnology  
Technical University of Denmark (DTU)

April 2012



## **Preface**

This thesis is presented to fulfil the criteria for obtaining a Ph.D. - degree from the Technical University of Denmark (DTU). The present Ph.D. project was carried out at DTU Nanotech, the Department of Micro – and Nanotechnology, Geological Survey of Denmark and Greenland (GEUS) as well as DHI from October 2008 to April 2012. This work was supported by the Danish Council for Strategic Research (grant no. 2104-06-0006) and Copenhagen Energy through the Sensowaq consortium.

The project was supervised by Senior Researcher Mogens Havsteen Jakobsen, leader of the Surface Engineering Group (DTU Nanotech). Co-supervision was carried out by Professor Jens Aamand (Department of Geochemistry, GEUS) and Ph.D., M.Sc., Claus Jørgensen (Department of Urban and Industry, DHI). The last part of the research work dealing with microfluidics and electrochemical detection was co-supervised by Assistant Professor Arto Heiskanen (Bioanalytics, DTU Nanotech). The thesis contents include results described within one peer-reviewed publication, one submitted paper and one article that is ready to be submitted.



## Acknowledgement

“Silent gratitude isn’t much use to anyone.” Here, I would like to thank people who have great contributions in making me privileged to present my three years of work in the form of a thesis. Without them, it wouldn’t have been a reality.

First of all, I am deeply grateful to my supervisor, Mogens Havsteen Jakobsen (Senior Researcher, Leader of surface engineering group, DTU Nanotech). From the day I joined this project, he has been there to support me as a supervisor, as an adviser and sometimes as a colleague. Beyond this, I found in him a person who listens to me patiently and understands my queries and worries in a soft manner that always leads to a pleasant conclusion. I am extremely lucky to have a supervisor like him who has been a constant source of inspiration, encouragement and care.

I thank my co-supervisors, Claus Jørgensen (Department of Urban and Industry, DHI) and Jens Aamand (Professor, Department of Geochemistry, GEUS) for their wonderful support throughout this project. They have been extremely cordial and constantly motivating over the entire course of the project.

Special thanks to Arto Heiskanen, who co-supervised the last spell of the project. His supervision at a crucial turning point was extremely beneficial to bring about important break-through in the project. The time he spent for useful discussions and corrections of the thesis draft was priceless.

In the Surface Engineering Group, I am indebted to René Bergmann, who has always been helpful in making good presentations and documents. I am grateful to my group members especially Ida Thygesen who always motivate me with her dynamic personality. I also extend my gratitude to Søren Vang Fischer, Natalie Kostesha and Nicola Mirotta.

I owe many thanks to the enthusiastic Spire Kiersgaard (Lab Technician, GEUS), who helped me in performing experiments in the immunochemistry lab.

I should also mention a few people who were generous to share their time and knowledge in the micromilling lab. I am thankful to Álvaro José Conde, David Sabourin, Per Thor Jonassen and Maciej Skolimowski.

I must thank my wife, Susan Kurian for her continued support and encouragement. I was continually amazed by her willingness to proof read the thesis draft and make necessary format changes in the final draft. Her support as a life-partner in taking care of our affectionate and darling one year old Jonathan during my busy days was unconditional and extraordinary. I realise that, she is the real power booster in my whole life.

Finally, I am thankful to my parents, in-laws and family who gave immense support. Special thanks to my sister-in-law, Ms. Sarah Kurian who gifted me a Nikon D5000 DSLR camera which was greatly useful to capture pictures of the sensor prototype during the project.

*This thesis is dedicated to my bundle of joy*

*Little Jonathan*

*for bringing in unconditional love, happiness and relaxation during what would have  
been an otherwise stressful period*

## List of Publications

- Published

### **Optimization of immunochemistry for sensing techniques to detect pesticide residues in water**

Basil Uthuppu, Natalie Kostesha, Jens Aamand, Claus Jørgensen, Spire M. Kiersgaard, Mogens Havsteen Jakobsen

Part of: Sensors Applications Symposium (ISBN: 978-1-4244-8063-0), 2011, Wiley-IEEE press,

Type: - Article in refereed conference proceedings

Presented at: IEEE Sensors Applications Symposium 2011, San Antonio, TX, USA

### **Real-time Detection of Pesticides in Ground Water using Immunoassay Based Electrochemical Setup**

Basil Uthuppu, Natalie Kostesha, Jens Aamand, Claus Jørgensen, Mogens Havsteen Jakobsen

Type: - Conference Poster

Presented at: NanoBio Europe 2010, Münster, Germany

- Submitted

### **Optimization of an immunoassay of 2,6-dichlorobenzamide (BAM) and development of regenerative surfaces by surface modification with newly synthesised BAM hapten library**

Basil Uthuppu, Jens Aamand, Claus Jørgensen, Spire M. Kiersgaard, Natalie Kostesha, Mogens Havsteen Jakobsen

Type: - Full Paper, submitted to Analytica Chimica Acta on 2 November 2011

Status on 8 December 2011: Under review

- Ready to submit

### **An amperometric immunosensor with an in-built micro flow-injection analysis ( $\mu$ FIA) system for quantitative determination of 2,6-dichlorobenzamide (BAM) herbicide residue in ground water**

Basil Uthuppu, Arto Heiskanen, Ida Thygesen, Claus Jørgensen, Jens Aamand, Mogens Havsteen Jakobsen

Type: - Full Paper, ready to submit

- Oral Presentations

### **Real-Time Detection of Pesticides in Ground Water Using Immunoassay Based Electrochemical Setup**

Presented at: INASCON 2010, Baarlo, The Netherlands



**Immunoassay based electrochemical sensor for quantitative detection of BAM in ground water**

Presented at: 4th Annual Meeting of Danish Water Research Platform (DWRP) 2010, GEUS, Copenhagen, Denmark

## Abstract

Access to clean and safe-drinking water is essential to health and it is a basic human right. These days, nearly a billion people of the world's population do not have access to this precious commodity. Along with many other causes, pollution of water sources by pesticides poses a real threat to the availability of clean water. Thus, the need of rapid, reliable and on-site early warning systems to monitor the quality of water becomes as important as its preservation. This work describes the design and development of an automated microfluidic biosensor based on immunological methods (immunosensor) to determine quantitatively the presence of pesticides in ground water. A herbicide residue, 2,6- dichlorobenzamide (BAM) is chosen as a model system in this research.

The thesis describes how an existing, highly selective and sensitive BAM immunoassay is optimized to transfer it from a lab-based end-point analysis technique (ELISA) to a portable, onsite monitoring system. The optimization of this heterogeneous competitive immunoassay is achieved by a unique approach in which the immunosorbent is engineered by using a newly synthesised BAM hapten library. Additionally, the improvisations made to the existing BAM hapten synthesis route resulted in the isolation of haptens for the parent herbicide (dichlobenil) itself. The affinity constants of new BAM haptens were estimated and compared with the existing BAM hapten. These results were correlated with their regeneration performances. Based on this, one of the newly synthesised BAM haptens (named as hapt D) was chosen for further development of the BAM immunosensor. This immunosensor employs a cost effective, miniaturizable, amperometric detection technique.

This thesis details the design and fabrication of a microfluidic platform in order to incorporate the optimized BAM immunoassay and the electrochemical detection method. A modular approach was adopted for the fabrication of the microfluidic platform in order to make the device simple to integrate, automate and maintain. The microfluidic platform has an in-built micro flow-injection analysis ( $\mu$ FIA) system and it is a novel characteristic of the microfluidic device prototype. The microfluidic device was automated using Lego<sup>®</sup> Mindstorms<sup>®</sup> servomotors to control its micro pumps and valves.

By confirming (amperometrically) the regeneration capability of the optimized immunosurface and generating a standard curve for BAM inhibition assay, the developed Amperometric BAM ImmunoSensor (ABIS) prototype provides the proof of concept. The possibility of interfacing ABIS with the macro world using a nearly developed auto-sampling unit has also been considered in the thesis.



## Resumé på dansk

Manglen på rent drikkevand er en alvorlig problemstilling for menneskeheden. Sammen med mange andre årsager repræsenterer forurening med pesticider en reel trussel mod tilgængeligheden af rent drikkevand. Behovet for hurtige, pålidelige og on-site varslingssystemer til overvågning af vandkvaliteten på et tidligt stadie bliver derfor ligeså vigtig som det rene vands bevarelse. Dette arbejde beskriver udformningen og udviklingen af en automatiseret mikrofluidisk biosensor, der er baseret på immunologiske metoder (immunsensor) til kvantitativ bestemmelse af tilstedeværelsen af pesticider i grundvand. Ukrudtsmiddelresten, 2,6-dichlorbenzamid (BAM) er udvalgt som modelsystem i dette studie.

Denne afhandling beskriver, hvordan et eksisterende yderst selektivt og sensitivt BAM immunoassay optimeres til overførsel fra en laboratoriebaseret teknik (ELISA) til et transportabelt on-site overvågningssystem. Optimeringen af dette heterogene kompetitive system er opnået ved en unik tilgang, hvori immunosorbenten konstrueres ud fra brugen af et nyligt syntetiseret hapten-bibliotek. Endvidere resulterede forbedringerne, af den eksisterende BAM hapten syntesevej, i isoleringen af haptener til selve det oprindelige ukrudtsmiddel (dichlobenil). Affinitetskonstanterne for de nye BAM haptener blev vurderet og sammenlignet med det eksisterende BAM hapten. Disse resultater blev korreleret til deres regenereringsevner. Baseret på disse resultater, udvalgte et af de netop syntetiserede BAM haptener (benævnt som hapten D) til videreudvikling af BAM immunosensoren. Immunosensoren anvender en omkostningseffektiv, miniaturiserbar, amperometrisk detektionsteknik.

Denne afhandling beskriver desuden designet og fremstillingen af en mikrofluidisk platform, der gør det muligt at integrere det optimerede BAM immunoassay og den elektrokemiske detektionsmetode. Til fremstillingen af denne platform anvendtes en modulær tilgang, som gør enheden enkel at integrere, automatisere og vedligeholde. Den mikrofluidiske enhed blev automatiseret ved hjælp af Lego<sup>®</sup> Mindstorms<sup>®</sup> servomotorer til at kontrollere dens pumper og ventiler. Dette design inkorporerer et indbygget mikro-flowinjektions analyse system ( $\mu$ FIA) og er et nyt særkende for den mikrofluidiske enhed.

Ved amperometrisk validering af regenereringskapaciteten af den optimerede immunooverflade og ved at måle en standardkurve for BAM inhiberingsassayet, leverer den her udviklede Amperometriske BAM ImmunoSensor (ABIS) prototype metodens proof of concept. Muligheden for at forbinde ABIS med makroverdenen ved brug af en nyudviklet automatisk prøvetagningsenhed er også taget i betragtning i denne afhandling.



## Table of Contents

1	Introduction.....	1
1.1.	Preserving precious water .....	1
1.2.	Pesticides and water pollution .....	3
1.3.	Pesticide analysis .....	5
1.3.1	Conventional techniques .....	5
1.3.2	Emergence of Immunoassays .....	5
1.3.3	Immunoassay – Principle .....	7
1.3.4	Immunosensors .....	7
1.4.	BAM - A model system for immunoassay based analysis .....	8
1.5.	Aim of the thesis project .....	10
1.6.	Thesis contributions .....	11
1.7.	Thesis overview .....	12
1.8.	Conclusion .....	13
2	Optimization of BAM immunochemistry .....	15
2.1.	The motivation for optimization of immunochemistry.....	15
2.1.1	BAM immunoassay .....	15
2.1.2	From ELISA to immunosensor .....	17
2.1.3	Synthesis of a library of new haptens .....	18
2.2.	Experimental .....	20
2.2.1	Reagents, buffers and materials .....	20
2.2.2	Instruments.....	21
2.2.3	Synthesis of Haptens.....	21
2.2.4	Synthesis and characterization of different conjugates.....	26
2.2.5	Assay method.....	26
2.2.6	Kinetic study of HRP-TMB reaction .....	27
2.2.7	Affinity constants.....	27
2.2.8	Regeneration cycles .....	27
2.3.	Results.....	28
2.4.	Discussion .....	34
2.5.	Conclusion .....	40
3	A modular $\mu$ FIA-based immunosensor.....	41
3.1.	Introduction.....	41
3.2.	Materials and methods .....	42
3.2.1	Miniaturized peristaltic pump .....	45
3.2.2	Miniaturized valves.....	47
3.2.3	Immunochip .....	49
3.2.4	Electrochemical detection module .....	50
3.2.5	Reservoir modules .....	53
3.2.6	Interconnection .....	54
3.3.	Experimental .....	56
3.4.	Results and discussions.....	57
3.5.	Conclusion .....	63
4	Characterization of the detection techniques .....	65
4.1.	Introduction.....	65
4.1.1	UV-Vis spectrophotometry .....	65
4.1.2	Electrochemical detection .....	66
4.2.	Experimental.....	67
4.2.1	Materials and methods .....	67

4.2.2	Experiments .....	69
4.3.	Results and discussions.....	71
4.3.1	Spectrophotometric detection using ABIS prototype .....	71
4.3.2	Characterization of the electrochemical detection unit.....	73
4.4.	Conclusions.....	78
5	Electrochemical BAM immunosensor .....	79
5.1.	Introduction.....	79
5.1.1	FIA based immunosensing.....	79
5.2.	Experimental .....	81
5.2.1	Materials .....	81
5.2.2	Experiments .....	81
5.2.3	Automating the system .....	85
5.3.	Results and discussions.....	87
5.3.1	Regeneration with amperometric detection .....	87
5.3.2	Standard curve .....	87
5.4.	Conclusion .....	89
6	Discussion.....	91
6.1.	Designing the system prototype.....	91
6.1.1	Regenerating the immunosurface .....	92
6.1.2	Designing of a continuous, in-line monitoring system .....	93
6.1.3	Making the ABIS prototype portable, maintainable and automated...	94
6.1.4	Designing for cost-effectiveness.....	94
6.2.	The in-built $\mu$ FIA core – a functional key element .....	95
6.3.	Stability of the reagents .....	95
6.4.	The ABIS prototype – room for improvement .....	96
6.5.	Interfacing with the macro-world .....	97
6.6.	Conclusion .....	99
7	Conclusions and Outlook.....	101
7.1.	Project achievements .....	101
7.2.	Recap of thesis contributions .....	101
7.2.1	A unique approach to optimizing the BAM immunoassay.....	101
7.2.2	Synthesis of new BAM haptens .....	101
7.2.3	Isolation of new dichlobenil haptens .....	102
7.2.4	Novel design of in-built standalone $\mu$ FIA .....	102
7.3.	Scope for future work .....	102
7.3.1	Interacting with the macro-world.....	102
7.3.2	Alternatives to PDMS .....	102
7.3.3	Managing air bubbles.....	103
7.3.4	Making the system real-time.....	103
7.3.5	Multiplexing with multiple residues .....	103
7.4.	Final remarks .....	103
References.....		105
Appendix I .....		111
Appendix II.....		117
Appendix III.....		139

## List of Figures

1.1	A Global map indicating the population living in water-stressed areas by 2025 [1]	2
1.2	Different processes that may be undergone by a pesticide once it is released into the environment [2].	4
1.3	Structures of dichlobenil and 2,6- dichlorobenzamide (BAM).	9
2.1	Structures of a) BAM hapten (hapt A) and b) the anthraquinone entity (EQ-0028)	16
2.2	A schematic representation of labelled competitive heterogeneous BAM immunoassay.	17
2.3	Chemical structures of three newly synthesised BAM haptens	20
2.4	a) hapt A synthesis route given by Bruun et al. [3], b) improvised general route adopted for hapten library synthesis in this work, c) chemical structures of nitrile haptens (potential dichlobenil haptens)	22
2.5	The UV-Vis Spectrum depicting absorption spectra of Ovalbumin	29
2.6	The UV-Vis Spectrum depicting absorption spectra of EQ 0013	29
2.7	Absorption spectra of hapt A, hapt B and hapt D	30
2.8	The kinetic curves showing Horse Radish Peroxidase (HRP) reaction with TMB substrate	32
2.9	Standard curves generated by active hapten surfaces	33
2.10	Regeneration results of three different immobilized hapten conjugates	34
2.11	Hydrolysis of nitrile group into amide by KOSiMe <sub>3</sub> in THF via an intermediate salt which is insoluble in THF	36
3.1	Micromilling machine. Inset shows tool bits used for micromilling	43
3.2	Hydraulic Bonding Press	44
3.3	Components of a multi-roller	46
3.4	A pumping inlay with 8 integrated channels made of PDMS (left panel) and a rotor bed made of 10 mm thick PC.	46
3.5	Different steps involved in the assembly of the miniaturized peristaltic pump module	47
3.6	A schematic cross-sectional view of the valve [4]	48
3.7	Different steps of the valve assembly	49
3.8	A bonded immunochip.	50
3.9	A bonded mixing chip	51
3.10	Screen Printed Electrode from Dropsens [5]	51
3.11	The components of the electrochemical detection chamber	53
3.12	Components of a reservoir module	54
3.13	Ball Joint Interconnection Block (BJIB)	55
3.14	The completely integrated microfluidic system developed for Amperometric BAM Immunosensor (ABIS) prototype.	56
3.15	A schematic diagram of the built-in flow injection manifold used for the ABIS prototype	60



3.16	The specially designed two mm thick connection blocks with BJIBs on both sides	61
3.17	Pump calibration	62
4.1	Spectrophotometric BAM immunoassay in the flow system (6 regeneration cycles).	71
4.2	Voltammogram of 2.5 mM potassium ferricyanide system	74
4.3	Cyclic voltammograms of 2.5 mM $K_3Fe(CN)_6$ at different scan rates.	75
4.4	FIA amperometry of $K_3[Fe(CN)_6]$ with the same concentration	75
4.5	Amperometric detection of different $K_3[Fe(CN)_6]$ concentrations in $\mu$ FIA	76
4.6	Cyclic voltammograms of commercially available TMB substrate and its oxidized form TMB (ox).	77
5.1	A schematic representation of the electrochemical BAM immunosensor	83
5.2	LEGO NXT brisck, three servo motors and the connecting shaft	85
5.3	Scen shot of an example of NXT program	86
5.4	A sigmoidal standard dose response curve generated with 8 BAM standrds	88
6.1	A schematic view of the operational principle of the sampling unit.	98
6.2	The sampling unit	99

## List of Tables

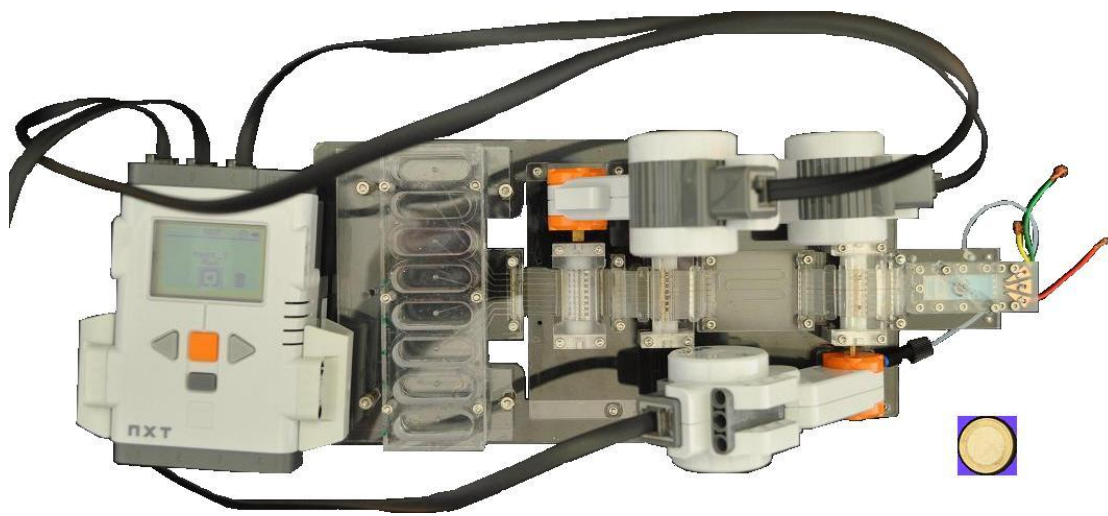
2.1	Characterization of hapt-OA-EQ 0028a conjugates by UV-Vis spectroscopy	31
2.2	constants ( $K_{\text{aff}}$ ) of HYB 273 towards the active haptens	33
2.3	The dependence of structural aspects on the nature of interactions between BAM haptens and HYB 273	38
5.1	Pump-valve operations corresponding to different steps of the standard curve generation experiment	84



## List of Abbreviations

$\mu$ FIA	micro Flow Injection Analysis
Ab	Antibody
ABIS	Amperometric BAM ImmunoSensor
Ag	Antigen
Ag*	Labelled Antigen
BAM	2,6-dichlorobenzamide
BJIB	Ball Joint Interconnection Block
BSA	Bovine Serum Albumin
CAS number	Chemical Abstract Service registry number
CE	Capillary Electrophoresis
CNC	Computerized Numerically Controlled
Da	Dalton
DDT	(dichlorodiphenyltrichloroethane
DHI	Danish Hydraulic Institute
DTU	Technical University of Denmark
EC <sub>50</sub>	Effective Concentration
ELISA	enzyme-linked immunosorbent assay
EQ 0028	Photoreactive anthraquinone entity
FAST	Fluidic Array Systems and Technology
FIA	Flow Injection Analysis
FIIA	Flow Injection Immunoanalysis
GC - MS	Gas Chromatography coupled with Mass Spectroscopy
hapt	hapten
HPLC - MS	High-Pressure Liquid Chromatography coupled with Mass Spectroscopy
HRP	HorseRadish Peroxide
HYB 273	Hybridoma 273
IC <sub>50</sub>	Concentration at while 50% of Inhibition is obtained
K <sub>aff</sub>	affinity constants
MAC	maximum admissible concentrattion
NMR	Nuclear Magnetic Resonance
NOVANA	National Action Programme for the Water Environment and Nature
OA	Ovalbumin
OD	Optical Density
PBS	phosphate buffered saline
PBST	PBS with Tween® 20
PC	polycarbonate
PCB	Printed Circuit Board
PDMS	polydimethylsiloxane
PMMA	poly(methyl methacrylate)
SPCE	Screen-Printed Carbon Electrodes

THF	<b>tetrahydrofuran</b>
TLC	Thin Layer Chromatography
TMB	3,3',5,5' - <b>tetramethyl benzidine</b>
UV	UltraViolet
UV-Vis	Ultraviolet–Visible



ABIS – Amperometric BAM ImmunoSensor

*a functioning prototype*



# Chapter 1

## Introduction

---

### 1.1. Preserving precious water

Water, is perhaps, one of the most undervalued precious resources that we humans use. History speaks of glorious civilizations that thrived and prospered around water bodies. This is understandable given the role of water and its usage in sustaining life and supporting socio-economic activities for mankind. Why to look into the past alone? The future as envisioned by space exploration and research is substantially motivated by the need to find the existence of water outside our planet, and subsequently perhaps the possibility of life on other planets. Therefore water has had a long and indisputable role in nurturing life as we know it today. There is nothing to suggest that this will not be the case in the foreseeable future. Yet, we take its availability and use for granted.

The World Water Council reports that of all the freshwater on this planet, about 70% lies trapped in ice-caps and glaciers. About one fifth of the remaining 30% freshwater lies in remote areas - inaccessible to humans. Three-fifth is often not usable because it occurs at the wrong time or place in the form of monsoon and floods, for example. It is the remaining one-fifth which needs to be carefully considered and used. This (the remaining 6% of freshwater) is only about 0.0008% of the total water available on this planet [1]. In other words, if all the water on this planet could be stored in a five-litre container, the water available for managed usage by the human race is only about what fits onto a teaspoon! However, efficient water management still remains a developing science.

How much longer can we ignore the need to manage our water resources more carefully? Till the turn of this century, there was not much debate over water as a renewable and limited resource. Instead, the availability of water was probably even assumed to be unlimited. Rivers and streams were viewed as cheap and dependable sources of water and exploited in all possible ways. Often, they also served as prime



avenues for waste disposal. These days nearly a billion people of the world's population do not have access to clean and safe water [2].

Depending on future rates of population growth, it is estimated that between 2.7 billion to 3.2 billion people may be living in either water-scarce or water-stressed conditions by 2025 (Figure 1.1) [3].

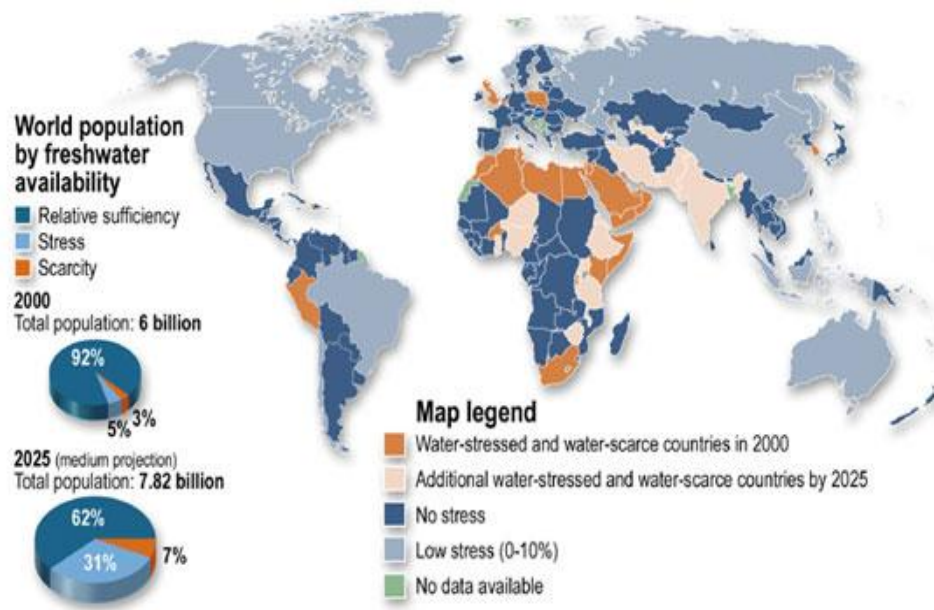


**Figure 1.1: A Global map indicating the population living in water-stressed areas by 2025 [4].**

These prospects are scary and not at all impossible. In fact, this is probably the reason why freshwater is largely being seen as the oil of the 21<sup>st</sup> century. Water is today, a commodity that is not only getting scarce and expensive, but also capable of fuelling armed conflicts amongst populations trying to secure its availability. There is an emergent need to use effective water management strategies.

As opposed to water quality monitoring, water preservation is a much discussed topic. Awareness programmes highlight the importance of efficient water use. Collection and storage of clean drinking water are also a significant part of these discussions. Just as important as water preservation, is the need to closely monitor the quality of the water resources. Elaborate laboratory techniques are employed to evaluate drinking water quality. Though capable of yielding sensitive quality indications, these approaches can be time-consuming and cumbersome because it is needed to collect and deliver samples to the laboratories. Hence, there is a growing demand for devices for *in-situ* drinking water quality assessment. On the face of it, these can be seen as

portable systems that indicate water quality nearly immediately. When effectively used, these devices can be employed as early warning systems which can fairly quickly indicate intentional water contamination as well. This introduces a whole new relevance within the scope of national security where a rapid, reliable and continuous monitoring mechanism can be a critical necessity.

The development of one such early warning device is the main focus of this research. The research problem specifically considers groundwater contamination caused by pesticides.

## **1.2. Pesticides and water pollution**

Pesticides are chemicals that are used to control and/or eliminate plant and animal pests and diseases. The development and application of pesticides has been considered as one of the fundamental contributors to the green revolution by controlling a wide variety of pests and weeds that would otherwise diminish the quantity and quality of food produce. Along with genetically modified plants, pesticides have been instrumental to intensify agriculture in order to satisfy the urgent need of increasing crop production demanded by population explosion and lack of sufficient arable land. Unfortunately, they now threaten the long-term survival of major ecosystems by disruption of predator-prey relationships and biodiversity. Along with many other causes, pollution of water sources by pesticides poses a real threat to the availability of clean drinking water.

Pesticides were used extensively on the assumption that they would either be retained in the upper soil or degraded by microorganisms, so they would not enter into the ground water. However, in reality, a pesticide may undergo a number of processes such as adsorption, transfer, break-down and degradation, once it is released into the environment. Depending on the physical and chemical characteristics of the pesticide and the soil, transfer of pesticide happens through volatilization, spray drift, run-off, leaching etc. into the environment (Figure 1.2). Water bodies are the most vulnerable media to be polluted by pesticides. Ground water contamination by leaching of pesticides is more fatal, because flushing a plume of contamination from ground water may take many years. Unlike surface waters, ground water does not dilute the contaminants that have accessed it. Cold temperatures, limited microbial activity, lack

of sunlight and low oxygen level deep under the soil may also diminish the breakdown process of pesticides.

In many countries, the main source of drinking water is the ground water. In

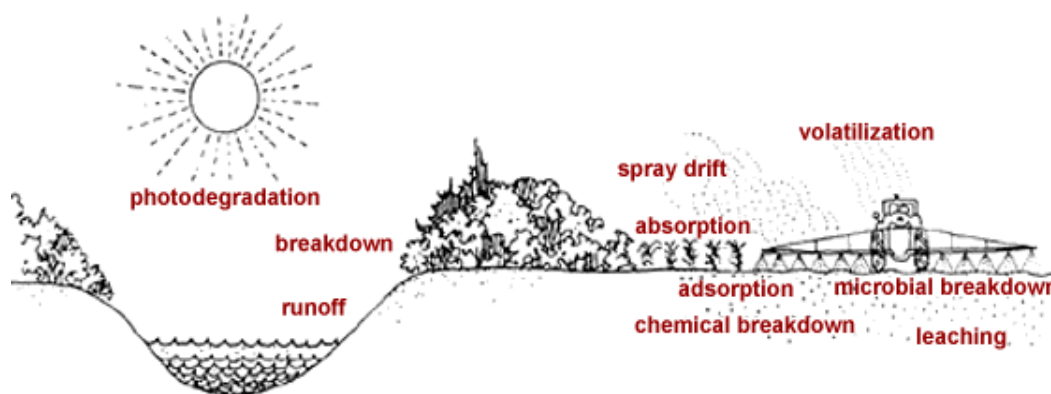


Figure 1.2: Different processes that may be undergone by a pesticide once it is released into the environment [5].

Denmark, the drinking water supply is totally based on ground water [6]. Under the National Action Programme for the Water Environment and Nature, NOVANA, the Danish ground water monitoring programme analysed 34 pesticides and metabolites along with a number of other analytes. The results show that more than 25% of the wells have the presence of pesticides and their metabolites. The most frequently found pesticide group consists of triazines and their metabolites. 25% of the water supply wells contain 2,6-dichlorobenzamide (BAM), a metabolite of herbicide dichlobenil and 10% have more than the maximum admissible concentration (MAC) value of 0.1  $\mu\text{g/L}$  [7].

All pesticides are basically toxic as they intend to destroy or control pests or weeds. This inherent toxicity makes them potentially hazardous to all living organisms. These organic molecules are normally also less degradable. In some cases, the degradation products are even more toxic and more easily spread in the environment than the original pesticide compounds. Monitoring the presence of pesticides or pesticide residues in water resources becomes so important these days to ensure the quality of drinking water and to minimise the risk of oral exposure to such undesirable compounds.

### **1.3. Pesticide analysis**

The European Union has set the permissible limit for an individual pesticide in drinking water to 0.1 µg/L. Similarly the permissible limit for the total quantity of pesticides in drinking water is set to 0.5 µg/L [8]. Detection and quantification of such a low level presence of pesticides in water and other sources require highly sensitive analytical techniques.

#### **1.3.1 Conventional techniques**

Traditionally, methods like gas chromatography coupled with mass spectroscopy (GC - MS) [9, 10], high-pressure liquid chromatography coupled with mass spectroscopy (HPLC - MS) [11-13], HPLC coupled with UV [14] and capillary electrophoresis (CE) [15] are being employed to quantitatively detect the low level presence of pesticides in environmental matrices. In spite of the advantages of these conventional techniques such as high sensitivity and selectivity, they are all laborious, time consuming, expensive and require highly skilled technicians to perform analyses. Most of them have tedious and prolonged sample pre-treatment steps such as purification, concentration and derivatization which make them extremely complex techniques with bulky instrumentation. A time consuming sample preparation procedure associated with single sample analysis, makes the conventional methods difficult to perform for a large number of environmental samples that are to be monitored at regular intervals. In the present scenario, where the availability of clean and safe water is seriously affected by the pesticides and their residues, considerable attention should be given to the development of early warning systems comprising of easy-to-use, cost effective monitoring techniques for rapid, robust and sensitive determination of pollutants. In the past few decades, a considerable effort has been invested in research and investigations concerning the development of improved techniques for pesticide analysis. Immunoassays have emerged as a good alternative to the conventional methods.

#### **1.3.2 Emergence of Immunoassays**

Immunoassays have been widely used in clinical chemistry [16, 17] and endocrinology [18] since their appearance in the form of an analytical tool in 1960 [19]. Surprisingly, immunochemistry did not find any practical application in analysis

of pesticides or other environmental contaminants until 1971. Initially, immunochemical methods were misconceived as methods that could be applied only in the analysis of biological compounds such as hormones, proteins, viruses, bacteria and pharmaceuticals. At that time, environmental chemists were entirely satisfied with the conventional techniques available for analysis of environmental pollutants. And also, techniques like gas- and liquid chromatography were greatly successful in analysing early compounds of interest in this field. Development of specific antibodies (the key components of all immunoassays) against small organic environmental pollutants, which are too small to produce an immune response, requires careful engineering of rational haptens to create immunogens with carrier proteins. One should consider these factors as the reasons for the subsequent introduction of immunochemical methods into the environmental analysis compared to the clinical field [20, 21]. In 1971, Ercegovich *et al.* [22] presented immunoassays for DDT, malathion and aminotriazole, making the first strong suggestion to environmental chemists to consider immunoassays as an analytical method for environmental monitoring. Since then, with better hapten design strategies, the immunoassay technique has found a greater acceptance in the environmental analysis indicated by the growing number of publications in the field and emergence of companies marketing commercial products for immunoassays in environmental analysis [21, 23-32].

Immunoassays are based on highly specific and highly sensitive interactions between an antigen and its corresponding antibody. Antibodies, also known as immunoglobulins (molecular weights of 150 000 Da) are soluble proteins produced in the immune system of vertebrates as a result of the defensive mechanism activated upon the introduction of a foreign body in their body fluids. Any molecule or pathogen capable of eliciting such an immune response is called an antigen. Normally antigens with molecular weights less than 5000 Da, such as those of pesticides, are not antigenic, because the immune system would be unproductive if it responds to small molecules that include intermediates and products of cellular metabolism. However, it is possible to elicit immune response if such small molecules or their derivatives are covalently attached to large proteins as carrier molecules. These small molecules/derivatives are called haptens and the hapten–carrier molecule conjugate forms the immunogen. The antibodies produced in response to such immunogens

have the ability to bind the hapten part when they are free. An individual antibody binds only a particular molecular structure within the antigen. In other words, this binding is extremely specific. As an analytical technique, immunoassays, the current '*state of the art*' in the field of pesticide analysis, make use of the extraordinary binding properties (affinity and specificity) of an antigen-antibody interaction. After the reaction, measurement of the bound sites reflects the analyte concentration in the medium. These occupancies are estimated by a signal produced by a tracer which is attached either to the antibody or to the antigen, since the binding reaction itself does not generate any measurable signals. Based on the labels that give the quantification of the immunological reaction, immunoassays are classified as fluorescent [33], chemi-luminescent [34], enzyme [35], plasmon-resonance [36] and radio isotope [37] assays.

### 1.3.3 Immunoassay – Principle

The main principle of immunoassay technique can be illustrated by the following chemical reaction.

$Ab + Ag + Ag^* \leftrightarrow AbAg + AbAg^*$ , where Ab is an antibody, Ag is an antigen and  $Ag^*$  is the corresponding labelled antigen. The analyte Ag and labelled antigen  $Ag^*$  compete for a limited amount of binding sites on Ab. The extent of binding of  $Ag^*$  which is a measure of  $AbAg^*$  depends on the concentration of the analyte Ag [30].

### 1.3.4 Immunosensors

Conventional immunoassays developed for pesticides in water are normally performed in a particular laboratory or institute. These methods pose many advantages over the existing chromatographic methods in terms of cost, speed, simplicity and number of simultaneous analyses. However, to extend this technique to a continuous analysis format in order to monitor the water quality over long periods of time, there is a need to set up new systems. Initiatives and developments in such directions have been introduced into the field of environmental biosensors. Biosensors are analytical tools which combines a biological recognition element with a suitable transducer capable of translating the biological event into a measurable physical signal. When the recognition element of a biosensor is an antibody, the sensor can be called an immunosensor. Unlike conventional immunoassays, an immunosensor is

capable of detecting the analyte continuously and selectively to provide data in real-time. Based on the employed transducer technique, immunosensors can be classified as, for instance, optical [38-40], piezoelectric [41, 42], electrochemical [43-45], micromechanical [46, 47].

#### **1.4. BAM - A model system for immunoassay based analysis**

After realizing the potential of applying immunochemical methods (especially immunoassays) to the field of environmental monitoring, many research groups around the world have developed a number of immunoassays for pesticide analysis. A detailed list can be found in literature [28]. Mogens Havsteen Jakobsen (the main supervisor of this thesis project) has participated in the development of monoclonal antibodies for a variety of pesticides belonging to the group of s-triazines [48] and the degradation product of the herbicide - Dichlobenil, 2,6-dichlorobenzamide (BAM) [49]. The latter monoclonal antibody shows very low cross-reactivity towards structurally related compounds. A quantitative enzyme-linked immunosorbent assay (ELISA) was developed based on competitive binding of the antibody between BAM in solution and BAM hapten immobilized in the micro-wells. The assay is now validated and used as a technique in routine analysis in Denmark to quantify BAM in ground water samples.

Dichlobenil is a nitrile herbicide (2,6-dichlorobenzonitrile, CAS No. 1194-65-6) which has been applied particularly in non-agricultural areas such as industrial sites, railway lines, motorways, car parks, private gardens etc. It has also been applied in surface waters to control submerged and floating water-living weeds. The principle metabolite of dichlobenil in soil is 2,6-dichlorobenzamide (BAM) [50]. BAM may reach natural water resources and can raise potential threats against the well-being of species living in such habitats. This is because BAM has lower sorption tendency to soil. It is more persistent and more mobile than dichlobenil and has high water solubility. The toxicity studies of dichlobenil and BAM during the past 40 years have been reviewed by Bjorklund *et al.* [51].who reported that consumption of a few hundred mg/kg of BAM can cause acute toxicity in mammals.

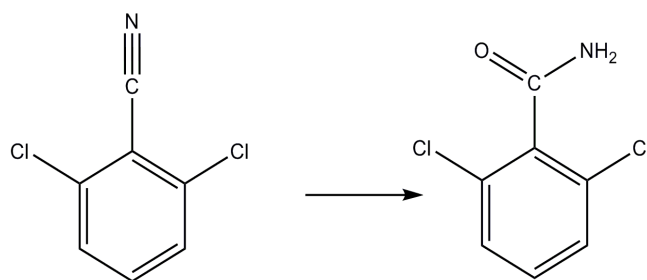


**Figure 1.3: Structures of dichlobenil and 2,6- dichlorobenzamide (BAM).**

Bjorklund *et al.* also reviewed various analytical strategies based on different chromatographic techniques available for determining both dichlobenil and BAM in environmental matrices [52]. The review reveals that these methods require various sample preparation strategies including sample pre-handling steps, sample pre-concentration steps, extraction techniques and sometimes derivatization of the analytes. This makes the process extremely laborious, skill demanding and time consuming. Moreover, design, development and success of these chromatographic techniques greatly depends on the basic physical and chemical properties such as vapour pressure, water solubility, octanol-water distribution coefficient, solid matrix-water distribution coefficient etc. of the analytes. However, the immunoassay method for BAM analysis in water as described by Bruun *et al.* [49] is highly specific, cost-effective, sensitive and requires no sample pre-treatments steps as opposed to the chromatographic analysis approach. A detailed description of the development of a competitive ELISA technique based on BAM immunoassay with a low coefficient of variation (CV) is presented by Bruun *et al.*

Presently, a rapid and robust in-line monitoring method for pesticide analysis in water is required. This is especially important and relevant for a country like Denmark where the ground water serves as the main resource for drinking water. As explained, biosensors are good candidates for this purpose. The availability of the above mentioned, in-house BAM immunoassay tool box has been chosen as a model system in the development of an electrochemical biosensor. The ultimate goal of the overall project is a well-validated, multi-analyte electrochemical immunosensor. This thesis presents a detailed description of the process of developing such a sensor.



## 1.5. Aim of the thesis project

The aim of the project is to develop a prototype of a portable (miniaturized), automated and continuous in-line monitoring system based on an electrochemical immunosensor that can perform quantitative detection of the herbicide residue, - 2, 6-dichlorobenzamide (BAM), in water. The system is intended to be used at drinking water production units as an early warning mechanism. Ideally, the final set up is intended to be used for field work - unattended - for at least a few weeks. This demands a number of repeated analysis cycles with proper calibration of the system which means, the immunochemical reaction (BAM immunoassay) should be repeated on the same immunosorbent many times when it is performed in the sensor. This requires the regeneration of the immunosurface after each analysis cycle. In this regards, a detailed study of the immunochemical reaction is necessary to optimize it in order to transfer it from plate-based ELISA to a continuous monitoring sensor system.

During the course of this project the following points were considered as milestones:

- i. Optimization of BAM- immunoassay (competitive ELISA) in order to transfer it to an in-line sensor
- ii. Design and development of a microfluidic platform with an electrochemical detection scheme
- iii. Evaluating regeneration of the immunosurface using an electrochemical detection scheme
- iv. Verifying the stability of reagents used in the assay
- v. Automation of the miniaturized sensor unit
- vi. Integration of the miniaturized sensor unit with an auto-sampler which serves as an interface between the micro- and macro- worlds
- vii. Analysis of field samples with the fully automated prototype
- viii. Validation of the results with conventional ELISA.

Most of these milestones (i - v) have been realized as described in the following chapters of the thesis. The optimization of the BAM-immunoassay is achieved by using conventional ELISA. Highly selective and sensitive immunoreactions are investigated by using newly synthesized BAM hapten molecules immobilized as immunosorbents. This is in order to tune the immunochemical reactions envisaged to be used in a real-time, in-line sensor for repeated measurements. The next step is the integration of this optimized immunoassay with a suitable detection technique. An amperometric electrochemical method is investigated to be used as the detection technique. This integration demands the design and development of a suitable microfluidic platform which is to be realized using computerized numerically controlled (CNC) micro-milling fabrication techniques. Finally, the whole system needs to be suitably automated prior to field test. The aim in this regard is to utilize LEGO<sup>®</sup> Mindstorms<sup>®</sup> servo motors to achieve the desired automation.

## **1.6. Thesis contributions**

This thesis makes the following contributions through the research detailed in here.

- (i) It describes a unique approach towards optimization of a heterogeneous immunoassay by engineering the immunosorbent in order to use the same in a microfluidic device as the sensing mechanism of a biosensor (Chapter 2).
- (ii) It describes the synthesis of new BAM-haptens which were crucial for the above mentioned optimization (Chapter 2).
- (iii) The improvisation adopted for the synthesis of the existing BAM-hapten resulted in the isolation of new dichlobenil haptens for the parent compound of BAM (dichlobenil). The immense potential of such haptens is described in the discussion of Chapter 2.
- (iv) It describes the fabrication of a micro-fluidic platform (which is realized using a modular approach) with a novel design of a stand-alone, in-built flow injection analysis (FIA). This novel design will henceforth be referred to as  $\mu$ FIA (Chapter 3).

- (v) It details the design and development of an Amperometric BAM Immunosensor (ABIS) prototype to detect BAM concentrations in water using the innovations listed from i-iv (Chapter 3 - Chapter 5).

## **1.7. Thesis overview**

The research work described in this thesis is organized as follows:

Chapter 1 presents an introduction to the problem that this research work addresses. It discusses the current scenario regarding water pollution and the need for a suitable sensor device that can be used to quantify ground water pollution caused by pesticides, in particular by the herbicide residue 2,6- dichlorobenzamide (BAM).

Chapter 2 describes the experimental studies that focus on optimizing the BAM immunoassay used in the design of the sensor unit.

Chapter 3 describes the design and fabrication of the modular  $\mu$ FIA chip assembly which houses the sensor and detection units.

Chapter 4 details studies that aim to characterize the  $\mu$ FIA-based device and the electrochemical detection system. The  $\mu$ FIA-based device is characterized by using both spectrophotometric and electrochemical techniques.

Chapter 5 describes studies conducted to characterize the amperometric BAM immunosensor, (ABIS) prototype.

Chapter 6 presents the overall results of the research project. It discusses these results within the framework of the aims of the project (as detailed in Section 1.5).

Finally, Chapter 7 presents concluding remarks regarding the research described in this thesis. With respect to this, it presents the scope for future work and further applications for the device which is an outcome of this research activity.

Appendix I-III is a collection of papers (one refereed paper, a paper under review and a manuscript ready to be submitted) made over the course of the Ph.D. program.

## **1.8. Conclusion**

This chapter presented an insight to the importance of water quality monitoring. In this context it introduced the emergence of immunoassay based analysis techniques for pesticide analysis in groundwater. It detailed the aims of the research project described further in this thesis. It also enumerated the contributions made by this research/thesis and the organisation of the material in this work.



## Chapter 2

# Optimization of BAM immunochemistry

---

### 2.1. The motivation for optimization of immunochemistry

As mentioned in the introductory chapter (Chapter 1), the success of an in-line pesticide immunosensor for continuous measurements demands repeated analysis cycles to produce reliable and reproducible data. In the case of an immunosensor, the biosensing event (i.e. the immunoreaction) should be repeated many times. Depending on the adopted technique, this repetition requires that the immunosurface (where the sensing event takes place) is reconditioned/regenerated after each cycle. However, being a disposable end-point analysis technique, the plate-based ELISA does not deal with repetitive regeneration. Hence, when shifting from ELISA to a flow system the possibility of renewing the immunosorbent must be considered. In this chapter, a detailed study of BAM immunoassays is conducted to investigate the possibility of such repetitive regeneration of the immunosurface. All the studies are conducted in plate-based ELISA format. This chapter is based on the published paper and the submitted manuscript attached as Appendix I and II.

#### 2.1.1 BAM immunoassay

The immunoassay developed by Bruun et al. [49] for BAM detection is a labelled competitive heterogeneous immunoassay. The anti-BAM monoclonal antibody (HYB 273) involved in the described reactions was produced by carefully designing a BAM hapten (Figure 2.1(a)) and immunizing mice with this hapten molecule. As seen in the figure, the free carboxylic group present on the BAM hapten was instrumental for conjugation with the carrier protein (ovalbumin) in the formation of the immunogen. In the heterogeneous competitive assay format, the same BAM hapten-ovalbumin conjugate was used to immobilize on the surface. In order to make the immunosurface robust, a covalent immobilization was achieved by conjugating the BAM hapten-ovalbumin conjugate with an anthraquinone entity (EQ 0028, Figure 2.1(b)).

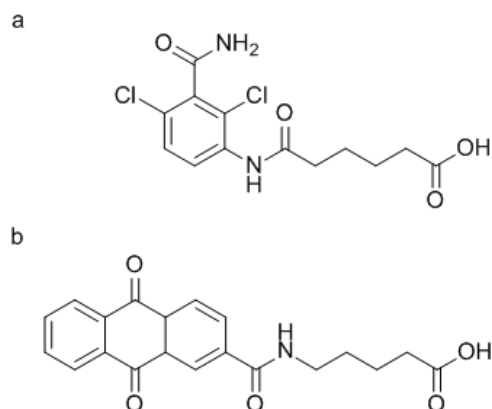


**Figure 2.1: Structures of a) BAM hapten (hapt A) and b) the anthraquinone entity (EQ-0028).**

This part of the overall conjugate is photosensitive capable of forming covalent bonds with polymeric substrates upon UV exposure. Such surface modifications are stable for years even under dry conditions. The synthesis of the anthraquinone entity and the conjugation procedure are described in [49]. A pre-mixed volume of the analyte BAM (BAM in water samples) and HYB 273 labelled with Horseradish Peroxidase (HRP) enzyme is incubated over the immunosurface. This results in a competition between free BAM in solution and the BAM hapten on the surface. Finally, incubation with 3,3',3,5'- tetramethyl benzidine (TMB), which is a chromogen and substrate for HRP, gives a signal proportional to the amount of HYB 273 attached on the surface. This signal is inversely proportional to the concentration of BAM in the analyte solution. In short, the binding of HYB 273 onto the BAM hapten immobilized surface is inhibited by the free BAM present in the sample to be analyzed. A schematic representation of the BAM immunoassay is shown in Figure 2.2. By using standard BAM solutions as samples in the above described procedure, a standard curve is generated and used later in determining the BAM concentration in unknown samples.

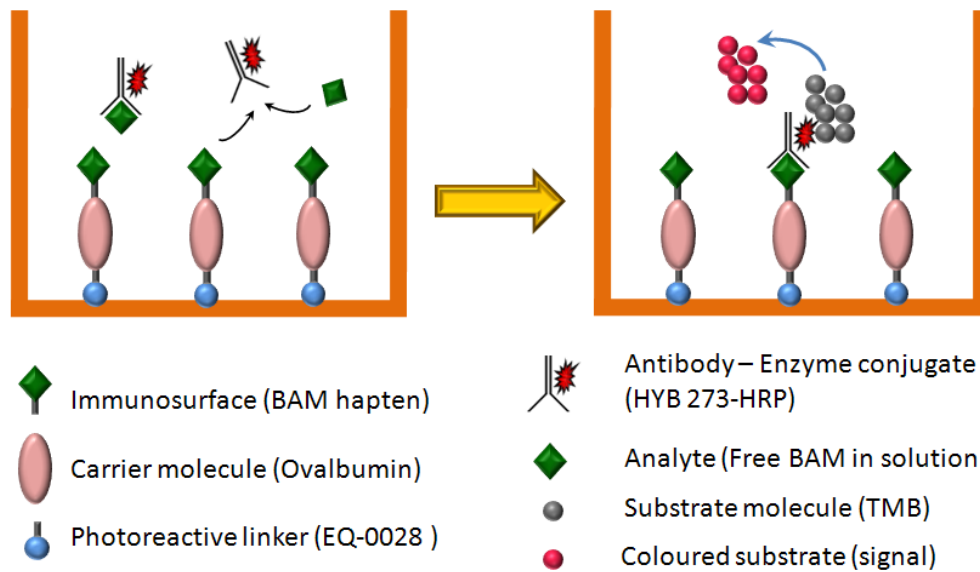


Figure 2.2: A schematic representation of labelled competitive heterogeneous BAM immunoassay.

### 2.1.2 From ELISA to immunosensor

ELISA, as it is conducted usually, is not suitable for the desired immunosensor. The use of conventional ELISA is inappropriate in continuous in-line sensing due to, for instance, the following factors:

- (i) The conventional immunoassays involve a multi-stage process, resulting in increasing complexity of analysis and in the requirement of qualified technicians.
- (ii) ELISAs are always run under laboratory conditions.
- (iii) The time for conventional immunoassays is longer due to the longer incubation processes.

Considering the project goals, it is necessary to move the above described plate-based conventional BAM immunoassay into a continuous monitoring system. Unlike the ELISA technology, which enables parallel analysis of many samples with internal calibration, the miniaturized, in-line immunosensing system runs each analytical cycle in a sequential manner. This requires that, after each cycle, the immunosurface (BAM hapten immobilized surface) has to be regenerated by disrupting the strong non-covalent interactions between HYB 273 and BAM hapten and at the same time



maintaining the surface activity for further assay cycles. This normally involves changing the pH or the use of surfactants and chaotropic agents. In a continuous flow system, a mild condition is appreciated to achieve the regeneration of the immunosurface. The preliminary work done in this direction at Cranfield University, showed that 100 mM glycine.HCl buffer of pH 2.0 is the most appropriate solution in case of BAM surface regeneration (data is not shown). In this project work, this result was adopted for regeneration purposes. Further studies also showed that attempts to regenerate BAM hapten immobilized surfaces with 100 mM glycine.HCl buffer resulted in a significant decrease in the signal after a number of cycles (8 cycles). It should be noted that, in these original assays, the same hapten was used for immunization as well as immobilization, and furthermore, the affinity of HYB 273 towards the free BAM and immobilized BAM hapten was comparable. In such a situation, during the inhibition assay, both the free BAM in the solution and the BAM hapten on the surface compete for a limited number of antibody binding sites based on the reversible equilibriums between HYB 273 – free BAM and between HYB 273 – BAM hapten. Hence, the HYB-hapten interaction can be changed by altering the affinity of the antibody towards the BAM hapten. Evidences for synthesizing structurally different competitors with respect to the immunizing hapten to enhance the analyte binding sensitivity of the antibody are found in literature [53-56]. In this project, this strategy is applied in a different way to tune the Ab-surface interaction in a heterogeneous inhibition assay to provide a better regeneration possibility for repeated continuous analysis.

### **2.1.3 Synthesis of a library of new haptens**

The above stated affinity tuning is achieved by making structural differences on the hapten immobilized on the surface. This is because the structure of the surface hapten with respect to the structure of the immunizing hapten has a strong influence on the equilibrium conditions. Hence by using the redesigned hapten on the surface the HYB 273 - surface hapten interaction can be lowered and thereby the regeneration possibilities can be improved. Various studies reported in literature describe how the structure of competing hapten is differed from that of the immunizing hapten by varying chain length and functional group of the spacer arm in the attachment site [57, 58]. It is not uncommon that antibodies show cross-reactivity to structurally similar, yet distinct, antigenic molecules [59]. Relatively minor changes in an antigen

structure may lead to considerable changes in the strength of the antibody-hapten interaction, because a relatively small component of an antigen is being recognized by the antibody and hence the same antibody can interact with structurally different antigens, but with lower affinity [60]. In a heterogeneous competitive assay, as in this project, altering the structure of immobilized hapten to tune the antibody – hapten interaction is an effective approach to achieve a more effective regeneration under mild conditions. This is significant because testing of different antibodies from different clones is out of the scope of this project and by keeping the same HYB 273 will retain the sensitivity/affinity of its analyte binding. Hereafter, the original BAM hapten is named as hapt A for simplicity. In the present research, we have synthesized three new haptens (Figure 2.3) – hapten B (hapt B), hapten C (hapt C) and hapten D (hapt D). They have the following features:

- (i) Like the original hapten (hapt A), the new haptens retain the amide group on the ring.
- (ii) hapt B differs from hapt A in the length of the linker.
- (iii) hapt C and hapt D differ from hapt A in the number of chlorine atoms on the ring.
- (iv) hapt D also differs from hapt A with respect to the position of the linker attached to the ring.

The newly synthesized BAM haptens are then conjugated with Ovalbumin(OA) and EQ-0028. The conjugates are characterized by UV-Vis spectroscopy to estimate the concentration in terms of OA and the extent of conjugation as the number of EQ-0028 per ovalbumin. The conjugates are immobilized on microtitre plates and the affinity of the anti-BAM antibody (HYB 273) to them is compared. It is shown that the surface activity towards HYB 273 can be changed in such a manner as to improve regeneration of the immunosurface. This was in accordance with the determined affinities.

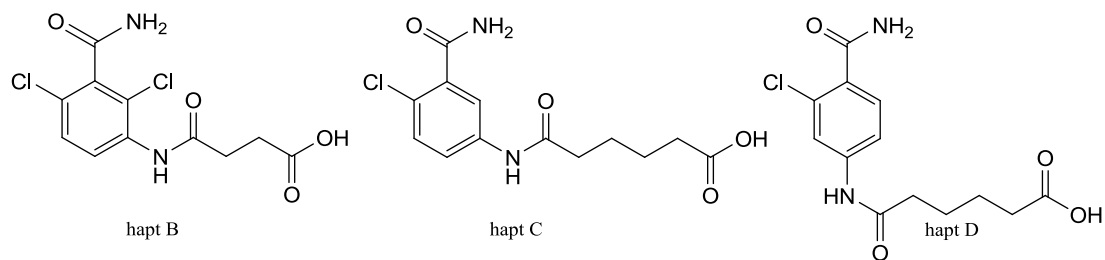


**Figure 2.3: Chemical structures of three newly synthesised BAM haptens (hapt B, hapt C and hapt D). Compared to hapt A, hapt B has a shorter linker, hapt C has the same linker but one of the chlorine atoms is missing on the ring, and hapt D has the same linker, but the position is moved from ortho to para relative to the amide functionality and one chlorine atom is missing.**

## 2.2. Experimental

### 2.2.1 Reagents, buffers and materials

2,6-dichloro-3-nitrobenzotrile (98%) [5866-98-8] was from Alfa Aesar, Germany, 4-amino-2-chloro-benzotrile (99%) [20925-27-3] was from Aldrich, Switzerland, 2-chloro-5-nitrobenzotrile (99%) [16588-02-6], methyl 4-chloro-4-oxobutanoate (methyl succinyl chloride, 97%) [1490-25-1] and potassium trimethylsilanolate ( $\text{KOSi}(\text{CH}_3)_3$ , 90%) [10519-96-7] were from Aldrich, USA, methyl adipoylchloride (97%) [35444-44-1] was from Aldrich, UK, lithium hydroxide monohydrate ( $\text{LiOH}\cdot\text{H}_2\text{O}$ , 98%) [1310-66-3] and acetic acid were from Sigma-Aldrich, USA, hydrochloric acid, petroleum ether, dichloromethane and ethanol were from Sigma-Aldrich, Germany, tetrahydrofuran (THF) was from Sigma-Aldrich, UK, ethylacetate was from Fluka, Mexico, iron powder (Fe), silica gel 60 (0.04-0.063) were from Merck, Germany and sodium carbonate ( $\text{Na}_2\text{CO}_3$ ) was from Sigma, USA. Benzotriazol-1-yloxy-tris (dimethylamino)phosphonium hexafluorophosphate (BOP) was from Novabiochem, Germany. N-ethyl-diisopropylamine (DIEA), dimethylsulfoxide (DMSO) and sulphuric acid ( $\text{H}_2\text{SO}_4$ ) were from Fluka, Germany, TMB-Plus substrate (3,3',5,5'-tetramethylbenzidine dihydrochloride) was from KEM EN TEC, Denmark, ovalbumin was from Sigma, USA., Bradford reagent was from Sigma-Aldrich, USA, BAM monoclonal antibodies (Bruun et al., 2000) were provided by Statens Serum Institut, Denmark, phosphate buffered saline (PBS) powder in pouches was from Sigma, USA, PBS with Tween® 20 (PBST) tablets were

from Fluka, Sweden. Sodiumbicarbonate ( $\text{NaHCO}_3$ ) was from Fluka, Germany. Glycin hydrochloride and BSA (Bovine Serum Albumin) were from Sigma, USA.

PBS buffer of pH 7.4 (1 M) was prepared by dissolving one pouch of buffer powder in 1000 mL of milli-Q water. PBST buffer of pH 7.4 (1 M) was made by dissolving one PBST tablet in 1000 mL of milli-Q water. Conjugation buffer was made by dissolving 1.68 g of sodium hydrogen carbonate in 200 mL of Milli-Q water (100 mM) and the pH was adjusted to 8.1. Regeneration buffer was made by dissolving 1.12g of glycine hydrochloride in 100 mL of Milli-Q water (100 mM) and the pH was adjusted to 2.

Polysorp microtitre plates were from Nunc®, Denmark. Milli-Q water purifier was from Millipore, USA and TLC aluminium sheets coated with silica gel 60 F254 with layer thickness of 0.2 mm were from Merck, Germany.

### 2.2.2 Instruments

The hot air oven was a BINDER with temperature and time control (Max. temperature: 250°C). UV reaction chamber was UV Stratalinker 2400 from Stratagene. The UV spectrometer was Shimadzu UV – 1800 (range: 190 – 1100) and the spectra were analysed by UVProbe 2.33 software. The microtitre plate reader was Thermomax with the software SOFTmax® from Molecular Devices, USA. The Plate washing instrument was Wellwash Ascent from Labsystems (Beverly MA, USA). The NMR was Varian Mercury 300 MHz and the software used to analyze the spectra was MestReNova

### 2.2.3 Synthesis of Haptens

Synthesis of hapten library was achieved by modifying the three stage synthesis route described by Bruun *et al.* [48]. The modified scheme (Figure 2.4(b)) made it possible to obtain nitrile derivatives of each of the new haptens (Figure 2.4(c)) giving altogether eight haptens named hapt A, hapt B, hapt C, hapt D, hapt E, hapt F, hapt G and hapt H. Final products and intermediates were identified using  $^1\text{H}$  NMR and the purity of the compounds was checked by Thin Layer Chromatography (TLC).

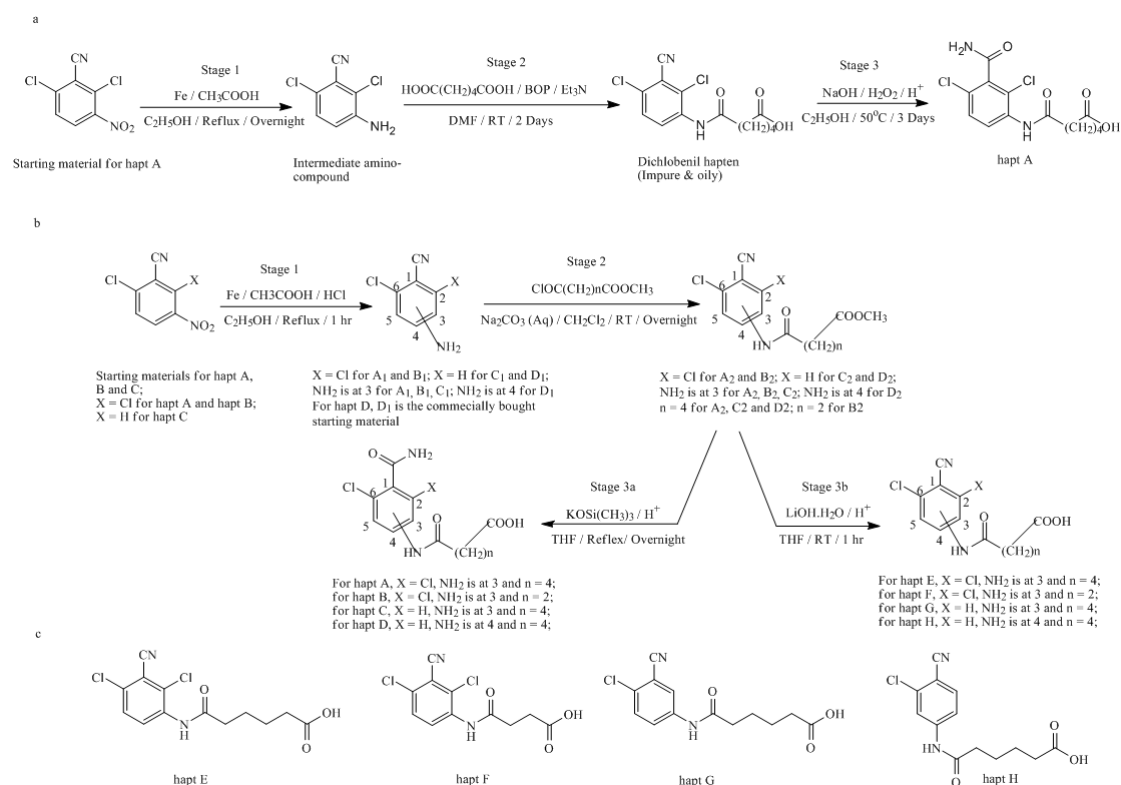


**Figure 2.4:** a) hapt A synthesis route given by Bruun et al. [49], b) improvised general route adopted for hapten library synthesis in this work, c) chemical structures of nitrile haptens (potential dichlobenil haptens).

### 2.2.3.a) Synthesis of hapt A

#### **3-amino-2,6-dichlorobenzotrile**

3-nitro-2,6-dichlorobenzotrile (10 g, 46.1 mmol) and iron powder (7.7 g, 138.1 mmol) were swirled in absolute ethanol (200 mL) in a round bottomed flask (R.B. flask) fitted with a water condenser and a dropping funnel in a nitrogen atmosphere. Acetic acid (15.8 mL, 276.6 mmol) was added drop-wise to avoid vigorous reactions. The mixture was heated to reflux and followed by TLC and finally completed by the addition of conc. HCl (2 mL) after 1 hr of boiling. Milli Q water (750 mL) was added to precipitate the crude product. The crude product was then centrifuged and dried at 50°C. The product was extracted from the crude by the Soxhlet method using ethylacetate as solvent followed by purification by flash chromatography (eluent: ethylacetate / petroleum ether 1:1) and used in the next step. Yield: 97%. <sup>1</sup>H NMR (CDCl<sub>3</sub>) δ : 7.19 (d, 1H), 6.83 (d, 1H), 4.22 (s, 2H). *R<sub>f</sub>*: 0.38 (Ethylacetate / petroleum ether 1:1).

***methyl 6-(2,4-dichloro-3-cyanophenylamino)-6-oxohexanoate***

Purified 3-amino-2,6-dichlorobenzonitrile (1.53 g, 10 mmol) was dissolved in CH<sub>2</sub>Cl<sub>2</sub> (50 mL) in an R.B. flask. 5% w/v Na<sub>2</sub>CO<sub>3</sub> (125 mL) was added followed by drop wise addition of Methyl 6-chloro-6-oxohexanoate (methyl adipoylchloride, 7.2 mL, 30 mmol) dissolved in dichloromethane (25 mL). The reaction mixture was stirred at room temperature till completion indicated by TLC. On completion, the mixture was transferred to a separatory funnel and the organic layer was washed with 5% w/v Na<sub>2</sub>CO<sub>3</sub> solution three times. The product was then isolated from the organic layer by evaporating CH<sub>2</sub>Cl<sub>2</sub> after drying over MgSO<sub>4</sub>. Yield: 99.5%. <sup>1</sup>H NMR (CDCl<sub>3</sub>) δ : 8.61 (d, 1H), 7.69 (s, 1H), 7.41 (d, 1H), 3.67 (s, 3H), 2.49 (t, 2H), 2.37 (m, 2H), 1.72 (m, 4H). R<sub>f</sub>: 0.32 (Ethylacetate / petroleum ether 1:1).

***6-(3-carbamoyl-2,4-dichlorophenylamino)-6-oxohexanoic acid (hapt A)***

Methyl 6-(4-chloro-3-cyanophenylamino)-6-oxohexanoate (0.33 g, 1 mmol) and potassium trimethylsilanolate (0.8 g, 6 mmol) were dissolved in tetrahydrofuran (5 mL) and heated to reflux overnight in a nitrogen atmosphere. The brown precipitate formed was completely dissolved in Milli Q water and the aqueous layer acidified with 1 M HCl. The final product was extracted with ethylacetate, and the product obtained by evaporating the solvent after drying over MgSO<sub>4</sub>. Yield: 60%. Off-white powder obtained was shown to be pure by TLC. R<sub>f</sub>: 0.45 (Ethylacetate / acetic acid 95:5). <sup>1</sup>H NMR (DMSO-d<sub>6</sub>) δ : 12.1 (s, 1H), 7.88 (s, 1H), 7.75 (d, 1H), 7.51 (d, 1H), 2.47 (t, 2H), 2.3 (m, 2H), 1.64 (m, 2H), 1.56 (m, 2H).

2.2.3.b) Synthesis of hapt B

***methyl 4-(2,4-dichloro-3-cyanophenylamino)-4-oxobutanoate***

Purified 3-amino-2,6-dichlorobenzonitrile from 2.3.1.1 (7.5 g, 4 mmol) was dissolved in CH<sub>2</sub>Cl<sub>2</sub> (40 mL) in an R.B. flask. 5% w/v Na<sub>2</sub>CO<sub>3</sub> (80 mL) was added into it. Methyl 4-chloro-4-oxobutanoate (methyl succinyl chloride, 1.5 mL, 12 mmol) dissolved in CH<sub>2</sub>Cl<sub>2</sub> (15 mL) was added drop-wise. The reaction was then carried out as described in Section 2.3.1.2. Yield: 99.3%. <sup>1</sup>H NMR (CDCl<sub>3</sub>) δ : 8.6 (d, 1H), 8.04 (s, 1H), 7.4 (d, 1H), 3.72 (s, 3H), 2.77 (m, 4H). R<sub>f</sub>: 0.42 (Ethylacetate / petroleum ether 1:1).

#### ***4-(3-carbamoyl-2,4-dichlorophenylamino)-4-oxobutanoic acid (hapt B)***

The same procedure as in Section 2.3.1.3 was done for methyl 4-(2,4-dichloro-3-cyanophenylamino)-4-oxobutanoate (1.040 g, 3.5 mmol) with potassium trimethylsilanolate (2.7 g, 21 mmol) in THF (15 mL) to get hapt B. Yield: 60%. <sup>1</sup>H NMR (DMSO-d<sub>6</sub>) δ : 12.15 (s, 1H), 8.08 (s, 2H), 7.8 (s, 1H), 7.69 (d, 1H), 7.42 (d, 1H), 2.63 (t, 2H), 2.49 (m, 2H). R<sub>f</sub>: 0.28 (ethylacetate / acetic acid 95:5).

#### 2.2.3.c) Synthesis of hapt C

##### ***5-amino-2-chlorobenzonitrile***

2-chloro-5-nitrobenzonitrile (8.4 g, 46.1 mmol) was reduced with Fe powder (7.7g, 138.1 mmol), acetic acid (15.8 mL) and conc. HCl (2 mL) to 5-amino-2-chlorobenzonitrile as explained in Section 2.3.1.1. Yield: 85%. <sup>1</sup>H NMR (CDCl<sub>3</sub>) δ : 7.24 (d, 1H), 6.91 (d, 1H), 6.8 (dd, 1H), 3.91 (s, 2H). R<sub>f</sub>: 0.35 (ethylacetate / petroleum ether 1:1).

##### ***methyl 6-(4-chloro-3-cyanophenylamino)-6-oxohexanoate***

Purified 5-amino-2-chlorobenzonitrile (1.53 g, 10 mmol) was coupled with methyl 6-chloro-6-oxohexanoate (methyl adipoylchloride, 7.2 mL, 30 mmol) as explained in Section 2.3.1.2. Yield: 99%. <sup>1</sup>H NMR (CDCl<sub>3</sub>) δ : 8.12 (d, 1H), 7.77 (dd, 1H), 7.55 (d, 1H), 4.91 (s, 1H), 3.65 (s, 3H), 2.36 (m, 4H), 1.67 (m, 4H). R<sub>f</sub>: 0.23 (ethylacetate / petroleum ether 1:1).

##### ***6-(3-carbamoyl-4-chlorophenylamino)-6-oxohexanoic acid (hapt C)***

Hydrolysis of methyl 6-(4-chloro-3-cyanophenylamino)-6-oxohexanoate (0.3 g, 1 mmol) by potassium trimethylsilanolate (0.8 g, 6 mmol) was done as described in Section 2.4.1.3. to obtain hapt C. Yield: 70%. <sup>1</sup>H NMR (DMSO-d<sub>6</sub>) δ : 10.22 (s, 1H), 7.88 (d, 1H), 7.71 (d, 1H), 7.62 (dd, 1H), 7.56 (s, 2H), 7.34 (s, 1H), 2.31 (t, 2H), 2.20 (m, 2H), 1.50 (m, 4H). R<sub>f</sub>: 0.51 (ethylacetate / acetic acid 95:5).

#### 2.2.3.d) Synthesis of hapt D

##### ***methyl 6-(3-chloro-4-cyanophenylamino)-6-oxohexanoate***

4-amino-2-chlorobenzonitrile (commercially available, 1.5 g, 10 mmol) is coupled with methyl 6-chloro-6-oxohexanoate (methyl adipoylchloride, 7.2 mL, 30 mmol) as described in Section 2.3.1.2. Yield: 78%. <sup>1</sup>H NMR (CDCl<sub>3</sub>) δ : 8.14 (s, 1H), 7.95 (d,

1H), 7.58 (dd, 1H), 7.38 (d, 1H), 3.7 (s, 3H), 2.42 (m, 4H), 1.74 (m, 4H). *R<sub>f</sub>*: 0.26 (ethylacetate / petroleum ether 1:1).

***6-(4-carbamoyl-3-chlorophenylamino)-6-oxohexanoic acid (hapt D)***

Hydrolysis of methyl 6-(3-chloro-4-cyanophenylamino)-6-oxohexanoate (0.3 g, 1 mmol) by potassium trimethylsilanolate (0.8 g, 6 mmol) was done as described in 2.3.1.3. to obtain hapt D. Yield: 75%. <sup>1</sup>H NMR (DMSO-d<sub>6</sub>) δ : 10.62 (s, 1H), 8.17 (s, 1H), 7.95 (d, 1H), 7.70 (d, 1H), 7.52 (s, 2H), 7.28 (s, 1H), 2.41 (t, 2H), 2.35 (m, 2H), 1.65 (m, 4H). *R<sub>f</sub>*: 0.54 (ethylacetate / acetic acid 95:5).

2.2.3.e) Synthesis of nitrile derivatives of BAM haptens (hapt E, hapt F, hapt G, and hapt H - potential dichlobenil haptens)

Hapt E, hapt F, hapt G and hapt H were synthesized by a mild hydrolysis of corresponding stage 2 products with LiOH.H<sub>2</sub>O. 10 mmol of each Stage 2 products were dissolved in THF (40 mL). LiOH.H<sub>2</sub>O (60 mL of 0.5 M solution, 30 mmol) was added to it and stirred at room temperature for two hours. THF was boiled off and 10 mL of 1 M HCl was then added to precipitate corresponding nitrile haptens. The precipitates were dried in oven at 50°C overnight.

***6-(2,4-dichloro-3-cyanophenylamino)-6-oxohexanoic acid (Hapt E)***

Yield: 90%. <sup>1</sup>H NMR (DMSO-d<sub>6</sub>) δ : 12 (s, 1H), 9.86 (s, 1H), 8.02 (d, 1H), 7.7 (d, 1H), 2.45 (m, 2H), 2.22 (t, 2H), 1.56 (m, 4H) . *R<sub>f</sub>*: 0.61 (ethylacetate/acetic acid 95:5).

***4-(2,4-dichloro-3-cyanophenylamino)-4-oxobutanoic acid (Hapt F)***

Yield: 95%. <sup>1</sup>H NMR (DMSO-d<sub>6</sub>) δ : 12.18 (s, 1H), 9.98 (s, 1H), 8.05 (d, 1H), 7.7 (d, 1H), 2.68 (t, 2H), 2.48 (m, 2H). *R<sub>f</sub>*: 0.56 (ethylacetate/acetic acid 95:5).

***6-(4-chloro-3-cyanophenylamino)-6-oxohexanoic acid (Hapt G)***

Yield: 92%. <sup>1</sup>H NMR (DMSO-d<sub>6</sub>) δ : 12.03 (s, 1H), 10.55 (s, 1H), 8.2 (d, 1H), 7.83 (s, 1H), 7.64 (d, 1H), 2.34 (t, 2H), 2.21 (t, 2H), 1.54 (m, 4H). *R<sub>f</sub>*: 0.56 (ethylacetate/acetic acid 95:5).

***6-(3-chloro-4-cyanophenylamino)-6-oxohexanoic acid (Hapt H)***

Yield: 87%. <sup>1</sup>H NMR (DMSO-d<sub>6</sub>) δ : 12.03 (s, 1H), 10.63 (s, 1H), 8.05 (d, 1H), 7.61 (d, 1H), 2.36 (t, 2H), 2.21 (t, 2H), 1.53 (m, 4H). *R<sub>f</sub>*: 0.59 (ethylacetate/acetic acid 95:5).



## 2.2.4 Synthesis and characterization of different conjugates

To immobilize haptens on microtitre plates, the newly synthesized haptens (5 mole equivalents) were conjugated to 1 mL of 1 mg mL<sup>-1</sup> OA. To attain a photo-catalyzed covalent immobilization, rather than a normal physical absorption, an anthraquinone entity (EQ 0028, 10 mole equivalents) is conjugated to the hapten-ovalbumin conjugate. This conjugation process and the synthesis of EQ 0028 were described by Bruun *et al.*[48, 49]. The molar equivalence ratio during synthesis of hapten-OA-EQ 0028 conjugates was kept as 5:1:10. All conjugates were finally dialyzed against 1x PBS and stored at 4°C.

The antibody-Horse Radish Peroxidase (HYB 273 - HRP) conjugate concentration was determined by performing Bradford protein assay using bovine serum albumin (BSA) as the standard and was found to be 1.0 mg mL<sup>-1</sup>. Concentrations of all the haptens-OA-EQ 0028 conjugates were estimated by UV-Vis spectroscopy. From the UV-Vis data, it was able to calculate the number of anthraquinone entity per OA. Concentrations of OA and EQ 0028 are directly calculated from the UV-Vis data as they are photoactive (Eq. 1 and 2). Molar extinction coefficients of OA and EQ 0028 at 260 nm and 280 nm in PBS are found by measuring the absorbance of a series of solutions with known concentrations.

$$A_{conjugate}^{280} = \epsilon_{OA}^{280} C_{OA} + \epsilon_{EQ}^{280} C_{EQ} \quad (1)$$

$$A_{conjugate}^{260} = \epsilon_{OA}^{260} C_{OA} + \epsilon_{EQ}^{260} C_{EQ} \quad (2)$$

## 2.2.5 Assay method

Immobilization of hapt-OA-EQ 0028 conjugates on Polysorp<sup>®</sup> microtitre plates was always carried out by filling the wells with (100 µL/well) hapten-conjugate solutions of appropriate concentrations in 0.1x PBS. The plates were then irradiated with UV light (300 – 400 nm) at 34°C for 30 min, washed with 1x PBST four times and used for the assay immediately or sealed with a taped lid and stored at room temperature in darkness until use. During the competitive assays, the total volume of antibody or antibody with samples or standards in wells was always kept at 100 µL, because of the assumption that the surface provided by the 100 µL volume of hapten-conjugate solution was available for antibody-antigen interaction (hybridization). The plates

were incubated for 1 hr and then washed with 1x PBST four times. The TMB substrate volume was kept as 200 $\mu$ L/well to make the reaction kinetically independent of the substrate concentration. All assays except the regeneration experiments were conducted as end-point analysis by stopping the substrate reaction at a point of time by adding 1 M H<sub>2</sub>SO<sub>4</sub> (50  $\mu$ L/well) and the absorbances were measured at 450 nm.

### 2.2.6 Kinetic study of HRP-TMB reaction

Two plates were immobilized with hapt A and hapt D conjugates as described above. An inhibition assay was conducted with zero BAM in solution (to obtain maximum signal). Absorbance was recorded with no stop solution at 650 nm. The measurement was made after 15 minutes of adding the substrate until a constant absorbance was obtained every 5 minutes. A plot was generated with absorbance against time to find out the optimum duration for the substrate reactions.

### 2.2.7 Affinity constants

Affinity constants ( $K_{aff}$ ) of structurally different new hapten molecules were measured in order to quantify and compare the interaction of HYB 273 with them, on ELISA plates as described by Beatty et al. [61] with two-fold serial dilution of antibody and two different concentrations of each immobilized hapten conjugates. Accordingly, each plate was divided into two halves of 4 rows and 12 columns. The upper half was immobilized with hapten-conjugate of concentration [Ag] and lower part with [Ag]/2. A 2-fold serial dilution of HYB 273 was done in the direction of rows. The interaction between the antibody and each BAM-hapten were treated as sigmoidal dose-response curves; the data was fitted to the four-parameter logistic equation using GraphPad Prism software (version 4.03 for windows, GraphPad Prism, San Diego, CA, USA). A non-linear regression was performed to obtain effective concentration (EC<sub>50</sub>) values. Using EC<sub>50</sub> values,  $K_{aff}$  of anti-BAM monoclonal antibody to each BAM-hapten molecules were calculated according to the equation described in [61].

### 2.2.8 Regeneration cycles

To test and optimize regeneration conditions, microtitre plates were prepared as described in Assay method, keeping the immobilized hapten conjugate concentration the same. Preliminary investigations showed that a 100 mM glycine.HCl buffer of pH 2 was close to the optimal regeneration agent. In regeneration experiments, no stop

solution was used and the colour obtained by the substrate reaction was directly measured at 650 nm. After the first cycle of hybridization and substrate reaction, the coloured substrate was discarded and the plates were washed with 1× PBST four times. 100 mM glycine.HCl solution (pH~2) was added to each well (100µL/well) and incubated for 10 min at room temperature in a shaker at 200 rpm. The plates were again washed and used for next cycle of hybridization and substrate reaction. These processes were continued many times to check the ability of the surface to retain its capacity for further hybridizations. In order to bring the assay into an in-line sensor platform, this regeneration of surfaces is critical.

### **2.3. Results**

Careful selection of commercially available starting chemicals with small structural variations and linkers of different chain lengths made it possible to synthesise new haptens with new available motifs for binding pockets of HYB 273 which in turn resulted in reduction of hapten-HYB 273 interactions. This was evident from the inhibition assays performed with all 8 haptens and HYB 273. HYB 273 could bind with only three of them-hapt A, hapt C and hapt D. No nitrile derivative did bind to the antibody, since they lack the prime epitope, the amide group.

Figure 2.5 and Figure 2.6 show the absorption spectra of ovalbumin and EQ 0013 at different concentrations in order to determine molar extinction coefficients at different wavelengths.

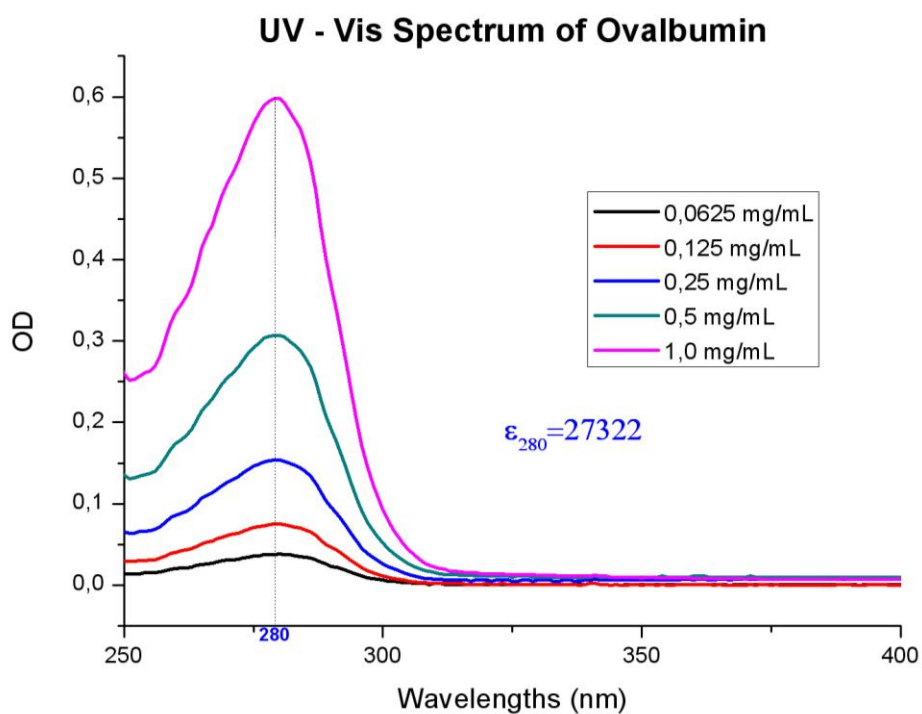


Figure 2.5: The UV-Vis Spectrum depicting absorption spectra of Ovalbumin.

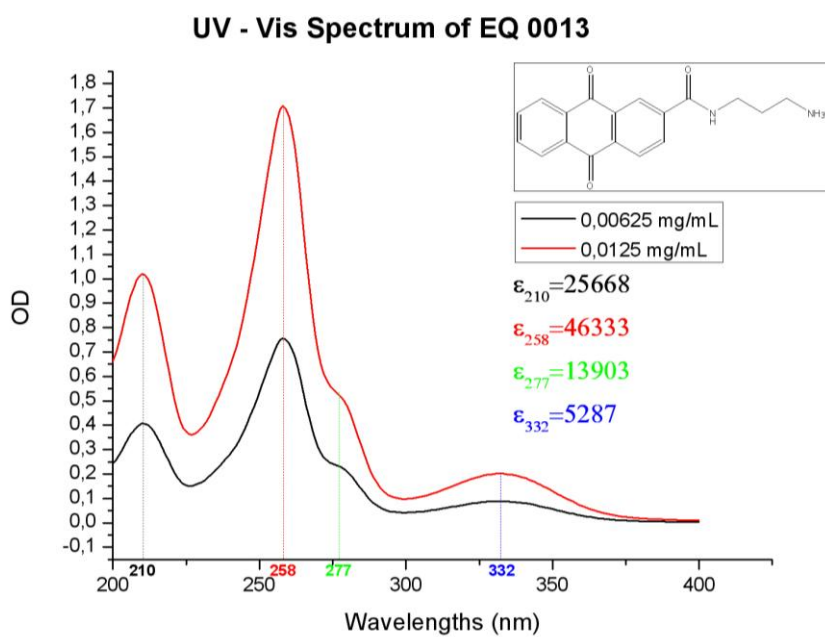
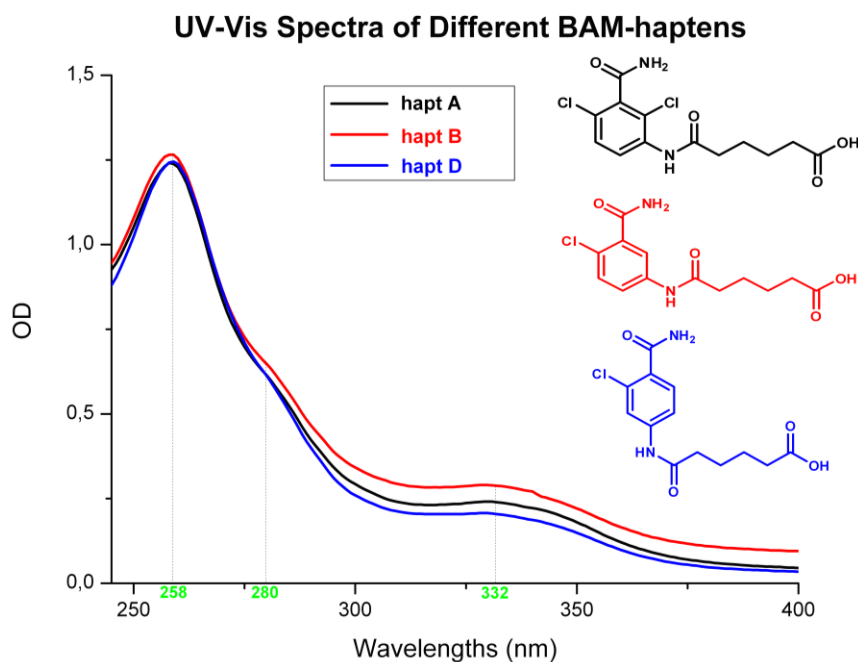


Figure 2.6: The UV-Vis Spectrum depicting absorption spectra of EQ 0013.

The results obtained from UV-Vis analysis of haptin-OA-EQ0028 conjugates are given in Figure 2.7 and the values are summarized in Table 2.1.



**Figure 2.7: Absorption spectra of hapt A, hapt B and hapt D.**

The concentration of OA was found to vary in a very small range in all of the conjugates (0.9 – 1.1 mg mL<sup>-1</sup>). To keep standard assay conditions, the concentrations of conjugates were adjusted to 0.9 mg mL<sup>-1</sup>. The number of photoreactive anthraquinone entities per OA was found to be four in hapt G-OA-EQ 0028 and it was two for all other conjugates.

**Table 2.1: Characterization of hapt-OA-EQ 0028<sup>a</sup> conjugates by UV-Vis spectroscopy.**

<b>Conjugates</b>	<b>Concentration (mg mL<sup>-1</sup>)</b>	<b>No. of EQ 0028 per OA</b>
hapt A-OA-EQ 0028	0.9	2
hapt B-OA-EQ 0028	1.0	2
hapt C-OA-EQ 0028	1.0	2
hapt D-OA-EQ 0028	0.9	2
hapt E-OA-EQ 0028	1.1	2
hapt F-OA-EQ 0028	0.9	2
hapt G-OA-EQ 0028	1.0	4
hapt H-OA-EQ 0028	1.0	2

<sup>a</sup>hapt: hapten; OA: ovalbumin; EQ 0028: photoactive anthraquinone entity.

The results of kinetic experiments done for hapt A and hapt D conjugates are shown in Figure 2.8. These results indicate that it takes at least 45 min for hapt A-immobilized surfaces and 40 min for hapt D-surfaces to reach a steady state situation during TMB (the substrate for HRP) reaction after the hybridisation of HYB 273 on immunosurfaces. This information is important, when the immunoassay is taken place in a flow system as a continuous non-end-point analysis.

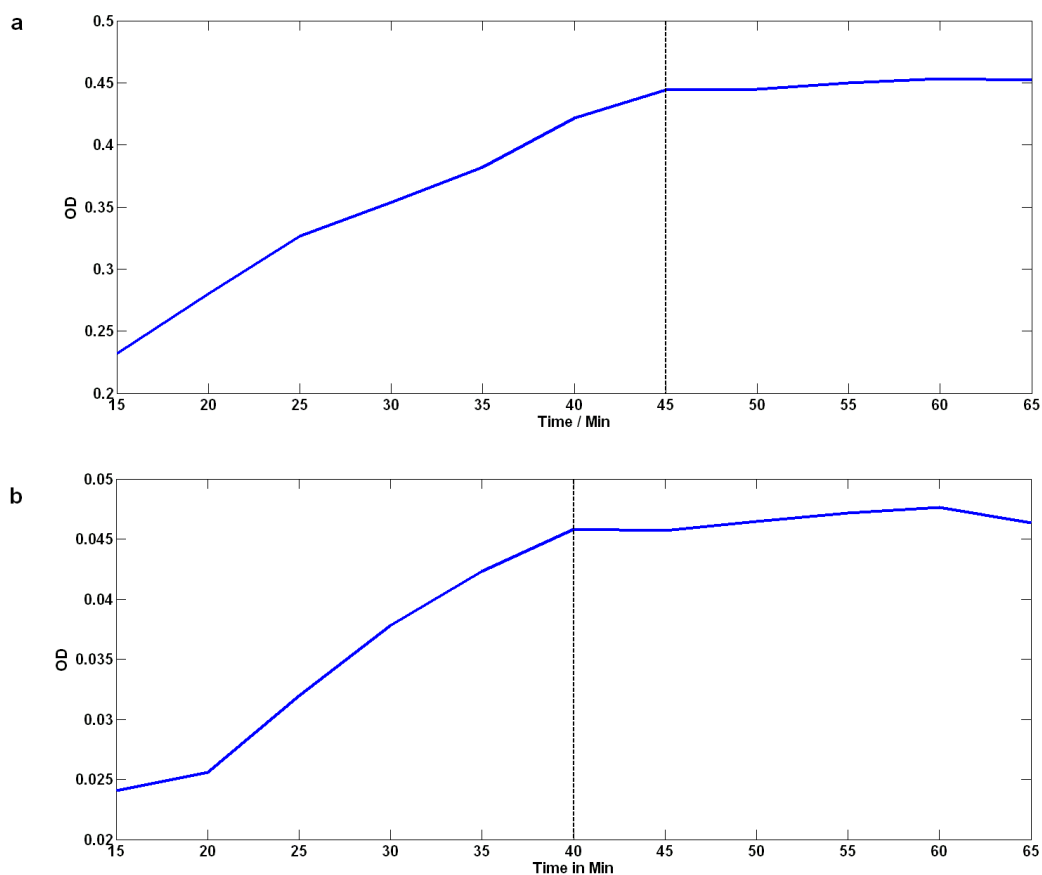


**Figure 2.8: The kinetic curves showing Horse Radish Peroxidase (HRP) reaction with TMB substrate on a) hapt A immobilized surface and b) hapt D immobilized surface. The absorbance are measured at 650nm without adding the stop solution.**

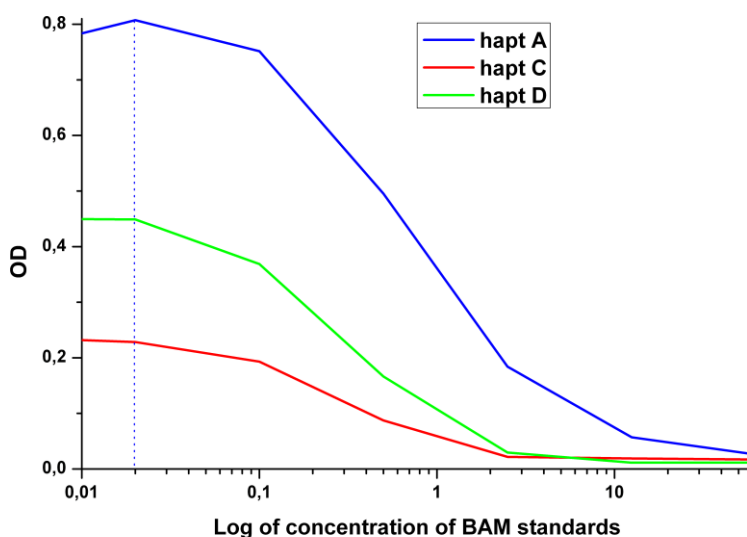
Since haptens B, E, F, G and H did not show any binding with HYB 273, it was decided to consider only the active haptens (hapt A, C and D) for further analysis. Standard curves were generated by inhibition assays with active hapten conjugates on surfaces and BAM standards ranging from  $0.0008 \mu\text{g L}^{-1}$  to  $62.5 \mu\text{g L}^{-1}$  in solutions. Direct OD values are plotted on the Y axis against the logarithmic concentrations of the BAM standards (Figure 2.9). Concentrations of hapten conjugates immobilized on microplates were the same. As expected, the original BAM hapten conjugate (hapt A-OA-EQ0028) had higher response to the antibody than the other two chemically modified new conjugates at all concentrations of BAM standards in solution. The reliable detection range is retained in new haptens as well (indicated by blue dotted lines).

Table 2.2 presents the affinity constants ( $K_{aff}$ ) of HYB 273 towards the active hapten conjugates.

**Table 2.2: constants ( $K_{aff}$ ) of HYB 273 towards the active haptens.**

Haptens	$K_{aff}$ . $\text{nm}^{-1}$
hapt A	0.5836
hapt C	0.2176
hapt D	0.3081

The antibody (HYB 273) showed lower affinities towards the newly synthesised haptens than the original hapt A. These results are in good agreement with the standard curves shown in Figure 2.9. We were not able to calculate  $K_{aff}$  to hapt B and nitrile derivatives (hapt E, F, G and H), due to the low affinity of anti-BAM antibody towards these haptens.



**Figure 2.9: Standard curves generated by active hapten surfaces (hapt A, C and D; none other than these did bind with HYB 273) with BAM-standards on micro-titre plates. Each OD value plotted is an average of 10 repeats.**



Figure 2.10 shows the signal following up to 25 analytical cycles with regeneration step between each cycle. Original hapten (hapt A) conjugate showed a steeper signal drop (blue line in Figure 2.10) though it had a good signal to noise ratio. After 25 cycles, the OD value reduced to approximately 40%. Among the three active conjugates, hapt C conjugate was the best in terms of regeneration (red line in Figure 2.10); but it showed a poor signal to noise ratio. However, hapt D conjugate showed an intermediate performance in both signal strength and regeneration capability. Combining these results with the affinity constants given in Table 2.2, hapt D seems to be the optional choice with respect to a signal-to-noise, regeneration capability and detection limit for surface immobilization when this assay is used in real-time sensor applications.

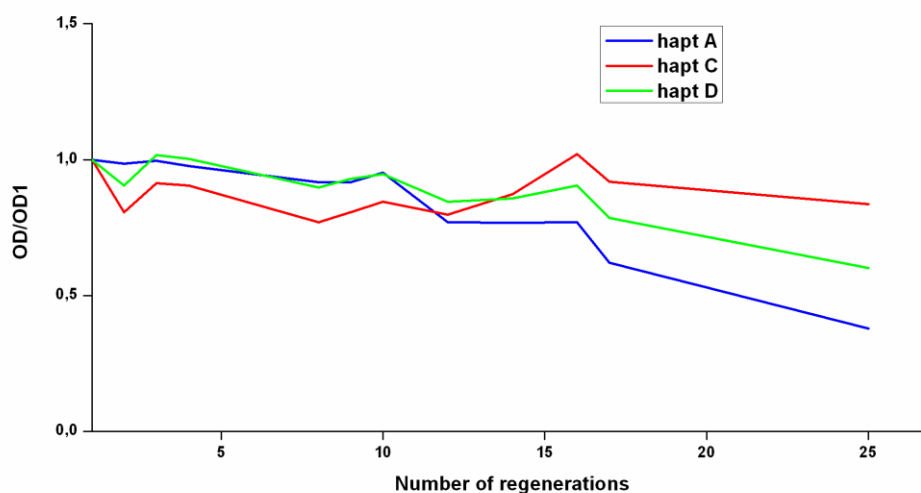


**Figure 2.10: Regeneration results of three different immobilized hapten conjugates.** In this experiment a 96-well polysorp microtitre plate was immobilized with the same concentration of the three hapten conjugates. In each cycle, same concentration of anti-BAM antibody was added to all the wells and incubated for one hour. After washing, TMB substrate solution was added and the OD values were read after 15 minutes. After washing, 100 mM glycine.HCl buffer of pH 2 was added for 10 min. to remove antibody. A new TMB substrate reaction was performed to confirm complete removal of the antibody. This analytical cycle was repeated until 17<sup>th</sup> cycle. After 17<sup>th</sup> cycle, eight more hybridization and stripping were performed without substrate reaction until the full cycle was repeated at the 25<sup>th</sup> cycle. All data are plotted relative to the signal intensity of the first cycle.

## 2.4. Discussion

As mentioned earlier, in this work the original synthesis route reported by Bruun *et. al* .[49] has been modified, keeping the same reaction sequence, but by improving the process in terms of reaction time, yield and purity at each step. As shown in Figure

2.4(a), three different stages were involved in the overall synthesis and product purity at each stage was crucial in the success of next stage reaction. In the reduction of nitro compounds to the corresponding amines (Stage 1), the yield and reaction time were improved by adding a catalytic amount of conc.HCl into the reaction mixture.

Purification of the resulting amines by flash chromatography technique improved the efficiency of next stage reaction. In the linker coupling reactions (Stage 2), instead of activating and coupling a dicarboxylic acid with a number of chemicals as described by Bruun et al., 2000, the acid chloride derivatives of the corresponding di-acids with the other end protected by methyl ester group were used. The reaction was carried out in a two-phase medium consisting of aqueous  $\text{Na}_2\text{CO}_3$  and  $\text{CH}_2\text{Cl}_2$  [62]. This two-phase reaction avoided the possibilities of formation of undesirable bi-products and dimer of the expecting product as impurities. Aqueous  $\text{Na}_2\text{CO}_3$  acted as proton acceptor and hydrolyzing agent for the excess reagent. Use of one side protected acid chlorides of diacids in this stage eventually helped in obtaining nitrile derivatives of haptens (Stage 3b, Figure 2.4(b)). It should be noted that esters resulted from Stage 2 and nitrile haptens obtained by Stage 3b were pure solid compounds rather than oily adduct reported by Bruun et al., 2000. Use of mild hydrolysing agent  $\text{LiOH} \cdot 2\text{H}_2\text{O}$  in THF helped to make the process simple in terms of hydrolysing only the ester group (without affecting the nitrile group on the ring) and effective in terms of increased solubility of ester in aqueous THF with respect to the traditional saponification by an aqueous alkali[63]. At room temperature, an aromatic nitrile hardly hydrolysed by  $\text{LiOH}$  and thus we obtained nitrile derivatives of haptens[64] (Figure 2.4c). These compounds have a potential value as dichlobenil haptens for immunization and development of useful immunochemistry for the herbicide itself.

In the new reaction scheme, both hydration of nitrile group (on the ring) and hydrolysis of the ester group (at the linker end) could be achieved in a single step by an anhydrous hydrolysis with  $\text{KOSiMe}_3$  in THF (Stage 3a, Figure 2.4 (b)). It was reported that on refluxing  $\text{KOSiMe}_3$  with a nitrile in THF, the intermediate salt gets precipitated (Figure 2.11)[65]. This means that the reaction can be controlled by stopping at the amide stage without going into carboxylic stage and any impurities can be washed off as the salt is insoluble in THF. Finally free amide can be obtained by a simple aqueous workup. At the same time  $\text{KOSiMe}_3$  in THF also functions as hydrolysing agent for the methyl ester at the linker end. The appreciable solubility of

KOSiMe<sub>3</sub> in THF and the easily cleavable silicon-oxygen bond made it capable of functioning as an organic soluble equivalent of O<sup>2-</sup> and thus converting ester directly to its anhydrous salt [66]. The free acid is subsequently liberated by acidification.

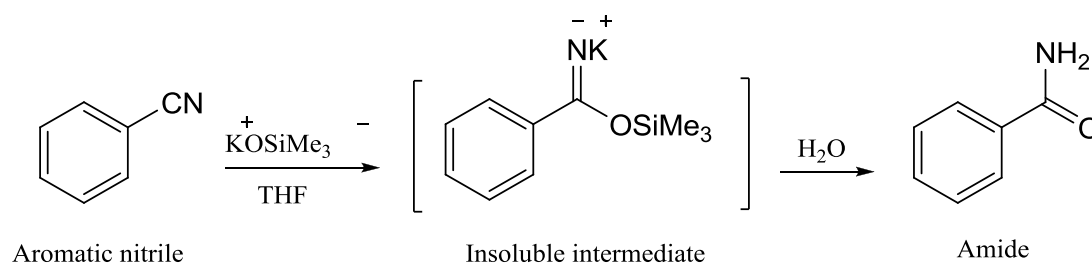


**Figure 2.11: Hydrolysis of nitrile group into amide by KOSiMe<sub>3</sub> in THF via an intermediate salt which is insoluble in THF.**

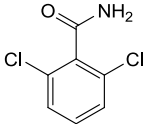
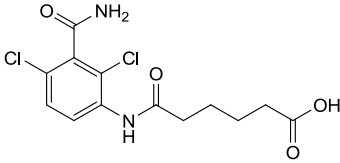
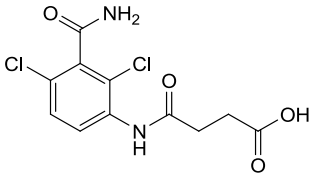
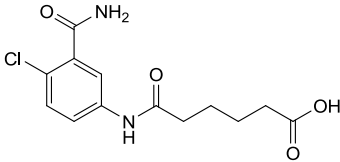
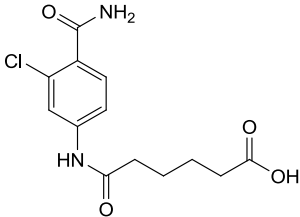
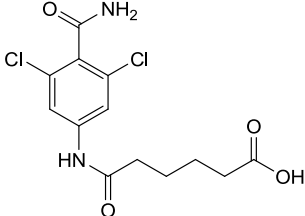
Interaction of HYB 273 with new haptens indicates clearly the importance of various epitope motifs in the binding process and how they can be tuned to manipulate the interaction in terms of regeneration aspects. The fact, none of the nitrile haptens bind to HYB 273 whereas free BAM molecules in samples and standards bind strongly to HYB 273 indicates that the amide group on the ring is the primary epitope for the antibody and the linker does not participate in the binding process at all. The next important motifs are the chlorine atoms on the ring. The role of their electronegativity in the binding mechanism is proved by the reduced  $K_{aff}$  values of hapt C and hapt D as compared to hapt A (Table 2.2). Thus losing one of these chlorine atoms can impart a considerable change in the interaction and affinity. Preservation of chemical structure, electronic distribution and special conformation on haptens has very important role in determining antibody affinity towards them [67].

The next important factor that affects the interaction is the steric hindrances exhibited by different haptens while the antibody molecules approach for binding. In the case of hapt D, the loss of one chlorine atom is compensated to some extent by the relieved steric effect by a change in orientation of the antigenic sites due to the para position of the linker relative to the most important epitope motifs. This is evident from the difference in  $K_{aff}$  values of hapt C and hapt D (Table 2.2). Recognition of target molecule moiety by antibody depends on the exposure of epitopes using favourable haptens [57, 58].

In hapt B, though it has retained all the major epitope motifs, reduction of the linker length almost totally inhibits binding. This explains the need of a spacer with a considerably long hydrophobic chain to present the main epitope motifs for effective binding when the antibody and haptens are in aqueous solutions. It should also be noted that the haptens are conjugated to ovalbumin molecules which are huge in size as compared to hapten molecules. A reduction in length of the spacer arm between the epitopes and OA would increase the steric factor for an effective binding with HYB 273. Importance of the linker length for effective binding during the development of immunizing haptens are reported [58, 68, 69]. The same is applicable for heterologous competitor haptens.

In heterogeneous assays, diffusion of antibody molecules and ease of availability of antigenic epitopes determine the extent of interaction. We manipulated the latter factor and tuned the interaction of HYB 273 with surfaces immobilized with various haptens. After considering all these factors, it is interesting to assume that a hypothetical hapten molecule with the main epitopes i.e., amide group and both the chlorine atoms on the ring and a linker of six membered chain at para position with respect to the amide would have a higher affinity than even hapt A for HYB 273. Above findings are summarized in Table 2.3 along with the structure of hypothetical hapten molecule. Our conclusion is that the amide group is the primary epitope, followed by the chlorine atoms while the spacer do not participate in the motif, but only serves to present the epitopes in the right way. Although we only have tested a small hapten library, it still gives insight to how changes in the hapten structure can affect on antibody/hapten interactions. Among the active haptens (hapt A, C and D), thus hapt D seemed to be a promising candidate for surface immobilisation as the immunochemistry shifts from ELISA to a flow system of an inline sensor.

**Table 2.3: The dependence of structural aspects on the nature of interactions between BAM haptens and HYB 273.**

Species	Structure	Nature of bonding with HYB 273	Comments
Free BAM		Very strong	All epitopes are present No steric effect
Hapt A		Strong	All epitopes are present. Steric effect due to meta positioned linker chain.
Hapt B		No binding	All epitopes are present. Linker is not long enough to present the epitopes for effective binding.
Hapt C		Weak	One of the epitope is missing. Meta positioned linker contributes considerable steric effect.
Hapt D		Intermediate	One of the epitope is missing. Para positioned linker relieves steric effect to compensate the missing chlorine to some extent.
Nitrile haptens	(Figure 2.4c)	No binding	The primary epitope is missing.
Hypothetical		Assumed to be as strong as free BAM	All epitopes are present. Steric factor is minimum. Linker is long enough to present the epitopes as if free BAM in aqueous solution.

Through this study, we have experienced that state of the art ELISA cannot be transferred as such into a flow system, since it is an end-point analysis with internal calibration. In fluidic systems, where different steps are in a sequential manner, reactivation of the surface is required for repeated reliable measurements and calibrations. Relatively mild conditions are appreciable for reactivation of surfaces in a  $\mu$ FIA-based flow system. This demands a proper balance between the interaction and the ease of removal of bound antibodies from the surface. On the basis of results presented, we were able to find the correlation in interactions between HYB 273 and various haptens, this knowledge can tremendously prove the regeneration step. From the obtained results we can conclude that hapt C binds the antibody too weakly to keep a good signal to noise ratio, but at the same time is best regarding regeneration. Hapt A has higher affinity and hence the best signal to noise ratio but at the same time faces the most difficulties in maintaining the surface activity. Hapt D with the intermediate affinity towards the antibody and with a reasonable signal to noise ratio is a promising candidate when this assay is moved to a fully automated immunosensing system in combination with  $\mu$ FIA techniques and miniaturized transduction methods. Regeneration experiments carried out on micro-titre plates were in good agreement with the affinity results.

Moving the optimized immunosensing assay to a fully automated  $\mu$ FIA set-up, several miniaturized transducer principles can be applied. Immunosensors can broadly be classified into micromechanical, optical, piezoelectric and electrochemical. We will use an electrochemical approach, in which the oxidized substrate solution will be passed by screen printed carbon paste electrode. A carbon paste electrode will act as the working electrode reducing the oxidized substrate where the current will be measured by a potentiostat. Initial experiments (data not shown) have shown an excellent quantitative correlation between the amount of oxidized substrate and the obtained current peaks with sensitivity in the same order as the conventional ELISA.

Other factors required for unattended on-site operation is the long term stability of the antibody and TMB substrate solutions. Preliminary results suggest that unattended operation for at least one month can be achieved.

## 2.5. Conclusion

An existing immunoassay between anti-BAM monoclonal antibody (HYB 273) and 2,6-dichlorobenzamide (BAM) on ELISA has been optimized and feasibility of using this well-established immunoassay as the sensing technique of a real-time, in-line sensor has been investigated. As a part of attaining reusable surface, a library of new haptens was synthesized. Interaction of HYB 273 with new haptens was investigated in detail and we were able to pick one of the new haptens (hapt D) with two changes in its chemical structure from the original hapten (hapt A), as a better surface for flow systems. However, in the future it would be interesting to perform a combinatorial analysis of a sequence of light and heavy variable chains of anti-BAM monoclonal antibodies and a library of hapten molecules. Such studies may help us to understand more about interactions between anti-BAM monoclonal antibodies and BAM-haptens and thus to improve the sensor properties.

By combining the optimised BAM ELISA with an electrochemical detection system, a real-time biosensor can be achieved for quantification of the pesticide residue BAM in ground water. A second generation of sensors which can quantify multiple analytes at the same time is a future goal of this project. By combining sensing technology, fluorescent and electrochemical detections we can improve not only the sensor sensitivity but also data reliability.

# A modular $\mu$ FIA-based immunosensor

---

### 3.1. Introduction

Plate-based heterogeneous immunoassay is a multistage, labour-intensive end-point analysis that includes sequential loading of different reagents, washing and incubation. Automation of liquid handling in microarray based immunoassays by complex robotic systems sets limits for themselves to be used in large hospitals for clinical applications only. Meeting project objectives requires automation of the BAM electrochemical immunosensor. In order to achieve this, immunochemistry optimized and established on ELISA plates (which is described in the previous chapter) should be transferred to a microfluidic platform where the combination of a set of fluidic unit operations is easily possible. When the solution volume is decreased, effective washing, evaporation and relative volumetric errors will become significant in plate based operation. On the other hand, well sealed microfluidic chips offer advantages in terms of portability, easy integration with one or more detection methods, low reagent volumes and easy automation of unit sequential operations. Increased surface area to volume ratio of  $\mu$ FIA-based chips facilitates the diffusion of an immunoreagent in the solution (free antibody) towards the surfaces with immobilized haptens, which is very significant in determining the sensitivity of a heterogeneous immunoassay, such as BAM detection. Careful design and fabrication, as well as reduction of the footprint of each individual analysis step allow parallelization of the processes on a  $\mu$ FIA-based chip, which is important for system calibration, repeatability and reproducibility of data. Modular approach (where the different modules responsible for different operations such as pumping, valving etc. are fabricated and then integrated into the complete system) makes the  $\mu$ FIA-based platform very simple and easy to operate. In this study, the final  $\mu$ FIA-based system was constructed by fixing the different modules onto a base plate using 2-mm screws and nuts.

This chapter describes the fabrication, integration and automation of different modules performing various functions such as pumping, flow switching (for



sequential loading of solutions, incubation and washing steps) and electrochemical sensing to bring the BAM immunoassay to the level of a lab-on-a-chip device. The various modules discussed involve

- Miniaturized peristaltic pump
- Miniaturized valves
- Immnochip
- Electrochemical detection unit
- Reservoir module
- Interconnections

### 3.2. Materials and methods

**Materials:** Depending on the intended application, selection of substrate material is the primary consideration for the fabrication of a microfluidic device. Silicon and polymers are the two materials widely used in fabrication of microfluidic devices [70-72]. In the present work, we have chosen thermoplastic polymers, such as poly(methyl methacrylate) (PMMA) (Röchling Technische Teile KG, Mainburg, Germany), polycarbonate (PC) (Bayer MaterialScience AG, Leverkusen, Germany), and a silicone based organic polymer, polydimethylsiloxane (PDMS) (made of Sylgard<sup>®</sup> 184 silicone elastomer kit — Dow Corning, Wiesbaden, Germany) for fabricating majority of the small individual units of the different modules. PMMA was used as the base material for fabricating the different parts of the ABIS prototype. Reasons justifying the choice of PMMA are for instance its low cost, low hydrophobicity, amenability for fabrication and modification [73] as well as most importantly its compatibility with the hapten immobilization technique [49] and the reagents used in the BAM immunoassay. PC was used to fabricate the upper chamber part of the reservoir module and rotorbed of the micropump. PDMS was used to make the inlays for pump and valves. The gaskets used in the reservoir module and electrochemical detection unit were made of PDMS.

**Machining:** Since PMMA was chosen to be the main substrate, one of the direct writing methods for polymer microfabrication, micromilling, which was easily accessible (in-house), less costly and relatively fast machining technique for

prototyping was used to fabricate all parts of the fluidic system under investigation. All the main components were fabricated using Computer Numerical Control (CNC) micromilling machine (Folken, Glendale, California) and a Mini-Mill/3Pro software system (Minitch Machinery Corporation, Norcross, GA, USA) which executes G-code generated by EZ-CAM15 Express software (EZCAM Solutions, Inc., New York, NY, USA). Designs of structures to be milled were drawn using AutoCAD and then converted to machine G codes with EZ Cam software. In micromilling, material is removed from the substrate with the help of cutting tools to fabricate the designed structures. The spindle rotates the tool and moves only in the Z direction. The stage moving in the X-Y plane creates the pattern on the substrate which is affixed on it. The shape of the fabricated structures is determined by the profile and diameter of the tool. Figure 3.1 shows a micromilling machine and example tool bits used for fabricating different parts of the microfluidic device.



**Figure 3.1: Micromilling machine. Inset shows tool bits used for micromilling.**

**Bonding:** After fabrication, the chip components with the microfluidic channels have to be closed with lids to obtain fully sealed fluidic channels. Different bonding methods such as adhesive bonding, thermal fusion bonding, solvent bonding, local welding etc. are described in literature [70, 73]. In the fabrication of ABIS prototype in this work, the three different PMMA-based chip components with channels were bonded to the corresponding lids (also made of PMMA) by using a direct bonding method, UV assisted thermal bonding, described in [74]. In this study, importance was given to the adequate bonding life-time of the chips and performance of chips with well sealed microfluidic channels without any clogging. After exposing the surfaces to be bonded to UV radiation (Dymax mercury UV light source, 400 W) for 60 s, the channel plate and the lid were pressed together by a laboratory press (PW10 hydraulic press, Paul-Otto Weber GmbH, Remshalden, Germany) for 40 min under a pressure of 20 bar at 85 °C. Figure 3.2 shows the PW10 hydraulic bonding press used for the same.



**Figure 3.2: Hydraulic Bonding Press.**

Following sub-sections describe in detail fabrication of the different modules developed to construct the ABIS prototype.

### 3.2.1 Miniaturized peristaltic pump

Many attempts have been made and documented to solve the issue of effective pumping of liquids through microfluidic devices [75, 76]. As a practical solution to this problem, one of the research groups at DTU Nanotech, the Fluidic Array Systems and Technology (FAST) group, has succeeded in designing and fabricating a mechanically actuated multi-channel peristaltic micropump, which is made of cheap and completely outside-clean-room fabricated components as described in [77]. The microfluidic system, described in detail in this chapter, is an adaptation of the concept developed by the FAST group. In this work, we have used an eight-channel peristaltic micropump for pumping different reagents into the immunochip where the BAM hapten is immobilized. The micropump comprises three main components: i) a multi-roller (Figure 3.3), ii) a pumping inlay made of PDMS (Figure 3.4, left panel), and iii) a rigid rotor bed made of PC (Figure 3.4, right panel). The fabrication details of these components are given in the supplementary material of [77].

As shown in Figure 3.3, the multi-roller is composed of eight stainless-steel pins (2 mm x 24 mm) fixed by two disc shaped nylon blocks with eight holes of diameter 2.1 mm each around a 4-mm brass shaft. The over-sized holes allow free rotation of the pins without a mechanical damage during the rotations. A ball bearing (ID: 4 mm/ OD: 9 mm) (VBX Bearings, Anaheim, California) is attached to each end of the shaft. The ball bearings are placed in housings made of 5 mm thick aluminium piece. Embedded 2-mm nuts and drilled holes of 2 mm in diameter in the ball bearing housings allow attachment of a multi-roller unit to base plate and rotor bed with 2-mm screws. The brass shaft is machined to facilitate interfacing with LEGO<sup>®</sup> Mindstorms<sup>®</sup> servo motors.

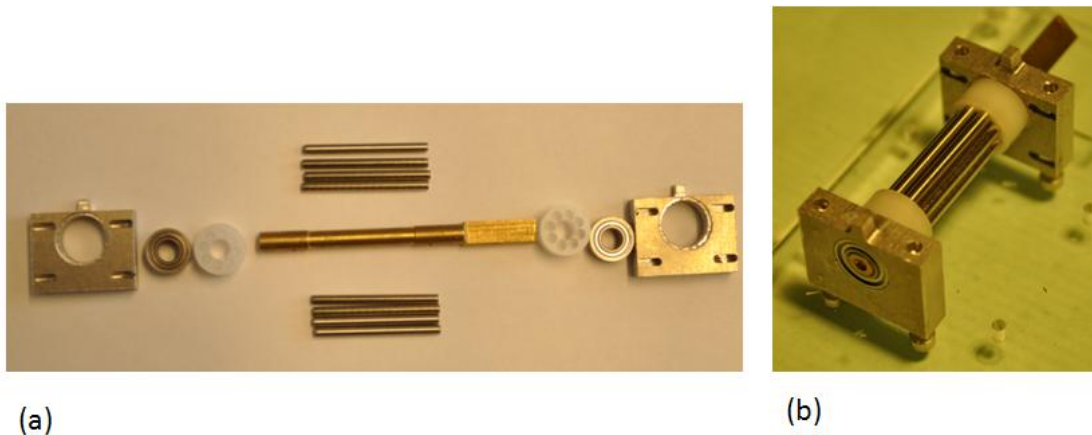


**Figure 3.3: (a) Components of a multi-roller of a miniaturized peristaltic pump, and (b) an assembled multi-roller.**

The pumping inlay with 8 integrated channels (Figure 3.4, left panel) was fabricated by casting PDMS inside a PMMA mould made by CNC micromilling. The channels are obtained by inserting 240- $\mu\text{m}$  optical fibres (Polymicro Technologies, Phoenix, Arizona, USA) through 250- $\mu\text{m}$  holes in the end pieces before injecting PDMS solution into the mould. Removing the optical fibers once the PDMS has been cured, results in the formation of eight integrated channels of 240  $\mu\text{m}$  in diameter spaced 2.25 mm apart (centre-to-centre) raised above the plane of the inlay with incorporated end brackets made of PMMA [77, 78].

The rotor bed (Figure 3.4, right panel) with a shape complementary to the multi-roller is made of 10 mm thick polycarbonate (PC) and provides a rigid support to the pumping inlay.

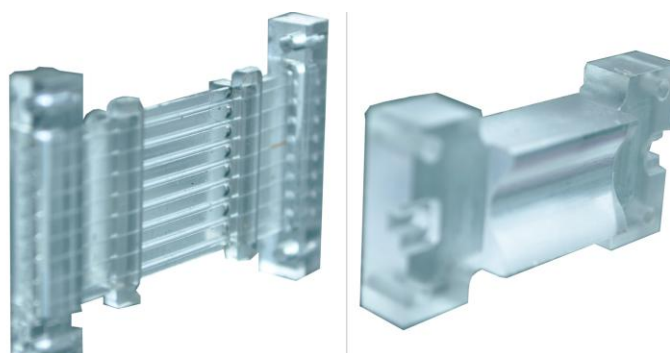


**Figure 3.4: A pumping inlay with 8 integrated channels made of PDMS (left panel) and a rotor bed made of 10 mm thick PC.**

When the three components of a micropump are screwed together (Figure 3.5), the channels of the inlay are compressed against the rotor bed during the rotations of the multi-roller. The combined rotation of the multi-roller and compression of the PDMS channels pushes the liquid in the direction of the rotation.

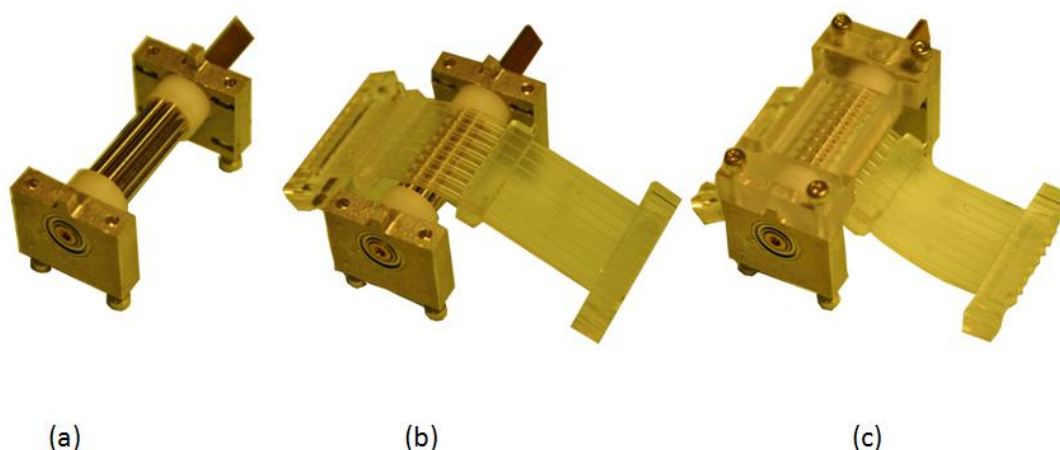


**Figure 3.5: Different steps involved in the assembly of the miniaturized peristaltic pump module: (a) an assembled multi-roller unit, (b) a PDMS pump inlay placed over the multi-roller, (c) a rotorbed screwed on the multi-roller to create the peristaltic effect on the pump inlay.**

### 3.2.2 Miniaturized valves

Fabrication of a number of miniaturized valves are reviewed in [8]. Most of them are fabricated by clean room processes with complex controlling procedures. In this project, a simple, mechanically actuated valve system, capable of controlling reagent flow in 8 channels independently, is used. Originally, a prototype of this valving approach was designed by the FAST group [79]. In a similar manner as described above in the case of the miniaturized peristaltic pump, the valve module consists of three components: i) a valve inlay made of PDMS, ii) two blocks of rigid supports, and iii) a brass shaft stacked with eight asymmetric discs made of PMMA. Each of the discs has a semi-circular recess on the edge. Figure 3.6 shows a schematic cross-sectional view of the valve.

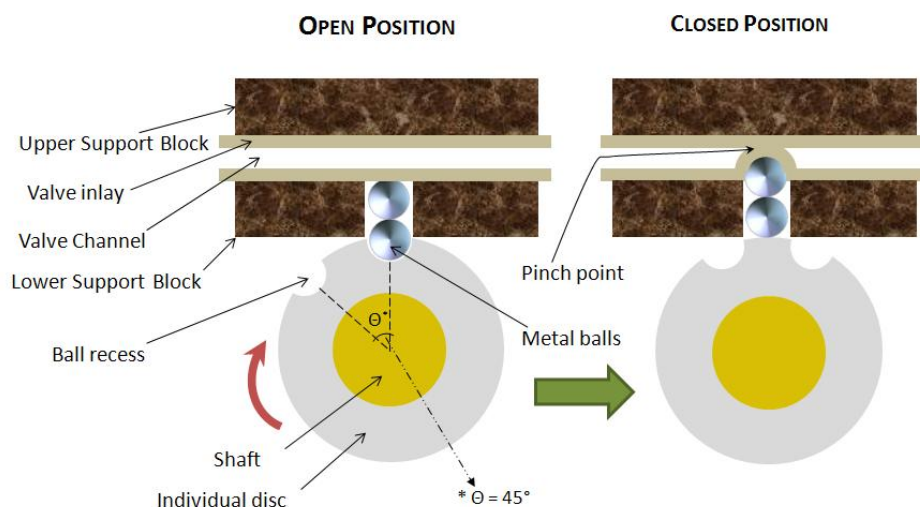


**Figure 3.6: A schematic cross-sectional view of the valve [79].**

The valve inlay is sandwiched between the two blocks of solid support (Figure 3.7). Two 1/16 inch stainless-steel balls (VBX Bearings, Anaheim, California) move up and down freely inside the slightly oversized holes drilled in the lower support block. 8 channels of the inlay, 8 holes in the lower support block and 8 discs on the brass shaft are aligned and screwed together in such a way that when the shaft rotates and consequently the discs rotate, the steel balls are either elevated (towards the edges of the discs) or recessed (into the semi-circular recessions). When elevated, the steel ball presses the inlay channel against the upper support block closing the channel. The angle of rotation of the shaft with respect to the position of recess on the disc determines which channels are opened or closed. The  $\mu$ FIA-based device designed for this project uses two such valve modules (Valve 1 and Valve 2). In Valve 1, each disc has a recess on its edge and the discs are separated by an angle of 45 degrees when stacked on the shaft. This means that one complete rotation of the shaft in steps of 45 degrees successively opens and closes each of the eight channels, provided the rotation starts at a position where channel 1 is opened. In Valve 2, only two channels are active and the recesses of the discs corresponding to these channels are aligned on the shaft by an angle separation of 45 degrees. It is also possible to close one channel independently, i.e., without opening any other channel by turning the shaft half-way (less than 45 degrees). This facilitates the possibility of having stop-flow in the system whenever needed, e.g., during incubation of antibody or substrate. Unlike in the pump inlay, the channels of the valve inlay are not elevated from the monolithic

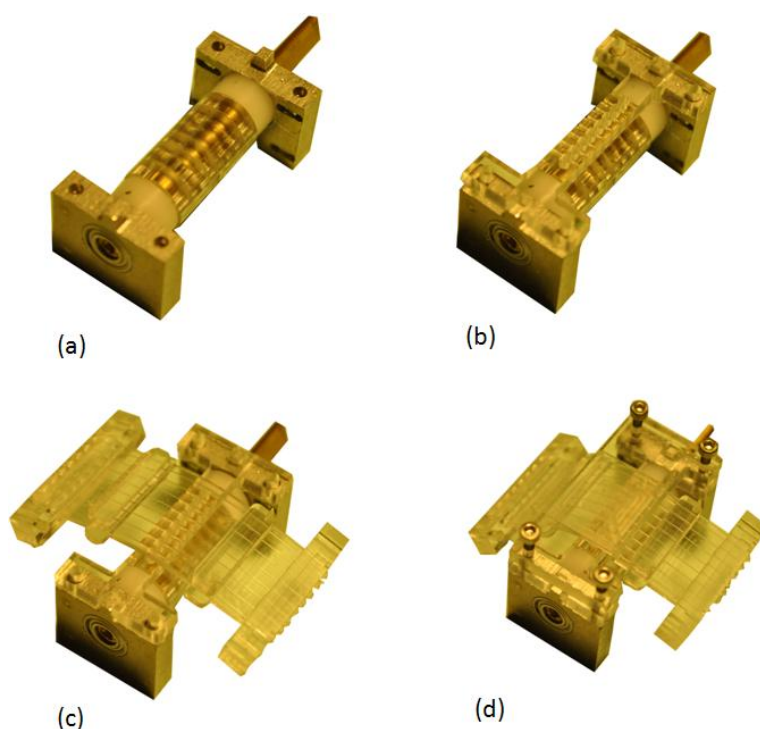


**Figure 3.7: Different steps of the valve assembly: (a) a shaft with eight PMMA discs assembled with ball bearings, (b) a lower rigid support with holes to bear steel balls placed over the discs, (c) a PDMS inlay placed over the balls, (d) a complete valve assembly including an upper rigid PMMA support.**

PDMS inlay-plane. This facilitates an easy closing of the channels by the steel balls (when pressed against the rigid support).

### 3.2.3 Immunochip

The most important module of this immunosensor is the immunochip in which the immunosurface is created by immobilizing BAM hapten. After considering factors including fabrication simplicity and dead-volume minimization, a simple microchannel of dimensions 150 mm x 0.5 mm x 0.4 mm (L x W x D) with a volume capacity of 30  $\mu$ L was micromilled on a 3 mm thick PMMA substrate. This channel plate is bonded to a 1.5 mm thick lid made of PMMA with inlet and outlet holes in a pattern that complements the channel plate. Figure 3.8 shows a bonded immunochip. Seven of eight inlets are interconnected to the immunochannel for the sequential loading of different reagents which is controlled by Valve 1. The eighth inlet allows a channel of the same width and depth as the immunochannel to keep an independent and continuous flow of base-line buffer to the detection module. Switching between



two of the three active outlets of the immunochip is controlled by Valve 2 to direct the flow from the immunochannel to either waste or the detector. The third active outlet leads the base-line buffer flow to the detector.

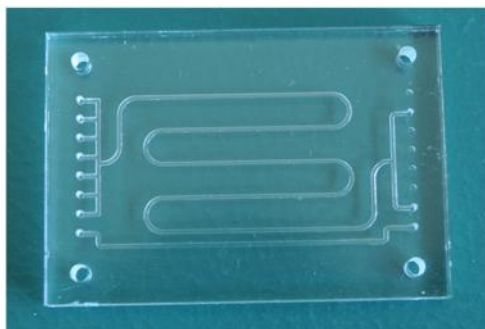


**Figure 3.8: A bonded immunochip.**

### **3.2.4 Electrochemical detection module**

The electrochemical detection module consists of a mixing chip and a leak-proof chamber for the electrode. The electrode has integrated terminals for easy connection to the potentiostat. The reagent (reactive substrate) to be detected is mixed with the baseline buffer (flowing to the detector) in the mixing chip.

#### **3.2.4.a) Mixing chip**

The mixing chip, fabricated in the same way as the immunochip, has a different channel shape (shown in Figure 3.9). The flow from the immunochip enters into the mixing chip at three active inlets of the mixing chip which is regulated by Valve 2. The undisturbed baseline buffer flow enters into one of these inlets and continues to the detector. One of the other two inlets takes the flow to the waste channel if the immunochannel of the immunochip is opened to it by Valve 2. Otherwise, the third active inlet receives the flow from the immunochannel to be mixed with the baseline buffer channel to flow to the detector for signal recording. After the detection this fluid is taken to the second waste channel.

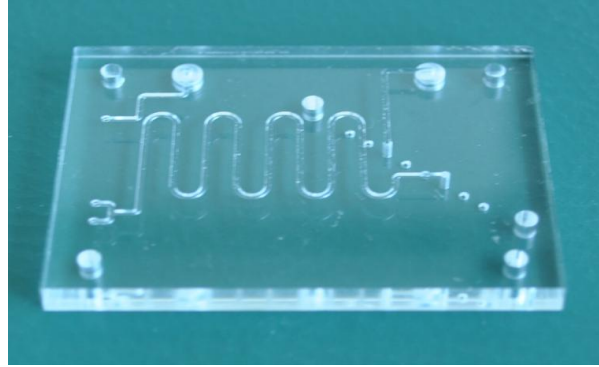


Figure 3.9: A bonded mixing chip.

#### 3.2.4.b) Electrode chamber

The various parts of the electrode chamber are shown in Figure 3.11. The electrode chamber is fabricated as two pieces (upper and lower) in order to accommodate a commercially available Screen Printed Carbon Electrode (SPCE) from Dropsens, (Llanera, Spain). A schematic view of the electrode is shown in Figure 3.10. A carbon working electrode (circular, 4mm in diameter), carbon counter electrode and silver/silver chloride reference electrode are screen printed on a ceramic substrate of dimensions 34 mm x 1 mm x 0.5 mm (L x W x T) with proper insulation layers between the leads. Carbon leads are guided to one of the edges providing three contact pads for external connections.

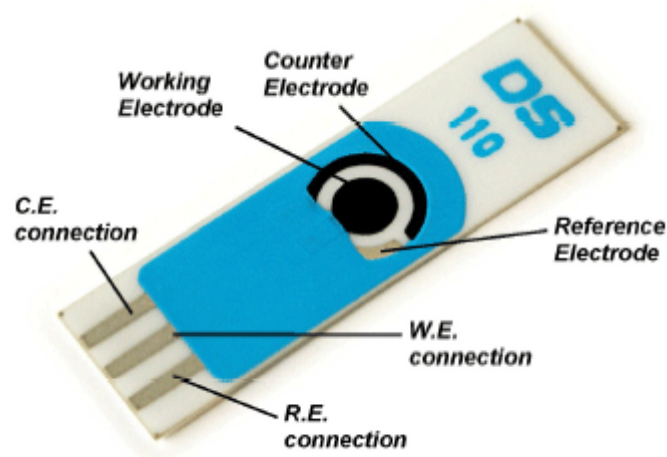
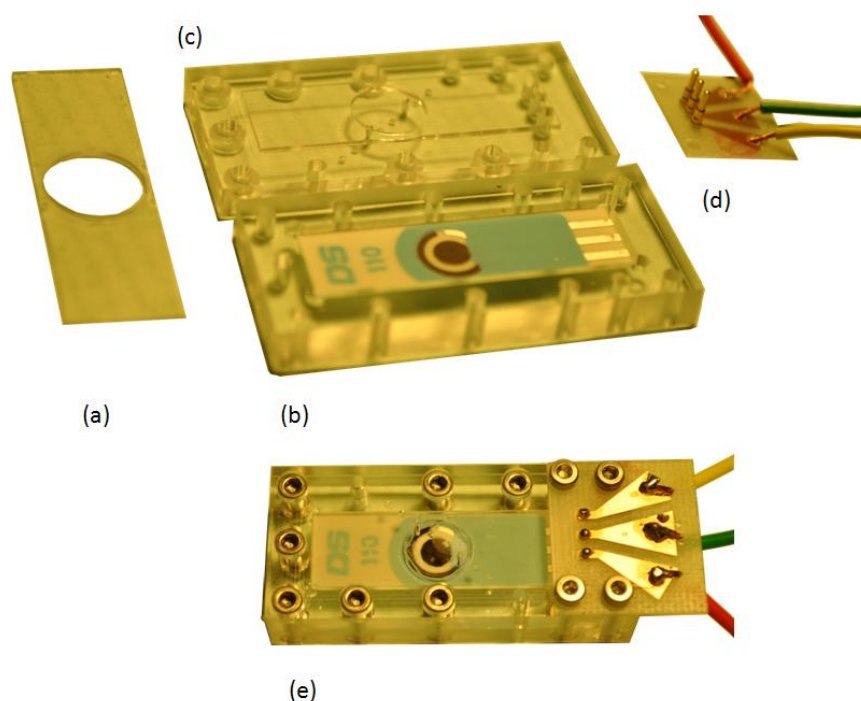


Figure 3.10: Screen Printed Electrode from Dropsens [80].

The lower half of the electrode chamber, fabricated of a 5 mm thick PMMA substrate is used to place the above described 0.5 mm thick SPCE in a 1.5 mm deep rectangular 'pocket'. The upper part has a 0.7 mm high counter-projection with a 0.8 mm deep circular chamber with 8.5-mm radius as shown in figure 1.8. When pressing the upper part against the lower part a space is provided for the 0.5 mm thick electrode and a 0.5 mm thick gasket (made of PDMS) on top of the electrode to ensure that this assembly is completely leak-proof. The gasket has a hole with 8.5 mm diameter aligned over the circular chamber. The circular chamber of the upper part with a volume capacity of 45  $\mu\text{L}$  serves as the actual detection chamber covering the circular area spanned by the working, counter and reference electrode of the SPCE. The upper surface of the upper half has the provision to connect the mixing chip with the electrochemical detection chamber using a specially designed double-sided interconnection block. The interconnection block has eight channels to link the mixing chamber to the detection chamber. Of these channels only two are active. One of these is an inlet to the detection chamber and the other acts as an outlet from the detection chamber to the waste channel through the mixing chip. Two diametrically opposite channels are activated for this purpose in order to minimize the presence of air bubbles. The upper half also has three holes (2 mm in diameter), which are aligned with the three contact pads of the electrode. Three spring-loaded contacts are soldered onto a Printed Circuit Board (PCB) as shown in Figure 3.8(d). The PCB is then screwed on top of the electrode chamber so that the contacts are inserted into the three holes in the upper half spanning through it to provide a connection with the electrode contact pads.



**Figure 3.11:** The components of the electrochemical detection chamber: (a) a PDMS gasket used to tighten the two halves together, (b) a lower half with a SPCE in a 1.5 mm deep pocket, (c) an upper half with a 0.7 mm deep counter protrusion and a 0.8 mm deep circular well, (d) a PCB with soldered spring loaded contact pins, and (e) an assembled electrochemical detection chamber.

### 3.2.5 Reservoir modules

The reservoir module consists of two parts. The upper part is made of 10 mm thick PC and has eight elliptical holes (each having 3 ml volume capacity when closed). The lower part is essentially a microfluidic chip (shown in Figure 3.12) made of a channel plate bonded with a lid (both are made of 2 mm thick PMMA). The channel plate has eight individual channels of width 0.5 mm and depth 0.4 mm. They are micromilled as shown in Figure 3.12. The upper part is screwed onto the chip. In order to make the reservoir leak-proof, a PDMS gasket is inserted between the two parts. The upper surface of the lid has elliptical grooves to accommodate the PDMS gasket. These grooves and the gasket are of the same shape as the elliptical holes of the upper part. The channels in the channel plate are micromilled in such a manner that when the upper and lower parts are screwed together, each channel originates from the centre of an elliptical reservoir. All of the eight channels end at a specific eight-hole interconnection junction where the pump inlay of the miniaturized peristaltic pump is connected.

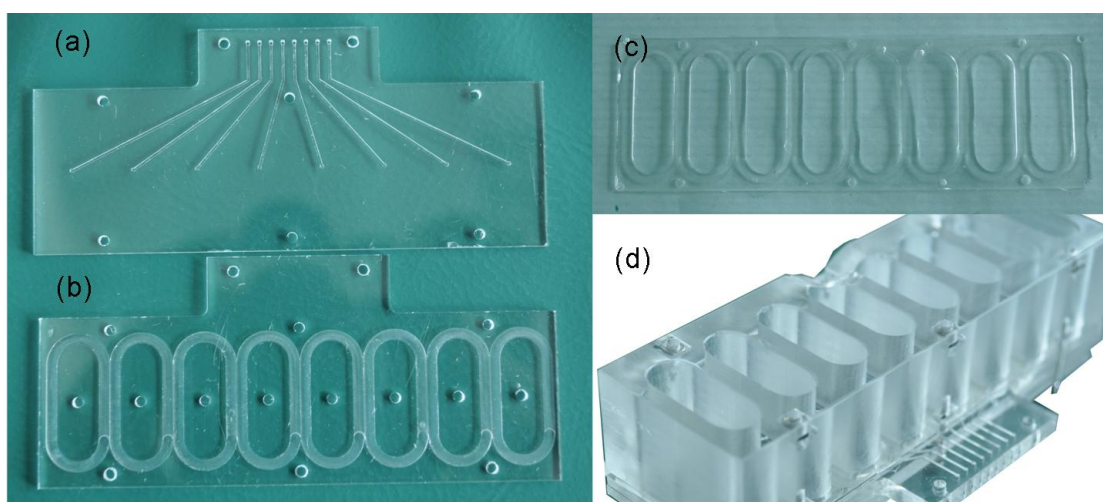


**Figure 3.12: Components of a reservoir module: (a) a channel plate of the lower part, (b) a lid of the channel plate with grooves to hold a PDMS gasket and the upper part, (c) a PDMS gasket, and (d) an upper part of a reservoir.**

### 3.2.6 Interconnection

The overall functioning of the microfluidic device described in this work was achieved by properly interconnecting the different modules that are intended for different functions and connecting the device with the external world. The fabrication of reusable, aligned, planar interconnections with minimal dead volumes and their characterization are well described by FAST group [78, 81]. An adaptation of the concept was used in this project to design and fabricate the necessary interconnections. The feature that has been instrumental for the development of all interconnections, starting at the reservoir outlet and leading to the inlet of the electrochemical detector, is the basic Ball Joint Interconnection Block (BJIB) described in [81]. A BJIB is implemented at both ends of the pump and valve inlays as shown in Figure 3.13. As is shown in the figure, at both ends of the inlays, there are eight PDMS ball joint features corresponding to eight embedded channels. They are housed in shell-like structures made of PMMA for stability and for easy attachment to any planar surface with a complementary feature of eight holes having the diameter of 0.8 mm (separated by a distance of 2.25 mm from centre to centre) which is flanked by two 2-mm holes (with a distance 25 mm from centre to centre). A closer look at the BJIB (Figure 3.13) used in this project reveals that it consists of a semi-spherical (dome like) structure with a projection of 0.5 mm from a cylindrical portion having an outer diameter of 1 mm and height of 0.5 mm. The dome like structure can perfectly

fit into a 0.8 mm hole on any planar surface and the cylindrical portion acts as an O ring made of PDMS. This plug-and-socket combination of BJIBs present at each end of an inlay and the characteristic planar 8-hole pattern available at the interconnection region makes the integration of different modules easy, tight and leak-proof.

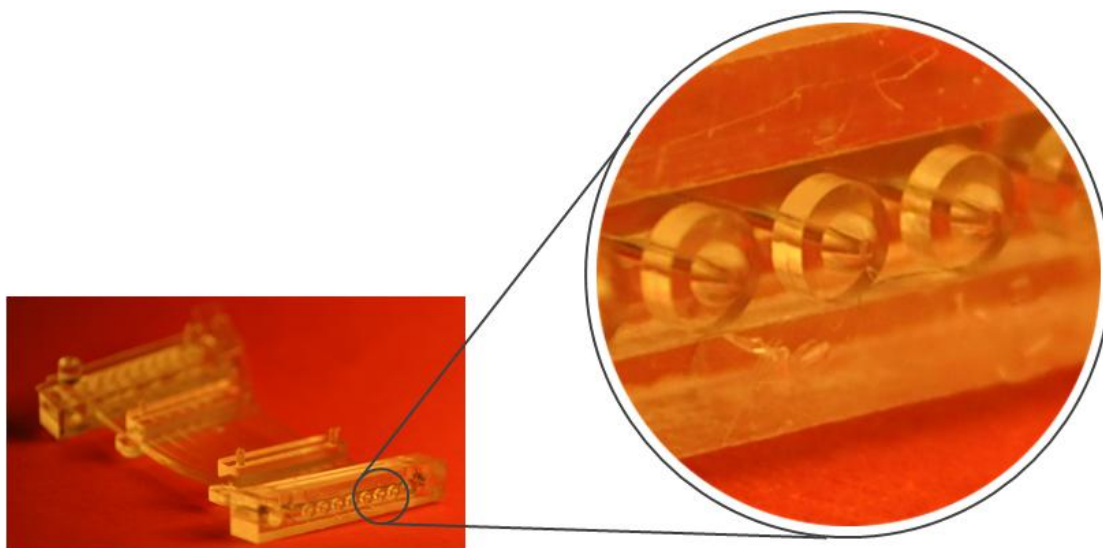


**Figure 3.13: A view of a Ball Joint Interconnection Block (BJIB) characteristic of fabricated PDMS inlays. A magnified image of the BJIB showing the dome like structures, the O rings, and the channels.**

The characteristic planar eight-hole interconnection feature is present as the outlet of the reservoir chip, inlet and outlet of both the immuno chip and mixing chip as well as inlet of the electrode chamber. The pump inlay is connected to the outlet of reservoir chip. The other end is joined to the inlay of Valve 1 with a 2 mm thick interconnection block (PMMA) having the 8-hole interconnection feature on both sides and eight integrated channels of 0.8 mm in diameter. The immuno chip is connected between the outlet of Valve 1 inlay and inlet of Valve 2 inlays. The outlet of Valve 2 inlay is joined to the inlet of the mixing chip. The outlet of the mixing chip and inlet of the electrode chamber are connected with a 3 mm thick PMMA shell with BJIBs (as PDMS inserts) on both sides with eight integrated channels of 240  $\mu\text{m}$  in diameter. The waste channels on the mixing chip are connected to the outer world by press-fit type connections [82], which are made by inserting an oversized element into an undersized recess. In this case, the waste channels end in the middle of circular well-like structures of 3 mm in diameter. A small piece of flexible silicone tube with 3-mm outer diameter is inserted into this hole. By pushing a tube whose diameter is

bigger than the inner diameter of the silicone tube (1 mm), the connection can be made tight and leak-proof. The entire  $\mu$ FIA-based ABIS prototype is shown in Figure 3.14.

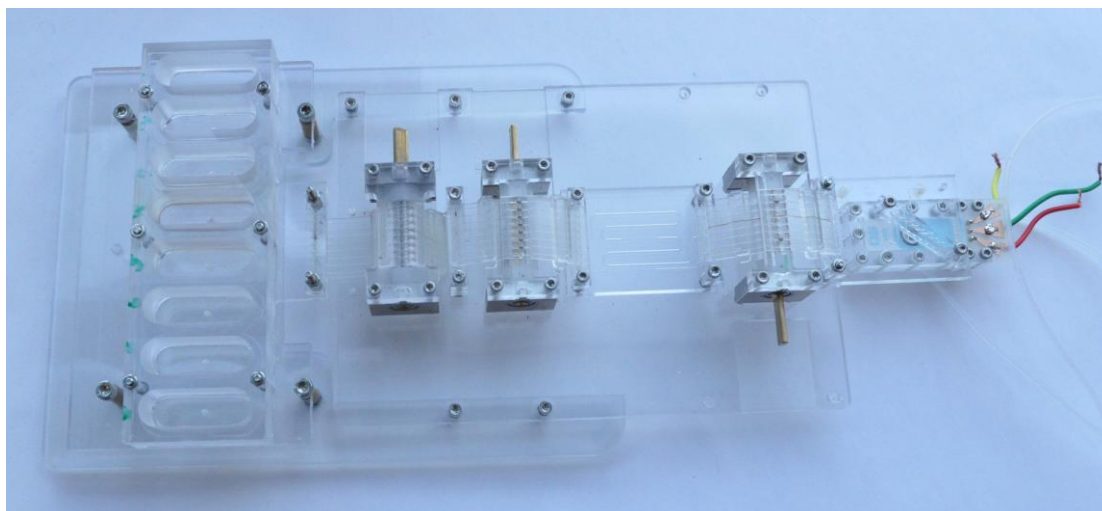


**Figure 3.14: The completely integrated microfluidic system developed for Amperometric BAM Immunosensor (ABIS) prototype.**

### **3.3. Experimental**

Since the above described microfluidic system is a customized version (for immunoassay applications) of the one described by the FAST group, experiments regarding leak pressure testing of the ball joint interconnection blocks [81], flow pattern of the miniaturized peristaltic pump [77] and validation of the miniaturized valve for mixing and routing [79] were not repeated. However, the pumping capacity and essentially the flow rate can be different for different pumps. Slight variations that may happen in the fabrications of the rotor bed and pump inlay or alignment of the three components while screwing them together can affect the flow performance. Flow rate characterization of the miniaturized peristaltic pump that has been used to construct the ABIS prototype was therefore performed.

After integrating the different modules, except the detection chamber, onto a base plate, flow rate of each channel was estimated. The LEGO<sup>®</sup> servo motor that drives the pump was run for five minutes at four different speeds expressed in % power (40%, 50%, 60% and 75%). Each channel originating from an individual reservoir

was connected to the rest of the system one by one with the help of Valve 1. The outlet of the immunochip was opened to the waste channel of the mixing chip so that milli Q water flowing out of the system was collected in previously weighed Eppendorf tubes. Flow rate was calculated in  $\mu\text{L min}^{-1}$  for each channel at different speeds by measuring the final weight of each Eppendorf tube with collected water. The flow rate determination of each channel was made with three repetitions.

Experiments to assess and confirm the overall functionality of the fluidic system, especially the performance of the valves and the detection unit are described in the next chapter.

### **3.4. Results and discussions**

With the aim of combining the BAM immunoassay with electrochemical detection, a microfluidic system as the platform was successfully developed. The modular approach adopted for the purpose yielded many advantages to the system. In this approach, the successful modules can perform distinct operations to accomplish desired functions and they contain everything necessary to accomplish this. Each module is composed of smaller structural units. This brings about fabrication simplicity into a level of making 3-dimensional structures even from 2-dimensional drawings. Another advantage of this approach is the interchangeability of the different modules. The array order of the different modules is easily interchangeable depending on the intended application of the final microfluidic system. In other words, the same modules can be used to construct different systems for different applications. By keeping common features for interconnections on each module, easy integration is possible between different modules and assembly of the modules onto the base plate. In the system described here, holes for screws and nuts of 2 mm in diameter make the integration simple and easy. Issues regarding PDMS inlay changes, removing air-bubbles from the detection chamber, exchange of immunochips with different surfaces, replacement of electrodes etc. are dealt quite easily in such systems to ensure high level of maintainability. This requires disassembling and reassembling of the concerned module by merely dealing with a few screws and nuts.

Choosing PMMA and PDMS as primary substrates for microfabrication of the ABIS prototype benefited in many ways. In addition to the well known qualities of these



materials, such as low cost, possibilities of outside clean room fabrication, fast prototyping [83], making patterns on PMMA by a direct writing technique, such as CNC micromilling, was readily accessible in-house. Bonding of PMMA pieces together to make well sealed microfluidic chips by thermal bonding was comparatively easier. A prior UV treatment clearly helped to perform the bonding at a temperature lower than  $T_g$  of PMMA (100 – 122 °C) [70] which in turn helped to reduce the risk of channel deformation. Above all, the various aqueous solutions used in BAM immunoassay are highly suitable when using PMMA, which would not be the case when using organic solvents. PMMA shows better flexibility towards the chosen fabrication technique, micromilling than PC especially in the fabrication of microchannels. And also UV assisted thermal bonding was easier for PMMA materials than for PC. Another favorable factor to be considered is the feasibility of transferring the BAM hapten immobilization procedure from ELISA plates (polystyrene) to PMMA based microchannels. Since the immobilization process involves a UV activated covalent bond formation, PMMA is considered to be a better substrate to fabricate the immunochip than PC (PC is known for its ability for blocking UV radiations). While considering the other utilized polymer substrate, PDMS, it is obvious that the system under study would not have been possible without the PDMS inlays used in micropumps and valves. PDMS is well known for its elasticity [84] which has been instrumental for its suitability in the miniaturized peristaltic pump and valves used in this project. Another significant property of PDMS is its ability to generate tight seals to flat surfaces while compressing (ability to function like O rings). The PDMS ball joint features available at the ends of the inlays thus make the interconnections of various modules possible. PDMS layers are also used as gaskets to keep the reservoir module and the electrode chamber leak-proof. However, PDMS adsorbs protein molecules and results nonspecific binding of biomolecules (the antibody, HYB 273 in this case) due its hydrophobicity which is considered as one of the drawbacks of the material [85]. The use of a detergent, Tween<sup>®</sup> 20 in the assay buffer reduces this effect significantly in the case of ABIS.

Once assembled, preliminary attempts to test the function of the miniaturized pump and valves, using the above mentioned PDMS inlays, gave a desired performance. The function of the pump and valves were significantly influenced by the alignment characteristics of the essential three components – the rigid support, PDMS inlay and

multi-roller/disc-shaft. Extra care was taken to ensure that all the eight channels of the pump inlay were closed at the point of contact while it was squeezed against the rigid support by the multi-roller. This is essential for the proper peristaltic pumping operation. In the case of the valves, the extent of the inlay-squeezing was controlled by the upper rigid support. In this case, when each of the stainless steel balls is elevated on the underlying disc edge, each of the corresponding channels has to be closed completely. The main areas of concern regarding these assemblies lie in the PDMS inlays fabrication. The inlays themselves are highly vulnerable to be torn while mounting them on the corresponding assembly unit, if necessary care has not been taken. The insertion of optical fibres (diameter 240  $\mu\text{m}$ ) into the holes (diameter 250  $\mu\text{m}$ ) present in the PMMA mould and successful removal of the fibres after curing of the PDMS inlays (channel creation) are long and tedious processes. Trapped air bubbles in the PDMS solution during injection and curing may destroy the channels and affect the mechanical stability of the inlay as a whole. This can be avoided to some extent by degassing the PDMS solution in a vacuumed desiccator before injecting it into the mould and providing extra holes in the mould lid through which the air bubbles can escape. Mechanical properties of the PDMS inlays were found to be substantially better with fewer chances of embedded air bubbles when they were cured at room temperature. This slow curing facilitates more effective transport of air bubbles toward the holes in the mould lid and further out of the mould.

The most important feature of the microfluidic system developed during this project is its ability to function as a Flow Injection Analysis (FIA) system. FIA is based on the injection of a liquid sample into a moving continuous carrier stream of a suitable liquid. The injected sample forms a zone which is then transported to a detector that records signals continuously [86]. A close look at the design of the immunochip (Figure 3.8) and its function along with the mixing chip reveals the built-in FIA system in a microfluidic environment. The immunochannel itself behaves as the loop of this FIA system. The bypassed baseline buffer provides the background signal as it flows to the detector continuously. As shown in the schematic diagram of the microfluidic system with built-in FIA function (Figure 3.15), Valve 2 controls the injection of reacted substrate into the baseline buffer by a carrier stream which is the same as the baseline buffer, but originates from a different reservoir in this design. Diffusive mixing of the reacted substrate plug is facilitated by the narrow mixing channel. The

channel is made long enough to ensure the complete mixing of the two solutions which flow through it. Unlike the conventional FIA system, the  $\mu$ FIA of ABIS has a separate baseline buffer flow to record the background signal prior to the injection of the reactive sample plug from the loop by the carrier stream. This introduces a dilution factor in the detected signal. However, the obtained output signal depends on the concentration of the electroactive substance in the loop. Another advantage of the design is that the employed reagents and washing solutions as part of the immunoassay are bypassed to the waste using  $V_{21}$  (Figure 3.15). This keeps the electrode surface clean and thereby eliminating the effect of electrode fouling on the recorded signal.

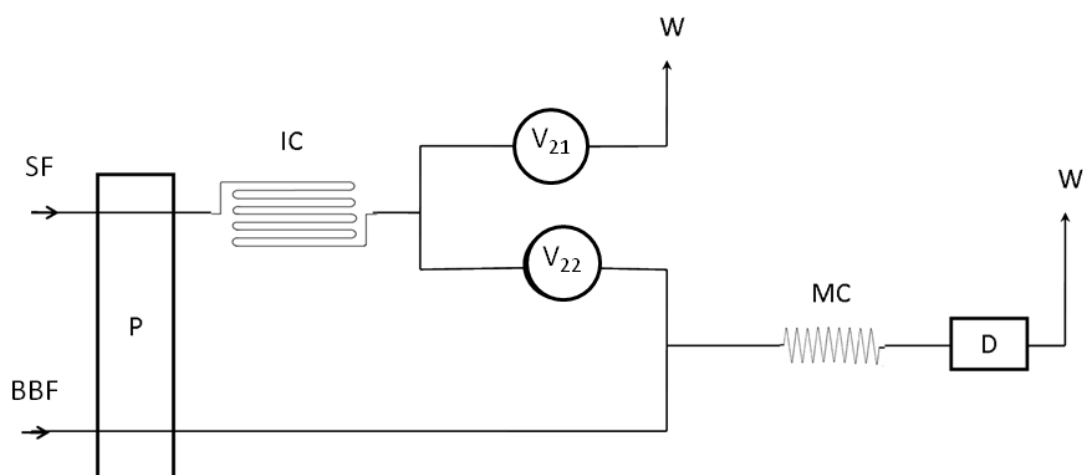


**Figure 3.15: A schematic diagram of the built-in flow injection manifold used for the ABIS prototype. (SF-substrate flow, BBF-baseline buffer flow, P-miniaturized peristaltic pump, IC-immunochannel, V1,V2-valves, MC-mixing channel, D-detector chamber, W-waste).**

The electrochemical detection unit developed for the ABIS prototype in this project is very simple, compact, leak-proof and uses inexpensive Screen Printed Carbon Electrodes (SPCEs). As mentioned before, the sequentially added fluids into the immunochannel are completely bypassed to the waste by Valve 2 with respect to the electrode chamber. This enhances the electrode surface life-time and protects it against fouling. A complete encapsulation of the SPCE is achieved by constructing the chamber as two halves. The PDMS gasket inserted between the two halves ensures a tightly closed chamber when they are screwed together. The PCB with spring-loaded contacts gives better performance than the commercially available cable

connector when connected to the potentiostat. However, the circular electrochemical chamber micromilled into the lower surface of the upper half is susceptible to air bubbles originating from the flow of the baseline buffer. The inlet and outlet of the electrochemical chamber are kept as far apart as possible. This is to reduce the occurrence of bubbles by basing the electrochemical chamber on a wall-jet design so that the entire volume containing the analyte easily fills the whole chamber.

Another important feature to be mentioned in this discussion is the characteristics of the interconnections between the individual modules. The BJIBs available at the ends of the inlays and the complementary planar eight-hole structure present on the various chips facilitate a ‘plug-and-socket’ like alignment while screwing them together. Thus the interconnections are very effective and stable since no external tubing is required at any interconnection junction. This helps to reduce the flow resistance of the entire system to a great extent. Special connectors having BJIBs on both sides of 2 mm thick planar blocks are used to connect two planar surfaces with the complementary 8-hole structure (eg. mixing chip and detection chamber). Figure 3.16 illustrates this design.

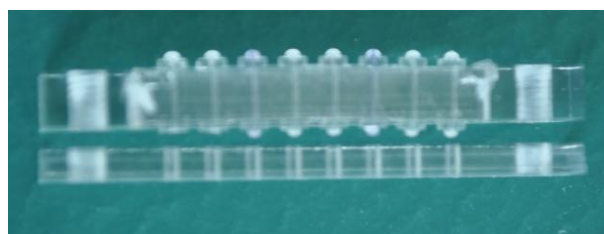


**Figure 3.16: The specially designed two mm thick connection blocks with BJIBs on both sides used to connect the mixing chip with the detection unit.**

Figure 3.17 shows the results of pump calibration. The ordinates are the mean value of flow rates (each obtained as average of three runs for a channel) of eight channels for corresponding motor powers. The error bars indicate the standard error of mean (SEM). The line plot is a linear fit of the means. From the figure it can be observed that the flow rate of the channels increases linearly with the applied power to the LEGO servomotor. Since the error bars (SEM measures) for greater pump power are

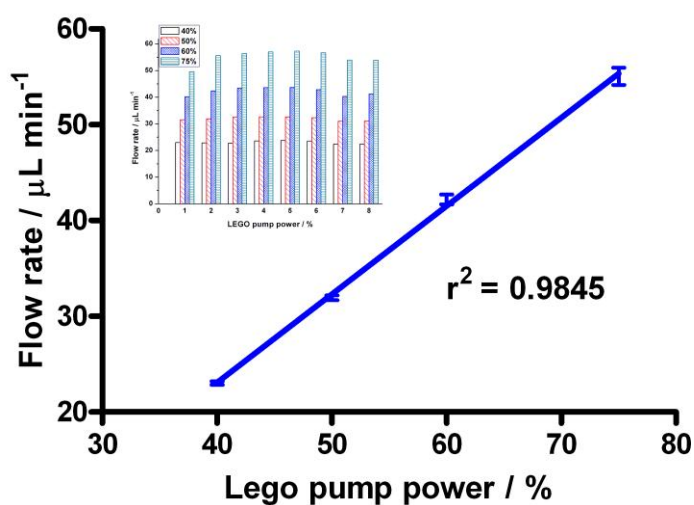


Figure 3.17: Pump calibration: Flow rate dependence on the applied power to the LEGO servomotor.

bigger, it can be inferred that disparity in flow rates is slightly higher at higher applied power. The flow rate tends to deviate from linearity below a certain pump power. The insert shows the behaviour of each channel separately at different applied power. Ideally, all the channels are expected to behave in the same manner at a particular level of motor speed. However, as the bar diagram shows the middle channels are more consistent in this regard compared to the channels at the sides of the PDMS inlays. In this project, the speed of the LEGO motor was set to be at 50%, at which the channels showed a flow rate of  $31.06 (+/-0.24) \mu\text{L min}^{-1}$ . At this speed the pump inlay also showed better durability. This also simplified the automation protocol given that the volume capacity of the immunochannel is approximately  $30 \mu\text{L}$ .

### 3.5. Conclusion

Development and fabrication of a  $\mu$ FIA-based microfluidic device is achieved to integrate the affinity reaction (bio-sensing event) and electrochemical reaction (detection of the bio-sensing event) as an important step in developing an in-line electrochemical BAM immunosensor prototype. The adopted strategy consists of both top-down (micromilling) and bottom-up (assembling micromilled units into different modules) approaches as a combination. The final 'stand-alone' device is made of a number of modules that perform specified functions. The modular approach makes the system easy-to-construct, easy-to-maintain and easy-to-automate.

The miniaturized pump used for pumping different liquids in the microfluidic device is well calibrated. A flow rate of  $30 \mu\text{L min}^{-1}$  is chosen for the ABIS prototype. By combining the design features of immunochip and mixingchip with the help of miniaturized valves, an in-built micro Flow Injection Analysis ( $\mu$ FIA) system is created and used to transfer effectively the biological sensing event into a physically measurable parameter. Because of the inevitable role of a microfluidic platform for miniaturization and automation of an immunosensor, fabrication of the device described in this chapter is considered as an important milestone in the development of the in-line electrochemical BAM immunosensor prototype - the project goal.



# Characterization of the detection techniques

---

### 4.1. Introduction

While developing an in-line biosensor as a whole, the selection of the detection technique depends on many factors such as cost, miniaturization possibilities, integration simplicity with the sensing element, ease-of-use, portability etc. Above all, it is important to note that while the biorecognition element determines the extent of selectivity and specificity, the sensitivity of the biosensor is greatly influenced by the transducer [87]. Another important factor that determines the applicable method of detection is how easily the sensing event can be translated to a physically detectable signal. It can be any type of optical property change (optical detection), redox process (electrochemical detection), mass induced stress (piezoelectric detection) etc. This chapter describes the two detection techniques, UV-Vis spectrophotometry and amperometry, that are chosen for the BAM immunosensor.

#### 4.1.1 UV-Vis spectrophotometry

In biosensors, optical transducers respond to a change in optical properties, such as absorption, reflectance, emission etc. associated with the biological sensing event. Normally, a change in intrinsic optical property of biomolecules involved in the biorecognition is not sensitive enough to be detected and often occurs in the deep UV region [88]. Most commonly, biosensors make use of various optical probes that are covalently labelled to the biomolecules. Enzymes are well known optical markers, since they catalyze reactions with high degree of specificity and the outcome of this reaction involves a colour change. This change can be detected by optical transducers. In this work the BAM immunosensor prototype is developed based on the well established ELISA as described in Chapter 2. During the course of achieving the project goal of developing the electrochemical BAM immunosensor, spectrophotometric detection was adopted for the initial experiments as a bench mark and also for the validation of micropumps and miniaturized valves described in Chapter 3. This was possible due to the fact that the substrate used for HRP is 3,3',5,5'- tetramethylbenzidine (TMB), which is optically as well as electrochemically



detectable [89, 90] in presence of hydrogen peroxide (co-substrate). The oxidised form of TMB has a blue colour and absorbs at 650 nm. Considering the advantages of sensitivity, easy automation with microfluidics, easy handling and cost effectiveness, electrochemical detection was chosen as the detection method for the ABIS prototype.

#### **4.1.2 Electrochemical detection**

For detecting very low amounts of an analyte present in small sample volumes, electrochemical immunoassay is gaining an increased significance as an ideal analytical technique that is simple to perform. The large number of review articles found in literature describing the progress of electrochemical biosensors for pesticide detection [91-98] emphasizes the significance of the detection technique in the research field. Electrochemical equipments are comparatively inexpensive, sensitive, miniaturizable, easy to handle, and provide the possibility to operate in turbid/colored media. Generally, electrochemical measurements can be performed for direct samples (without any sample pre-treatments). It is also well suited to (micro)fluidic systems so that automation is easily implemented. The above mentioned advantages of electrochemical detection were crucial for realizing the goal of this project in developing an automated ABIS prototype. Depending on the techniques applied to measure the electrochemical change associated with the biosensing process, there are three main electrochemical detectors, conductometric, potentiometric and amperometric. Conductometric detectors measure the change in conductance between two electrodes when the biological and associated chemical reaction takes place. Potentiometric detectors measure the change in potential at the working electrode due to accumulation of charge with respect to the reference electrode caused by the antibody-hapten binding at the electrode surface. Amperometric detection is based on measurement of the change in current passing between the working electrode (poised at a particular potential) and auxiliary electrode generated by directly oxidizing or reducing one of the products resulting from the biochemical reaction. The output signals of the amperometric detections have strong dependence on the concentration (linear/ sigmoidal dose-response) of the electroactive substance present in the analysed sample. In this project, oxidised TMB formed by the labelled heterogeneous competitive BAM immunoassay (described in 2.1.1) is measured amperometrically. The amperometric detection technique was chosen to enable the construction of a simple, sensitive, rapid and inexpensive detection unit for the BAM immunosensor.

A typical setup for amperometric analysis consists of a three electrode cell (working electrode, reference electrode and auxiliary electrode), connected to a potentiostat which functions as the voltage source and device for measuring current and voltage. In such a system, the current ( $i$ ) passing through the system between the working electrode and auxiliary electrode as the consequence of the potential ( $E$ ), at which the working electrode is poised, is recorded as a function of time ( $t$ ) to obtain an  $i-t$  curve. In the system developed in this project, the amperometric detection unit is coupled with a microfluidic chip assembly that has an in-built  $\mu$ FIA system. The electroactive substance formed in the loop of this  $\mu$ FIA, as a result of the labelled reaction associated with the biorecognition event is injected in to a baseline buffer flow. This results in change in current that flows between the working electrode and the auxiliary electrode according to the concentration of the electroactive material present in the injected plug. These changes are plotted as amperometric peaks against time (the  $i-t$  curve).

In this study, as mentioned earlier, TMB acts as the reporter molecule of the biosensing event. TMB was introduced as a better chromogen for HRP-based detection systems [99]. Horseradish peroxidase (HRP) conjugated with the antibody (HYB-273) catalyzes the oxidation of TMB in the presence of  $H_2O_2$ . The steady-state concentration of oxidized TMB (which can also be detected spectrophotometrically) is related to the concentration of analyte (in this case, as described in 2.1.1 it is inversionally proportional). Enzymatic oxidation of TMB by HRP/ $H_2O_2$  system in acetate buffer of pH 5 has been thoroughly characterized (spectrometrically) and reported in the literature [89]. The use of TMB as an electrochemically active substrate for HRP/ $H_2O_2$  system has been also reported [90, 100-102].

In this chapter, the spectrophotometric validation of BAM immunoassay in the flow system and the characterization of the electrochemical detection unit are described.

## **4.2. Experimental**

### **4.2.1 Materials and methods**

Potassium chloride, potassium ferricyanide and glycine hydrochloride were purchased from Sigma-Aldrich Corporation (St. Louis, MO, USA). Prestained TMB PLUS substrate used for BAM ELISA was purchased from KEM EN TEC Diagnostics

(Taastrup, Denmark). This is a ready-to-use substrate the components of which are not fully revealed. The same reagent was also used in electrochemical detection due to its better stability compared to the substrate made in-house by mixing TMB and H<sub>2</sub>O<sub>2</sub> (unstable even at 4 °C). The assay buffer used for the BAM immunoassay in the flow system was 0.01 x PBS of pH 7.4 with 0.05% Tween 20 (a detergent). PBS with Tween® 20 (PBST) tablets were from Fluka (Stockholm, Sweden). Dissolving one tablet of PBS with Tween® 20 in 500 mL of milli-Q water yielded 0.01 M PBS containing 0.05% Tween® 20 (containing 0.14 M NaCl and 0.0027 M KCl). The regeneration buffer was prepared by dissolving 1.12g of glycine hydrochloride in 100 mL of Milli-Q water (100 mM) and the pH was adjusted to 2.

UV-Vis spectrophotometric detection was performed by UNICAM Helios Uni-9423 spectrophotometer under 'rate' mode. The rate application is used to record time-dependent changes of the sample absorption at a specific wavelength. Hellma High-Precision flow-through cell made of quartz (type: 178.713-QS) with light path of 10 mm and volume of 8 µL was used as cuvette. This was connected to the outlet of the µFIA-based system (described in the previous chapter). The spectrum was recorded at 650 nm with a data sampling interval of 20 s and analysed by Visionlite software.

Screen Printed Carbon Electrode (SPCE) was used in the electrochemical detection unit and was purchased from Dropsens, (Llanera Spain). The electrode system from Dropsens (complete information of the company) comprises a screen printed carbon working electrode (Ø 4mm), carbon counter electrode and Ag/AgCl reference electrode. A CHI1010A potentiostat (CH Instruments, Inc., Austin, TX, USA) was used to perform all electrochemical experiments. The software associated with the instrument was used to record and analyze the data. In order to compare the electrochemical behavior of the ready-to-use commercial TMB substrate and in-house made TMB substrate, cyclic voltametric experiments were performed. For the characterization of the electrodes and detection using the immunosensor, amperometric measurements were conducted.

When the microfluidic assays were performed, the pump and valves were operated using Lego® servomotors under the control of an application program created by the LabView® based Lego® Mindstorms® NXT 2.0 software. In these experiments, BAM

immunoassays were performed in the inhibition format with zero BAM in the analyte sample in order to explore the possibility of maximum signal.

Mettler Toledo SevenEasy pH meter S 20, a product from Switzerland was used to measure pH of the different solutions.

## 4.2.2 Experiments

### 4.2.2.a) Spectrophotometric detection using BAM immunosensor prototype

After fabrication of the  $\mu$ FIA-based system comprising the miniaturized pump and valves, spectrophotometric detection was utilized to test the function of the BAM immunoassay under flow conditions. The format of the assay was similar to the one optimized for plate-based ELISA. The only difference was related to the incubation time. The optimized protocol using spectrophotometric detection was then applied to the assay based on electrochemical detection. The protocol adopted for the BAM immunoassay in the flow system was as follows:

1. Immobilization of BAM hapten in the immunochip: The immuno(micro)channel of the immunochip was filled with 30  $\mu$ L of hapt D (described in Chapter 2) which was diluted 10 times with 0.1 x PBS. Both sides of the chip were then irradiated in the UV chamber for 30 min to facilitate the photo-reactive covalent immobilization. After the completed immobilization, the chip was inserted into the microfluidic system.
2. Using Valve 1 and 2, the immunochannel was opened to the waste to allow washing of the unbound hapt D for 5 min with 0.1 x PBST.
3. The immunochannel was filled with HYB-273 solution (dilution: 1000 times with 0.1x PBS containing 0.05% Tween 20).
4. The system was kept under stop-flow in the channel for 15 min to allow complete binding of the antibody to the immobilized hapten.
5. The immunochannel was washed as described in step 2.
6. The immunochannel loop was filled with TMB solution (substrate).

7. The immunochannel was kept under stop-flow for 15 min to allow complete oxidation of the substrate.
8. Push the reacted substrate plug into the flow cell with the carrier stream (0.1x PBS) and run it for 5 min
9. The immunochannel was washed as described in step 2.
10. The immunochannel was filled with Glycine.HCl buffer (100 mM)
11. The immunochannel was kept under stop-flow for 3 min to allow complete removal of the bound antibody.
12. The immunochannel was washed as described in step 2.

Steps 3 to 11 were repeated several times to establish the regeneration capacity of the hapt D immobilized surface. A continuous base line buffer flow was maintained throughout the experiment in a separate channel in the immunochip (shown in Chapter 3). The flow rate of the micropump was adjusted to 30  $\mu\text{L}/\text{min}$  by setting the power of Lego motor at 50%. Valve 1 of the  $\mu\text{FIA}$ -based system was programmed to perform the sequential addition of different liquids from various reservoirs into the immunochannel. Valve 2 was used to control the outlets of the immunochip either directing the flow to waste or the detection cell through the mixing chip.

#### 4.2.2.b) Electrochemical characterization

Characterization of the screen printed carbon electrode (SPCE) and the electrochemical detection unit as well as the performance of the  $\mu\text{FIA}$ -based system (especially the function of valving) were done using the well-known potassium ferricyanide  $\text{K}_3[\text{Fe}(\text{CN})_6]$ . Cyclic voltammograms were obtained by filling the electrode chamber with 2.5 mM solution of  $\text{K}_3[\text{Fe}(\text{CN})_6]$  having 0.1 M KCl as counter electrolyte. The potential sweep was applied from 600 mV to -200 mV at scan rates 25, 50 and 100 mV/s. Using the information obtained from the CVs, an amperometric FIA experiment was performed using 1 mM  $\text{K}_3[\text{Fe}(\text{CN})_6]$  solution containing 0.1 M KCl. The immunochannel was filled with the solution, which was then fed into the detector. This procedure was repeated at five minute intervals. The electrode was poised at -200 mV vs. the built-in Ag/AgCl reference electrode. 0.1 M KCl solution

was fed into the detector chamber through the baseline buffer channel and the immunochannel was emptied each time using the same solution filled in one of the other reservoirs. Effectively the system worked like a Flow Injection Analysis (FIA) system. The reduction current was recorded as a function of time. To calibrate the electrochemical detector unit, the above described amperometric experiment was performed using six different standard solutions (3 mM, 1.5 mM, 0.75 mM, 0.375 mM, 0.1875 mM, 0.09375 mM) of  $K_3[Fe(CN)_6]$  prepared in 0.1 M KCl. 0.1 M KCl was also used as the the electrolyte during recording of the baseline. Reduction of  $K_3[Fe(CN)_6]$  was recorded as a function of time to obtain an  $i-t$  curve. All these experiments were conducted at room temperature.

### 4.3. Results and discussions

#### 4.3.1 Spectrophotometric detection using ABIS prototype

The result obtained from the spectrophotometric experiment is shown in Figure 4.1.

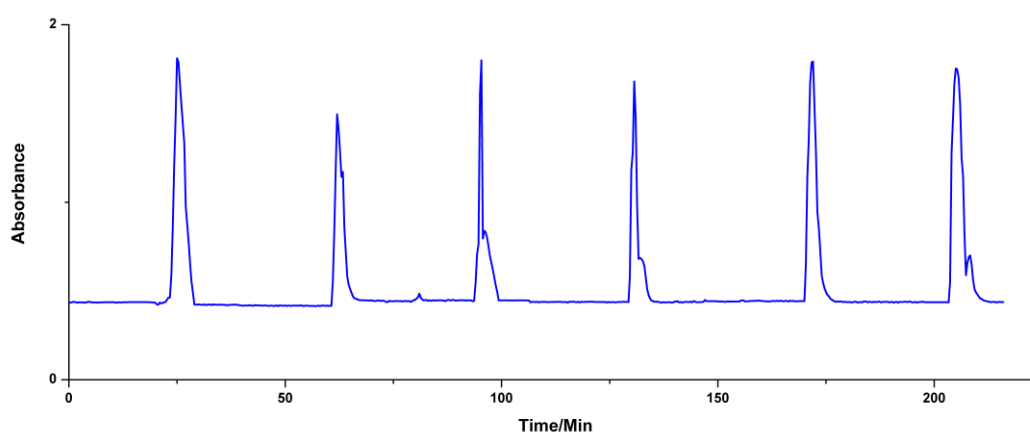


**Figure 4.1: Spectrophotometric BAM immunoassay in the flow system (6 regeneration cycles).**

The absorbance of oxidized TMB substrate at 650 nm is plotted as a function of time. The six peaks represent six identical BAM immunoassays performed in the flow system with a regeneration of the immunosurface between each assay. The injection of the oxidized substrate into the baseline buffer flow at the particular intervals is evident from sudden increase in absorbance. The baseline absorbance is then regained after each detection step. Each recorded absorbance peak has a tail that is characteristic of detection in FIA systems.

The well defined peaks in Figure 4.1 indicate that the BAM immunoassay functions as intended in its inhibition format within the immunochannel made of PMMA. The peaks also confirm that the UV assisted covalent immobilization of BAM haptens onto PMMA functioned successfully. High absorbance values reflect that at zero BAM in solution, the maximum number of binding sites of HYB 273 were available to bind with the surface immobilized BAM hapten (minimum inhibition). HRP conjugated to HYB-273 converts TMB substrate into its oxidized species which has its absorbance maximum at 650 nm. The commercially available ready-to-use TMB substrate solution contains H<sub>2</sub>O<sub>2</sub>. This H<sub>2</sub>O<sub>2</sub> deoxidizes the enzyme in order to maintain a suitable concentration of HRP which is otherwise continuously reduced by TMB, in the enzymatic reaction. Thus it acts as a co-substrate to amplify the signal with respect to the concentration of HYB-273 attached on the immunosurface. According to Josephy *et al.* [89], during incubation the oxidation of TMB takes place in two steps. The first intermediary product appears as blue, while the final product is yellow. Due to the presence of both intermediary and final product, the solution becomes green in the end of the incubation step. Aside from the characteristic tail, a shoulder also appears at the end of each peak. This can be attributed to the color change with time. The shape of the peaks (with a tail and well defined baseline) proves the successful control of the fluidics with the microvalves and thus achieves the function of a microfluidic Flow Injection Analysis (FIA) system. The flow rate (30  $\mu$ L/min) maintained by the micropump (50% power) helped to obtain absorbance of fresh aliquots of oxidized TMB at each data acquisition (conducted at the interval of 20 s) in a flow-through cell of 8  $\mu$ L capacity.

This experiment was performed as a quick validation of the BAM immunoassay in the flow system and the surface regeneration. The repetition of immunoassay in six cycles without any signal drop shows the successful regeneration of the immunosurface after each cycle. The difference in peak areas associated with each cycle is due the insufficient incubation time given for the substrate reaction (15 min). From the curve showing the reaction kinetics of the substrate oxidation (shown in Chapter 2), it is clear that the reaction rate has reached its maximum in 15 min. A small error at this point can make a huge difference in the signal strength, since no stop-reaction method is applied in the  $\mu$ FIA-based experiments.

Though the optical detection is simple and straight forward, the practical difficulties limit it to the level of lab based systems for bench mark analysis. Expensive instrumentation and difficulty to maintain stable optics at a miniaturized level reduce the possibility of having optical detection in an in-line sensor. The optical detection is also prone to problems due to appearance of air bubbles. To overcome the effect of factors, the electrochemical activity of the TMB substrate was crucial in developing the  $\mu$ FIA-based ABIS prototype.

#### **4.3.2 Characterization of the electrochemical detection unit**

The cyclic voltammogram of  $K_3[Fe(CN)_6]$  at the SPCE shown in Figure 4.2 matches with the one published elsewhere [103]. The shape of the cyclic voltammogram is qualitatively similar to what is predicted for a reversible redox couple, such as potassium ferricyanide/ferrocyanide. Since in this experiment, the potential was scanned from the most positive potential toward the most negative potential, ferricyanide was initially reduced to ferrocyanide, which then subsequently was oxidized to ferricyanide during the second half of the cycle. For a reversible process (as in the reduction of ferricyanide), the overall process is governed by the diffusion of the electroactive species to the planar electrode surface and the peak current is proportional to the square root of the scan rate as given by the Randle-Sevcik relationship,



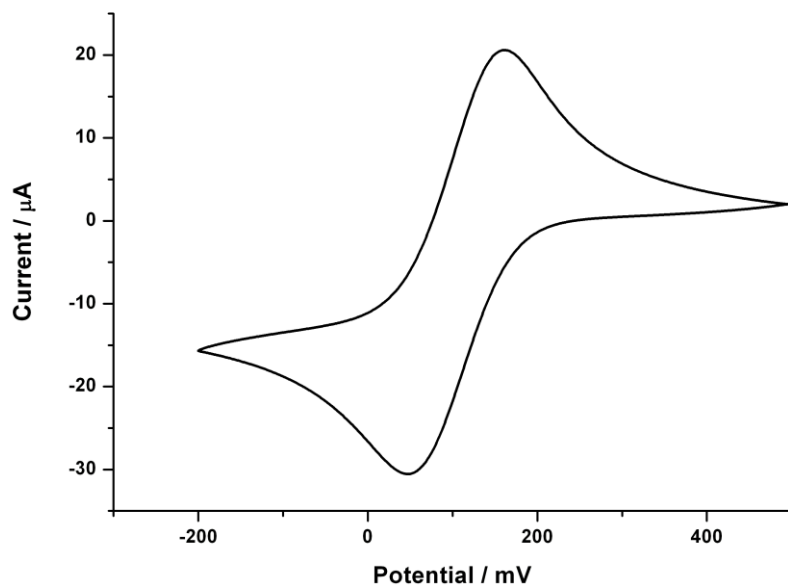


Figure 4.2: Voltammogram of 2.5 mM potassium ferricyanide system.

$$I_p = -k n^{3/2} A D^{1/2} C_O^\infty v^{1/2} \quad (x)$$

where  $k = 2.69 \times 10^5$ ,  $n$  is the number of moles of electrons transferred per mole of electroactive species,  $A$  is the area of electrode in  $\text{cm}^2$ ,  $D$  is the diffusion coefficient in  $\text{cm}^2\text{s}^{-1}$ ,  $C_O^\infty$  is the bulk concentration of the oxidized form of the electroactive species in  $\text{moles L}^{-1}$  and  $v$  is the potential scan rate in  $\text{volts s}^{-1}$ . Figure 4.3 shows a set of cyclic voltammograms obtained for 2.5 mM solution  $\text{K}_3[\text{Fe}(\text{CN})_6]$  over a range of scan rates on the SPCE. In this case, the normal expected behaviour of diffusion controlled reversible reactions, a linear relationship between the peak current and the square root of the scan rate is observed only upto a scanrate of  $100 \text{ mV s}^{-1}$ . Beyond that the system shows deviation from linearity, since SPCE is not the best option for conducting electrochemical reactions of potassium ferro-ferri cyanide systems.

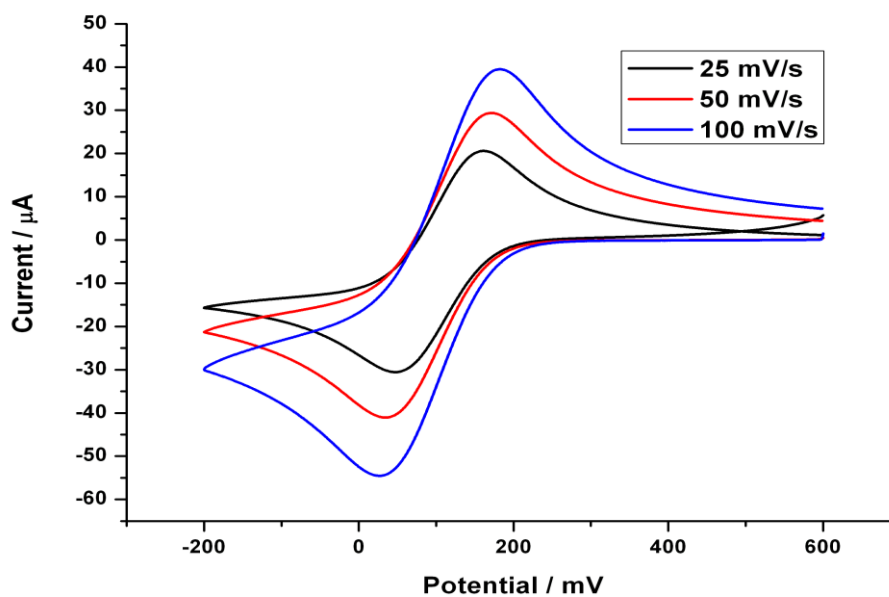


Figure 4.3: Cyclic voltammograms of 2.5 mM  $K_3Fe(CN)_6$  at different scan rates.

In Figure 4.4, the reduction current of  $K_3[Fe(CN)_6]$  is monitored using  $\mu$ FIA with amperometric detection.

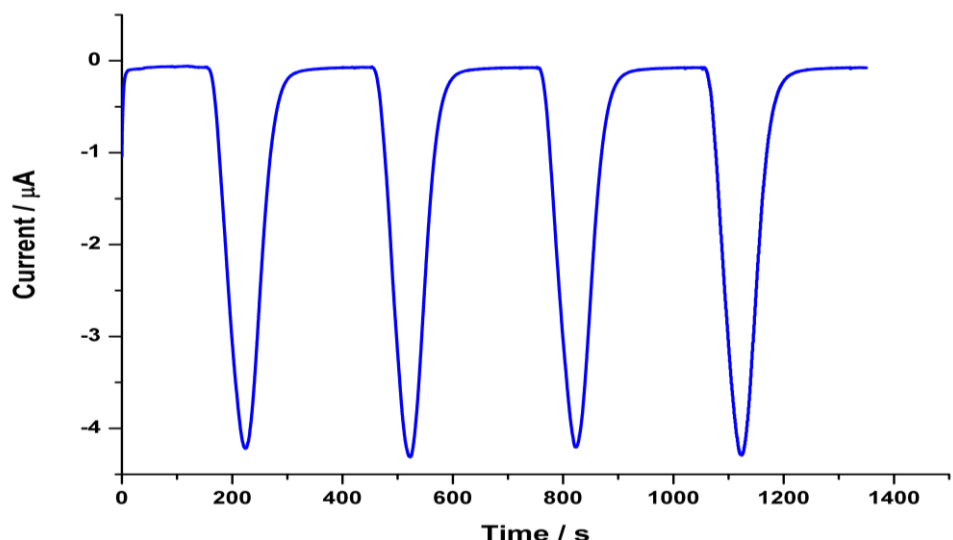


Figure 4.4: FIA amperometry of  $K_3[Fe(CN)_6]$  with the same concentration.

The cyclic voltammograms of  $K_3[Fe(CN)_6]$  shown in Figure 4.3 indicate that -0.2 V vs. the Ag/AgCl reference electrode during the amperometric detection provides a

sufficient over potential to effectively drive the reduction of ferricyanide . The recorded peaks are identical since the electroactive species in the loop has the same concentration during each repetition. In this case, when the immunochannel (the injection loop of the  $\mu$ FIA system) was filled with 2.5 mM  $K_3[Fe(CN)_6]$  solution and eluted to the detector a number of times, identical peaks were obtained with a variation in peak area less that 1%. On the other hand, the peaks shown in Figure 4.5(a) vary with respect to the concentration of  $K_3[Fe(CN)_6]$  solution in the loop, giving rise to a linear relationship between the obtained current and the concentration (Figure 4.5(b)).

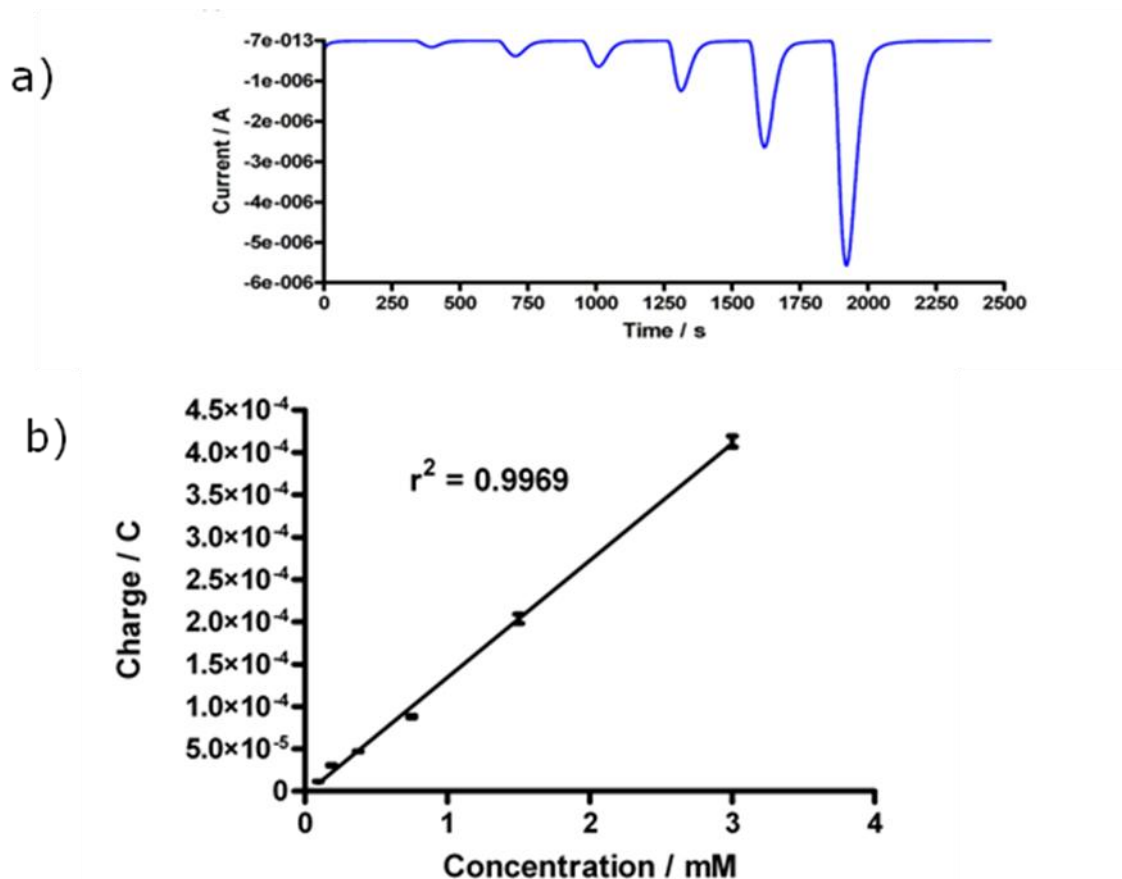


Figure 4.5: Amperometric detection of different  $K_3[Fe(CN)_6]$  concentrations in  $\mu$ FIA: (a) amperometric peaks obtained for different  $K_3[Fe(CN)_6]$  concentrations, (b) a plot of peak current versus concentration.

The well defined peaks of  $K_3[Fe(CN)_6]$  reduction demonstrate the  $\mu$ FIA-based system functions perfectly especially in delivering a constant flow rate and switching between the loading and injection mode using the valves.

In both experiments the area covered by each peak is proportional to the concentration of the electrochemically active substance responsible for the peak. In the ABIS prototype, the electroactive substance is the oxidized TMB substrate. It is reduced on the SPCE if the SPCE is poised at an appropriate potential. The obtained reduction current is proportional to the concentration of oxidized TMB is transported to the electrode surface by the applied flow. This is in return proportional to the amount of bound antibody-hapten conjugate in the immunochannel, which is inversely proportional to the analyte concentration. The CVs obtained for TMB and oxidized TMB (TMB (ox)) are shown in Figure 4.6. The black line represents the CV of the commercial TMB substrate, which contains  $H_2O_2$ . The red line represents the CV of TMB oxidized by 25 nM HRP. The shapes of the voltammograms are consistent with

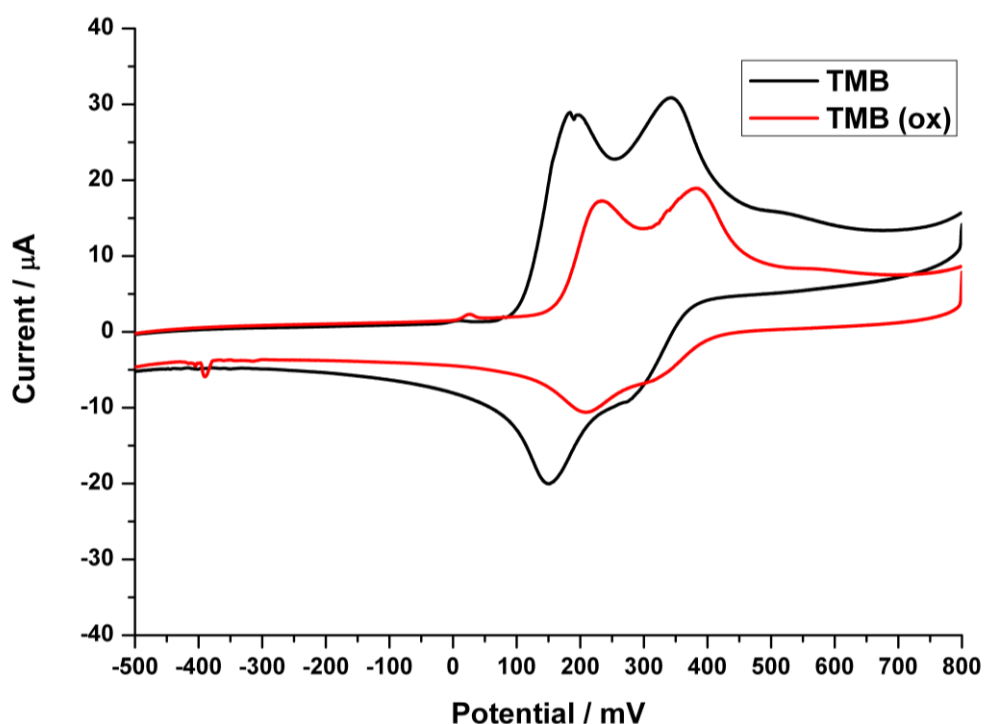


Figure 4.6: Cyclic voltammograms of commercially available TMB substrate and its oxidized form TMB (ox).

those described elsewhere [100, 101].

The peak currents of TMB (ox) are lowered because of the decrease of TMB concentration as the consequence of the enzymatic reaction. In the ABIS prototype, the TMB (ox) is detected without the addition of a stop solution. On the way to the detector, it is mixed with an equal volume of the baseline buffer (0.1x PBS). In this case, the slight deviation of peak positions (compared to the referred works) may be attributed to the absence of stop solution and variation of pH upon mixing with the counter electrolyte (baseline buffer). In this work, a potential of -100 mV against Ag/AgCl was chosen for the amperometric detection of TMB (ox) in the ABIS prototype. The voltammograms support this choice of potential at which the reduction of TMB (ox) is complete without any interference caused by the remaining unoxidized TMB.

#### **4.4. Conclusions**

In order to complete the design of the ABIS prototype, there is a need to identify a suitable detection mechanism. When using TMB as the reporter molecule of the biological sensing event in the BAM immunoassay, it is possible to adopt either an optical or an electrochemical detection technique. The research project described in this thesis focuses on the use of an electrochemical detection system, which is inexpensive, easy to handle, sensitive and suitable for easy miniaturization and automation. However, an optical detection method (as described in this chapter) was used as a bench mark to analyze and evaluate the performance of the microfluidic platform developed for the immunosensor. Quick spectrometric evaluation of the system confirms the successful function of the microfluidic device as an in-built FIA system and also the feasibility of shifting the BAM immunoassay from the plate-based ELISA format to a flow system. The preliminary electrochemical experiments performed using  $K_3Fe(CN)_6$  show that the electrode and the electrochemical detection unit function well. This indicates the possibility of using an electrochemical detection system for the in-line detection favoured by the research objectives of this project.

# Electrochemical BAM immunosensor

---

### 5.1. Introduction

The previous chapters described the different stages involved in the transformation of the conventional ELISA-based BAM immunoassay into an electrochemical BAM immunosensor for continuous in-line detection of BAM in ground water utilizing a modular  $\mu$ -fluidic platform approach. This chapter deals with the evaluation of the completely assembled microfluidics with electrochemical detection of BAM immunochemistry. This is performed by sequential feeding of different reagents required for conducting the BAM immunoassay into the immunochannel of the immunochip. During the electrochemical detection, the system as a whole functions as a microfluidic flow-injection analysis ( $\mu$ FIA) system. The various steps associated with this process are controlled by the miniaturized pump and valves which were automated by programmed LEGO<sup>®</sup> Mindstorms<sup>®</sup> servomotors.

#### 5.1.1 FIA based immunosensing

As a part of setting up new systems based on immunochemistry to monitor the presence of an analyte continuously over a long period of time, the idea of automated immunosensors has emerged. Along with expensive and complex centrifugal analyzers and air-segmented continuous flow systems [104], Flow Injection Immunoanalysis (FIIA) systems are pioneers in this area by joining batch immunoassay principles with simple flow injection methodology described by Ruzicka and Hansen in 1975 [86]. The strength of FIA lies in its ability of making a controlled and reproducible dispersion of a sample zone when it is introduced into an unsegmented continuously flowing carrier stream. A comprehensive review on the FIA application in various immunoanalysis techniques is found in literature [105]. Many examples of FIIA with electrochemical detection are reported, especially in the field of clinical chemistry [106-108]. The advantages and disadvantages of popular flow injection immunosensors based on different schemes, such as displacement, competitive binding and sandwich schemes are reviewed in [109]. When a heterogeneous enzyme immunoassay is coupled with FIA and amperometric

detection, the system explores the advantages of a flow system, selectivity of the immunoreactions as also sensitivity of an enzymatic reaction and amperometric detection. Carlo and Mascini have reported a FIA-based immunoassay with amperometric detection using HRP as a label for the determination of polychlorinated biphenyls [110]. The amperometric FIA techniques described in these applications rely on the use of an immunocolumn to carry out the antibody-antigen incubation and enzymatic reaction. The enzymatic reaction products are electroactive, which facilitates amperometric detection using commercially available FIA instrumentations. In some other cases, the immunoreactor and the detector are combined; hence the immunoreaction and the enzymatic reaction take place on the electrode surface [111, 112]. Such systems are prone to electrode fouling.

The prototype developed over the course of this project employs a unique approach where a chip-based flow-injection analysis system is built into the microfluidic platform developed for incorporating the immunoassay and the amperometric detection scheme. Such a system has the obvious benefit of being cost-effective as also being largely designed and developed in-house. The immunochannel (explained in Chapter 3) where the immunoreaction sequences and enzymatic reaction take place acts as the loop (of the in-built FIA) for the electroactive substance (which results from the enzymatic reaction) to be injected into a baseline buffer stream which flows into the detection unit. This relies on the proper integration of the fluidic chips with well-functioning, miniaturized pump-valve systems (described in Chapter 3). Such a miniaturized, chip-based, micro-fluidic FIA ( $\mu$ FIA) system is much easier to automate compared to conventional immunoassay techniques even in terms of multi-stage, sequential liquid-handling operations. However, it is important to note that the reuse of the immunosurface of the immunochip is a key issue to be considered in immunosensor development [109, 113]. In literature this issue has been barely addressed. Though no general conclusions have been drawn regarding the best regeneration conditions, this topic has been reviewed in literature [114]. Based on that, the preferred buffers to be used as desorbents are at acidic pH, such as glycine-HCl. The regeneration of the immunosurface used in BAM immunosensor based on the optimization reported in Chapter 2 is achieved by using glycine-HCl buffer at pH 2. This is tested in the electrochemical BAM immunosensor discussed in this chapter. In order to employ the final system for quantification of BAM in ground water, a

standard curve is generated by inhibiting the binding of HYB 273 onto the hapt D immobilized in the immunochannel with known concentrations of free BAM in solution.

## **5.2. Experimental**

### **5.2.1 Materials**

Since the format of the BAM immunoassay is the same as the batch immunoassays performed in plate-based ELISA and the integrated electrochemical BAM immunosensor is well depicted already, the various reagents and materials used for the experiments described in this section are the same as described in the previous chapters.

### **5.2.2 Experiments**

#### **5.2.2.a) Regeneration of immunochannel**

The regeneration of the immunochannel was tested by amperometric detection of the enzymatic product after repeated cycles of hybridization (immunoreaction between HYB 273 and hapt D immobilized in the immunochannel) and subsequent regeneration (disruption of HYB 273 – hapt D surface without affecting the immunological activity of the surface). The protocol adopted for this process is the same as given in section 4.2.2.a). In order to obtain the maximum current in each cycle, the inhibition assay was performed without added BAM in the solution (zero BAM).

#### **5.2.2.b) Standard curve generation**

A standard curve was generated by performing a number of competitive BAM immunoassays in the immunochannel with immobilized hapt D using different BAM concentrations in the standard solutions. Eight standard solutions of BAM with concentrations (in  $\mu\text{g L}^{-1}$ ) 62.5, 12.5, 2.5, 0.5, 0.1, 0.02, 0.004 and 0.0008 were prepared. 100  $\mu\text{L}$  of each BAM standard solution was mixed with 100  $\mu\text{L}$  of HYB 273 (1:1000 dilution of 1  $\text{mg mL}^{-1}$  HYB 273 stock solution with 0.01 M PBS containing 0.05% of Tween<sup>®</sup> 20) in a small 2 mL Eppendorf tube 15 min before it was introduced into the immunochannel for competitive reaction. The over all process was conducted in the automated prototype by repeating the different steps as given below.



1. Immobilization of BAM hapten in the immunochip: The immuno(micro)channel of the immunochip was filled with 30  $\mu\text{L}$  of hapt D ([115]) which was diluted 10 times with 0.01 M PBS. Both sides of the chip were then irradiated in the UV chamber for 30 min to facilitate the photo-reactive covalent immobilization. After the completed immobilization, the chip was inserted into the microfluidic system.
2. Using Valve 1 and 2, the immunochannel was opened to the waste to allow washing of the unbound hapt D for five minutes with 0.01 M PBST.
3. The immunochannel was filled with HYB-273+BAM standards (HYB dilution: 1000 times with 0.01 M PBS containing 0.05% Tween<sup>®</sup> 20).
4. The system was kept under stop-flow for 15 min to allow complete binding of the antibody to the immobilized hapten in the immunochannel.
5. The immunochannel was washed as described in step 2.
6. The immunochannel loop was filled with TMB solution (substrate).
7. The immunochannel was kept under stop-flow for 40 min to allow complete oxidation of the substrate.
8. The plug of reacted substrate was eluted into the detector with the base-line buffer (0.01 M PBS).
9. The immunochannel was washed as described in step 2.
10. The immunochannel was filled with Glycine.HCl buffer.
11. The immunochannel was kept under stop-flow for 3 min to allow complete removal of the bound antibody.
12. The immunochannel was washed as described in step 2.
13. Steps 3 to 12 were repeated several times with different concentrations of BAM standards in step 3 to obtain the standard curve.

Figure 5.1 shows the schematic of the electrochemical BAM immunosensor. This depicts how the integration of the different modules complements the overall function of the BAM immunosensor prototype.

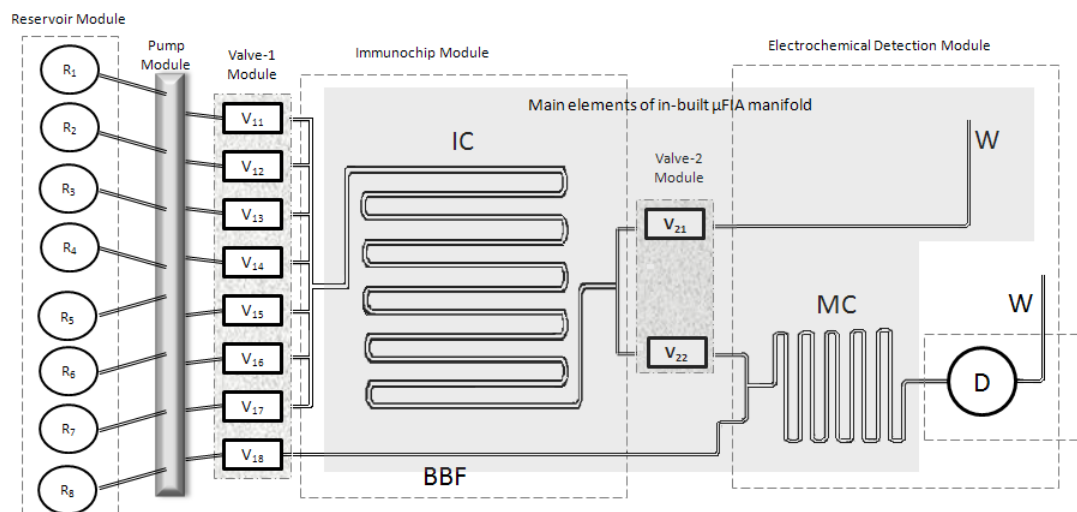


**Figure 5.1:** A schematic representation of the electrochemical BAM immunosensor. Each reservoir can be connected to the immunochip by dedicated valve of Valve-1 module. Valve V<sub>18</sub> is continuously open facilitating baseline buffer flow (BBF) to the detector. Among the active valves of Valve-2 module, V<sub>22</sub> is opened only when the electroactive substrate product is injected into the baseline buffer for recording the signal (in-built FIA function).

Table 5.1 enumerates the outline of the different operations associated with the pump and valve with respect to the various steps involved in the standard curve generation experiment.

**Table 5.1: Pump-valve operations corresponding to different steps of the standard curve generation experiment.**

Protocol Step #	From	Valve-1 Module								Valve-2 Module		Time (in mins)	To	Process
		V <sub>11</sub>	V <sub>12</sub>	V <sub>13</sub>	V <sub>14</sub>	V <sub>15</sub>	V <sub>16</sub>	V <sub>17</sub>	V <sub>18</sub>	V <sub>21</sub>	V <sub>22</sub>			
2	R <sub>2</sub>	0	1	0	0	0	0	0	1	1	0	5	waste	Washing of channel with assay buffer
* 3	R <sub>1</sub>	1	0	0	0	0	0	0	1	1	0	1.5	waste	Filling of channel with HYB+BAM standards
4	—	0	0	0	0	0	0	0	1	0	0	15	no flow in channel	Incubation for hybridization
5	R <sub>2</sub>	0	1	0	0	0	0	0	1	1	0	5	waste	Washing of channel with assay buffer
* 6	R <sub>4</sub>	0	0	0	1	0	0	0	1	1	0	1.5	waste	Filling of channel with TMB (substrate)
7	—	0	0	0	0	0	0	0	1	0	0	40	no flow in channel	Incubation for enzyme reaction
8	R <sub>5</sub>	0	0	0	0	1	0	0	1	0	1	5	detector	Signal recording
9	R <sub>2</sub>	0	1	0	0	0	0	0	1	1	0	3	waste	Washing of channel with PBST
* 10	R <sub>6</sub>	0	0	0	0	0	1	0	1	1	0	1.5	waste	Filling of channel with regeneration buffer
11	—	0	0	0	0	0	0	0	1	0	0	3	no flow in channel	Regeneration reaction
The sequence of these steps are repeated by using different BAM standards (in step 3) to obtain the standard curve														
<i>* It takes at least one minute to fill the channel with 30μL using a flow rate of 30μL/min.</i>														

### 5.2.3 Automating the system

To achieve the goal of the project, the operation of the final system needed to be automated. The automation was realized using a LEGO® MINDSTORMS® NXT kit. The kit itself consists of a programmable LEGO brick with inbuilt interfaces to

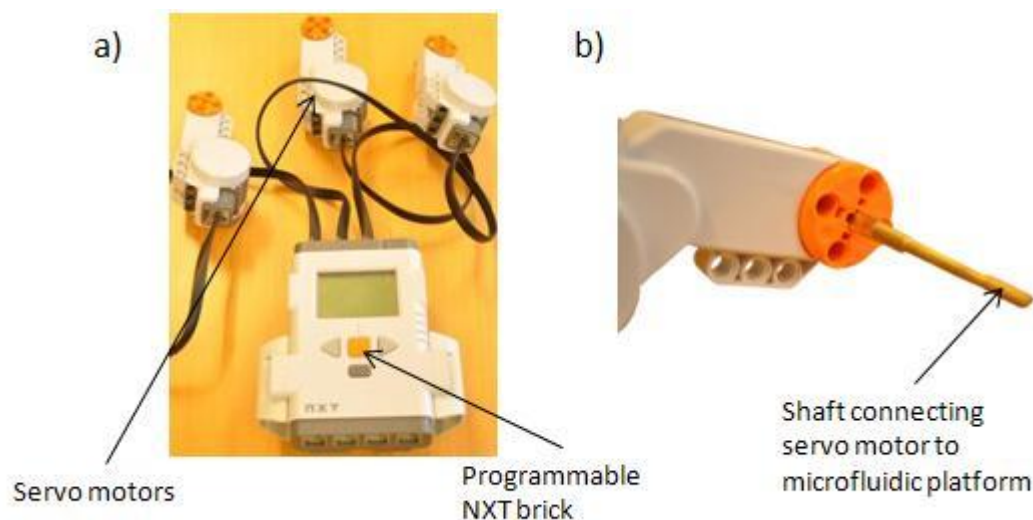


**Figure 5.2: a) LEGO NXT brick with three servo motors connected to each motor interface, b) custom designed shaft fabricated in-house to couple motor action to the mechanically actuated components of the ABIS prototype.**

sensors, motors and speakers. Figure 5.2(a) shows the NXT.

In this particular application, the NXT unit (i.e., the programmable LEGO brick) was used to control the three servo motors attached. The servomotors were connected to the respective mechanically actuated modules (pump and valves) on the ABIS prototype. This was achieved using specially fabricated brass shafts (as shown in Figure 5.2(b)). The first motor (Motor A) controls the miniaturized peristaltic pump. Motor A was suitably programmed to control the pumping of the required liquid reagents associated with the BAM immunoassay into the  $\mu$ FIA-based chip. The second motor (Motor B) was programmed to control the first valve module (Valve-1) thereby sequentially delivering the liquids required for the immunoreaction in the immunochip. In order to function properly, Motor B needs to be programmed so that the valves V11 - V18 are opened as desired at a different point in time during the operation of the system. The third motor (Motor C) was connected to the Valve-2 module. It was suitably programmed to operate valves V21 and V22 so that the

electroactive product (obtained from the electrochemical reaction which takes place inside the immunochip) could be injected into the baseline buffer flow on the mixing chip for detection.

The LEGO MINDSTORMS NXT software was used to programme the NXT brick for achieving the automation. The drag-and-drop user-interface (powered by National Instruments LabVIEW) enables clear and easy programming of the NXT. Figure 5.3 captures the screen shot of one of such programme used for the  $\mu$ FIA characterization experiment.

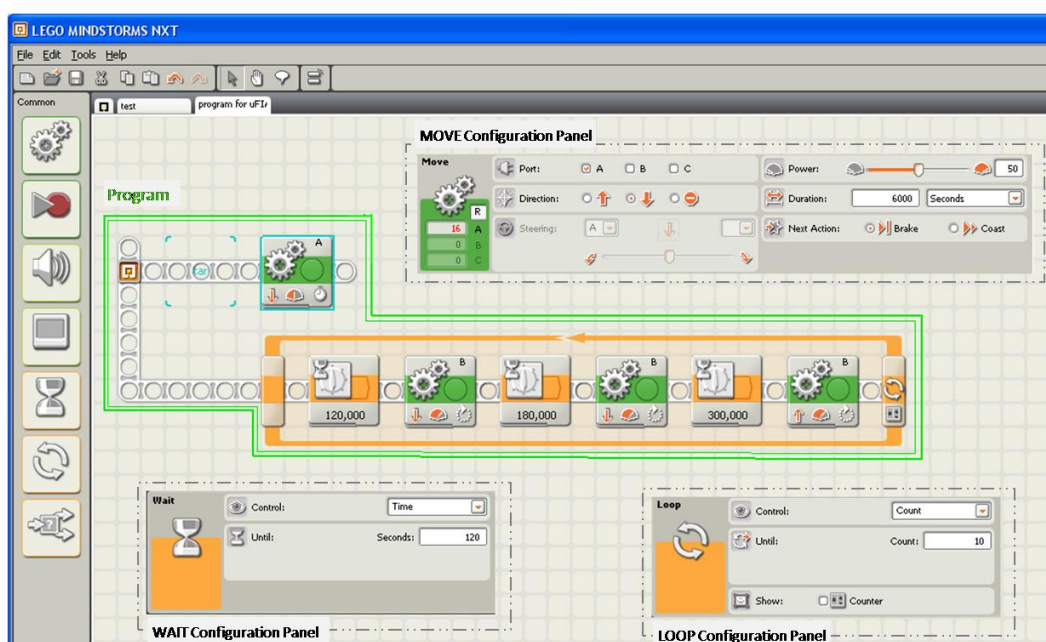


**Figure 5.3:** Screen shot of an example of NXT program used to control the pump module and the Valve-1 module of ABIS prototype. The chained blocks in the green box constitute the program. It controls two LEGO® servomotors parallelly, indicated as A and B. The MOVE block (meshed gears) controls the movement of the mechanically actuated modules of ABIS prototype (pump/valve) connected to the respective motors. The WAIT block (hourglass) decides the waiting time before the next step. The LOOP block (circular arrows) repeats a chain of functions for a defined number of times. The function parameters of various blocks are set in respective configuration windows. One example for each block is shown as inserts in the figure.

## 5.3. Results and discussions

### 5.3.1 Regeneration with amperometric detection

In the regeneration experiment where the BAM immunoassay was repeated in the inhibition format with zero BAM solution (to evaluate the maximum signal) at the same reaction conditions resulted in amperometric peaks with a %RSD of peak area of 20 (for 15 cycles). However, the signal observed with the 15th cycle retained almost 95% of the intensity of the signal produced by the first cycle. The high %RSD value may be attributed to the choice of enzyme-substrate incubation period of 15 min applied to each cycle. This was at the rising slope of the HRP-TMB kinetic curve (Figure 2.8 (b)). At this point of time, a tiny operational error may result in significant variations in the signal. The regeneration experiment primarily aimed to establish the feasibility of performing BAM immunoassay for a number of times without losing the immunosurface activity. This is considered to be a very important prerequisite in the development of an in-line monitoring system based on immunoassay. The result obtained in this experiment is supported by the findings described in [115] which showed the possibility of regenerating hapt D immobilized surface for a number of times (25 cycles of BAM inhibition assay with zero BAM in solution) without significant signal reduction on ELISA plates. In each cycle an incubation time of 15 min was given with 100 mM glycine HCl buffer (pH 2). Compared to this, hapt D immobilized immunochannel was regenerated under relatively mild conditions (incubation with 100 mM glycine HCl buffer at pH 2 for 3 min) by exploring the advantages of a microfluidic flow system. The increased surface to volume ratio available in the microfluidic immunochannel enhances the interaction of the immunosurface with the liquid reagents filled in it. Such a situation is equally beneficial for both formation and desorption of antibody – surface antigen complex and therefore results in better signal and stripping interactions for repeated BAM immunoassay cycles.

### 5.3.2 Standard curve

The standard curve obtained in electrochemical BAM immunosensor prototype is shown in Figure 5.4. To allow the enzymatic reaction of each standard solution to be complete, an incubation time of 40 min was applied. The area of the amperometric peaks obtained for each standard (ranging from  $62.5 \mu\text{g L}^{-1}$  to  $0.0008 \mu\text{g L}^{-1}$ ) was

plotted as a sigmoidal dose-response curve. An  $IC_{50}$  (the concentration at which 50% inhibition is obtained) value of  $0.1924 \mu\text{g L}^{-1}$  and a linear working range from  $12.5 \mu\text{g L}^{-1}$  to  $0.02 \mu\text{g L}^{-1}$  were obtained. These values are exactly the same as the ones reported for the plate based ELISA experiments [49].

The current design of the reservoir module does not provide separate chambers for different (premixed) antibody-BAM standard solutions. The use of a single reservoir for all the standards required prolonged washing steps to avoid foot prints of each analytical cycle. Such situations resulted in greater difficulty to obtain reproducible data. Though the reproducibility of the curve is not shown, the experiment provides the proof of concept achieved by the BAM immunosensor prototype.

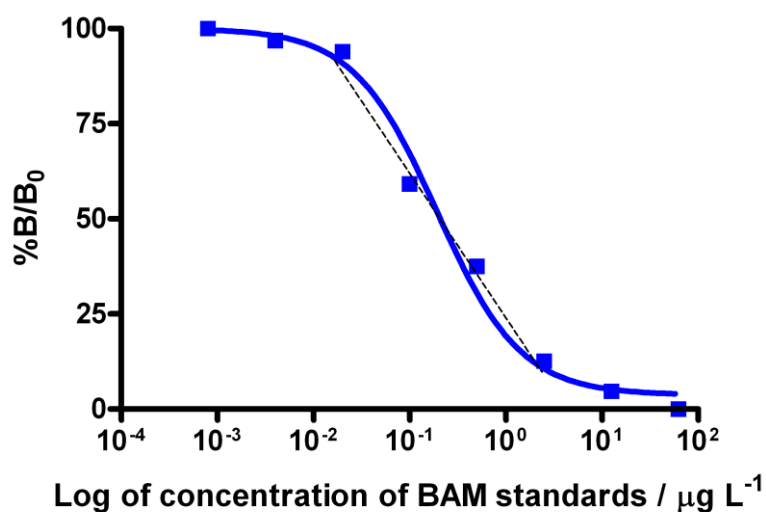


**Figure 5.4:** A sigmoidal standard dose response curve generated with 8 BAM standards. An  $IC_{50}$  value of  $0.1924 \mu\text{g L}^{-1}$  is obtained and the linear working range of the curve is shown as a dotted line.

This is a clear evidence for the fact that, in the heterogeneous BAM immunoassay, the reduced affinity of HYB 273 towards the immobilized hapten (hapt D which is chosen for surface immobilization after the optimization of BAM immunochemistry described in Chapter 2) is compensated by the increased surface area to volume ratio of microchannels. At the same time, use of the same antibody (HYB 273) helped to retain the analyte-antibody affinity. In short, by utilizing the advantages of

microfluidic platform, the modified heterogeneous BAM immunoassay is successfully shifted from ELISA plates to continuous flow analysis system.

## 5.4. Conclusion

This chapter described two experiments conducted to evaluate the function of the BAM immunosensor prototype. The regeneration experiment confirmed the reusability of the immunosurface. The standard curve experiment proved that using the same antibody and a suitably modified hapten (modified to improve reusability of the surface by decreasing hapten-antibody affinity) the sensitivity and the detection limit (from  $12.5 \mu\text{g L}^{-1}$  to  $0.02 \mu\text{g L}^{-1}$ ) of the ELISA-based BAM immunoassay are retained when performed in a flow system. This result emphasizes the immense potential of the prototype and also validates the proof-of-concept on which this research project is based. Although this prototype was used to detect a single pesticide residue (BAM), it can be easily tailored for many different applications. Modularity of the microfluidic platform used in the BAM immunosensor offers the possibility of constructing different systems for different applications by merely interchanging the array order of various modules. Having an automated in-built flow injection analysis system in a microfluidic environment ( $\mu\text{FIA}$ ) makes the system unique and facilitates easy integration with sensitive detection schemes.





# Chapter 6

## Discussion

---

This chapter discusses the overall project within the framework of the aims that were stated in the introductory chapter (Chapter 1) and the milestones achieved over the course of the work.

The world's increasing population and limited availability of clean and safe water has resulted in a situation where monitoring the quality of accessible (available) water is as important as its preservation. The primary goal of this project was to develop a sensor to be used in monitoring the contamination caused by pesticides in ground water. Being designed for laboratory-based analysis, neither the conventional methods of pesticide analysis (based on chromatographic techniques) nor the current '*state of the art*' ELISA method (which depends on plate based immunoassays) can serve as a continuous, on-site monitoring technique for pesticide quantification in ground water. As a practical solution, this project proposes the conversion of the plate based ELISA into a continuous in-line monitoring system. The sensor prototype detailed in the earlier chapters has been repeatedly referred to as continuous, cost effective, portable, real-time, automated and easy to handle. The following sections discuss these features in greater detail.

### 6.1. Designing the system prototype

The deciding factors for the selection of the model system and the techniques and methods used to achieve the prototype development were primarily based on the in-house availability and accessibility of resources and tool boxes. Previous research (conducted at the Surface Engineering Group of DTU Nanotech) involving the development of a quantitative enzyme-linked immunoassay for the detection of 2,6-dichlorobenzamide (BAM), a degradation product of the herbicide dichlobenil [49], provided the background and tool box for developing an electrochemical BAM immunosensor as a model system. The techniques (CNC micromilling) and materials (various polymeric substrates) adopted for the device fabrication were easily accessible in-house.

### 6.1.1 Regenerating the immunosurface

Chapter 2 of this thesis reports in detail the challenges of bringing a plate based ELISA into a continuous analysis format. A continuous immunoassay-based pesticide monitoring systems should be repeatable and reliably reproduce measurement data. Thus, the regeneration of the immunosurface is crucial to the function of the system.

The primary investigations for a suitable regeneration buffer to regenerate hapt A immobilized microtitre well plates was conducted at Cranfield Biotechnology Centre, Institute of BioScience and Technology, Cranfield University, Silsoe and commissioned by one of the project collaborators, DHI solutions, Denmark. They reported that after attempting with a number of solutions to regenerate a functional hapt A coated Polysorp™ surface, Glycine.HCl in the pH range of 1.9 and 2.3 was found to elute the bound antibody-conjugate completely. However, regeneration with 50 mM glycine.HCl pH 1.9 resulted in a decrease in the assay response after four regenerations, though %B/Bo values suggested that assay sensitivity could be maintained for at least 6 regenerations. Obviously, these results do not support the possibility of developing a continuous monitoring system based on BAM immunoassay without properly optimizing it. This was the motivation for approaching regeneration in terms of manipulating the affinity of HYB to the surface immobilized hapten.

In heterogeneous competitive immunoassays as in the case of BAM analysis, the performance of the method depends on two binding affinities –

- a) HYB 273 – analyte BAM affinity (*determines the sensitivity of detection*)
- b) HYB 273 – surface immobilized BAM hapten affinity (*determines the signal to noise ratio*)

In addition to this, when the BAM immunoassay was performed using the ELISA format, the diffusion of immunoreagents in the micro-wells significantly affected the signal intensity. In order to balance this effect, in ELISA based BAM assay, the antibody HYB 273 was chosen with comparable affinities to both analyte (free BAM in water sample to be analysed) and hapten (hapt A immobilized on the surface). In reality, hapt A is the same as the hapten used for immunizing mice to produce the monoclonal antibody, HYB 273. This in turn results in a strong antibody – surface

interaction and the potential difficulty for surface regenerations. Since the use of a different antibody was out of the scope of this project, chemically different new BAM haptens were synthesized (Figure 2.3) and their affinities towards HYB 273 were compared (Table 2.2 and Figure 2.9). The hapten with intermediate affinity (hapt D) showed a better regeneration capacity when compared to the original hapten (hapt A). The hapten with lower affinity (hapt B) showed the best regeneration capability (Figure 2.10). However, a very low affinity could possibly result in a weak signal-noise ratio. Hence hapt D was chosen as a better candidate for immunoassays in the flow system. Another advantage of the approach used in this project is that the hapten molecule was the immobilized entity. In terms of surface stability and regeneration this offered better prospects than antibody immobilization.

The regeneration was achieved by desorption of HYB 273-HRP conjugate from the hapt D immobilised surfaces without destroying the surface and/or losing its activity. This was facilitated by a change in pH (from 7 to 2). Since the protein molecules (ovalbumin) used to immobilize hapt D is structurally stable even at pH 2, there is less chance of surface removal due to ovalbumin denaturation (under the applied conditions) [116]. The covalent immobilization of hapt D also contributed to the robustness of the surface. Hence, due to the strong binding of the haptens on the surface, a slightly decreased HYB 273 – hapten affinity could result in better regeneration under mild conditions.

### **6.1.2 Designing of a continuous, in-line monitoring system**

When the optimized BAM immunoassay was transferred to the  $\mu$ FIA-based fluidic chip assembly (i.e., hapt D was used for surface immobilization rather than hapt A), the reduction in signal strength due to the diffusion was significantly compensated by an increase in surface area to volume ratio of the microfluidic channels. Furthermore, the binding motifs were more available to the antibody binding pockets due to a high surface area to volume ratio. This has possibly improved the binding affinity between hapt D and HYB 273 in the microfluidic channels when compared to that in the microtitre plates. This is evident from the significantly improved absorbance obtained when the BAM immunoassay was performed in the ABIS prototype (Figure 4.1) as compared to those obtained on ELISA plates (Figure 2.9). The regeneration experiments conducted in the BAM immunosensor both optically (Section 4.2.2.a))

and amperometrically (Section 5.2.2.a)) with hapt D as the immunosorbent demonstrated that a continuous analysis for BAM detection at least for a number of times is possible. This was crucial for the sensor to be employed as a continuous in-line monitoring system.

### **6.1.3 Making the ABIS prototype portable, maintainable and automated**

The microfluidic platform developed for the ABIS prototype is constructed using individual modules which perform different functions. Chapter 3 described how these modules function independently and how they are integrated to make the final prototype. The use of such miniaturized modules makes the system portable. The different parts of each module are easily replaceable and the modules themselves give a high degree of interchangeability. This makes the prototype easily maintainable, user friendly and easy to handle. The mechanically actuated components of the system, i.e., the miniaturized peristaltic pump and microvalves are constructed on a central shaft made of brass which is customized in such a way that one of its ends can be inserted into LEGO® Mindstorms® servomotors. This enabled the automation of the system.

### **6.1.4 Designing for cost-effectiveness**

The materials and fabrication technology used to develop the ABIS prototype were selected for their cost effectiveness. The entire sensor system was mainly constructed of polymeric materials using micromilling technology. In the final prototype, the choice and use of an electrochemical detection scheme provided a cheap and compact alternative (to other detection schemes like optical techniques, etc.). The use of the  $\mu$ FIA function to perform the immunoreactions and the consequent small quantities of reagents involved (in this scaled down version of an ELISA based immunoassay system) significantly reduces the overall reagent consumption. This contributes to the system to have low operational costs. For instance, the required amount of antibody to run one cycle of the immunoassay described in Chapter 4 and Chapter 5 is around 30 ng which is a very small amount compared to that needed for a lab-based ELISA (which needs at least a 150 ng/well to perform a similar assay).

## 6.2. The in-built $\mu$ FIA core – a functional key element

The immuno chip and mixing chip are designed to function complementarily (using Valve-2 module). This feature resulted in the creation of an inbuilt  $\mu$ FIA function, which is characteristic to the developed electrochemical BAM immunosensor described and discussed in this thesis.

This feature enables the system to function under both stop flow and flow conditions that are essential for the immunoassay. At the same time, it supports the controlled and highly reproducible injection of optically/electrochemically active substance into an uninterrupted flow of baseline buffer to record signals continuously. Careful design of the mixing chip and the double sided BJIB along with the press-fit mechanism (to accommodate external tubings) makes it possible to connect one or more detection methods to the  $\mu$ FIA core setup. A compact, leak-proof construction of an electrochemical unit provides a sensitive and cost effective detection method. The presence of Valve-2 and its link to a waste channel completes the loop of the  $\mu$ FIA and gives the possibility of diverting different reagents and washing solutions from the immuno chip to the waste channel. This helps to keep the electrode surface clean and prevents it from fouling.

## 6.3. Stability of the reagents

Investigation of the stability of various reagents used for BAM immunoassay is of great importance, as the final system is intended to function as an unattended, on-site, in-line monitoring system for at least a number of weeks. This reagent stability study was also commissioned by DHI Solutions and conducted at Cranfield Biotechnology Center, Cranfield University.

Stability trials conducted over the period of a month showed that the reagents used for BAM immunoassay were stable for at least 30 days. The antibody, HYB 273 – HRP conjugate retained its activity when stored at 4° C and mixed with glycerol to obtain a final concentration of 50% (v/v). The hapten coated polymeric surfaces were stable for one month when they were stored under dry conditions as well as in phosphate buffered saline (PBS) solution. The regenerated surfaces also showed the same behaviour. The TMB substrate solution used in the detection of bound antibody-HRP

conjugate was found to be stable in the presence of 50 mM KCl for at least 30 days at 4 °C.

#### **6.4. The ABIS prototype – room for improvement**

The use of PDMS for making pump and valve inlays has some drawbacks. The inlays are fragile and susceptible to tearing. The casting process is tedious and time consuming. Also, PDMS has a tendency to absorb substances, especially proteins and organic compounds. Both PMMA and PDMS are not compatible for organic solvents such as alcohols, acetone etc. This limits the application of the system to only assays with water based reagents. In BAM immunoassay all the reagents are water soluble. The application of Tween® 20, a detergent in the antibody solution reduces the risk of adsorption by PDMS. However, the use of these materials has to be reconsidered when developing a commercial product based on this prototype system.

In further development steps of the prototype, some design features can be improved. For instance, in the current system, the baseline buffer flows in one of the edge channels of the pump inlay. The edge channels show a slightly deviating performance when compared with the channels in the middle (Section 3.3). Moreover, it spans between the reservoir and the detection chamber without any valve options in between. This makes it impossible to get rid of any air bubble that can form in the channel. Such air bubbles end up in the detection chamber affecting the measurement. Another issue to be discussed is the removal foot prints of previous assay while doing immunosensing with samples and standards. This requires washing of the reservoir and the immunochannel with PBST and then emptying it. Under the complete automation, this step may take an extra time which will then disturb the successive steps in the program. In the current system, the program will run successfully, only if the starting positions of the servomotors controlling the valves are at the position where the first channel is open. There is no method to bring the valve to any unique position with the current setup and motors.

The regeneration results presented in Section 5.3.1 , shows a large %RSD value between the peaks. This was due to the fact that, the chosen incubation time was at the rising part of the kinetic curve of enzyme-substrate reaction. From the kinetic curve (Figure 2.8(b)), it is clear that with hapt D, an incubation time of 40 min is

needed to saturate the reaction. Based on this, generation of the standard curve was done using 40 min incubation time. This resulted in at least 80 min total processing time for one assay cycle. Thus, the performed assays cannot be described as rapid or realtime sensing.

## **6.5. Interfacing with the macro-world**

The prototype – as it is today – functions well in a laboratory environment. The current ABIS prototype has the following elements –

- a) An optimized immunoassay
- b) A well-functioning microfluidic platform
- c) An automated functioning setup
- d) A sensitive and cost effective detection scheme

In order to employ it outdoors, (as an on-site, in-line sensor) a suitable interface to the macro-world is very essential. Such an interface has already been developed as a part of this project by one of the collaborators, MikroLab in Aarhus. The interface is an automated, pre-sampling unit. This section presents a more detailed description of this interface.

As a sampling unit, it has pressure reduction valves to control the flow of the sample from the source (macro-world) to the sensor device (micro-world). The received samples are first filtered through the filtering membrane and then collected in a polymer container in the sampling unit.

The interface also has the ability to dilute the antibody with the assay buffer (PBST) as required by the detection protocol (up to 1:1000). Using syringe-piston pumps and precisely controlled step motors, it can perform the pre-mixing of precise volumes of diluted antibody and the sample. The pre-mixed solution is then made available to the  $\mu$ FIA-based immunosensor for further analysis. The unit also incorporates mechanisms to thoroughly clean the various loops and paths involved, so that possible memory effects due to previous cycles can be eliminated completely. In the microfluidic ABIS, this washing introduces procedural errors that can be avoided by shifting it to the sampler unit.





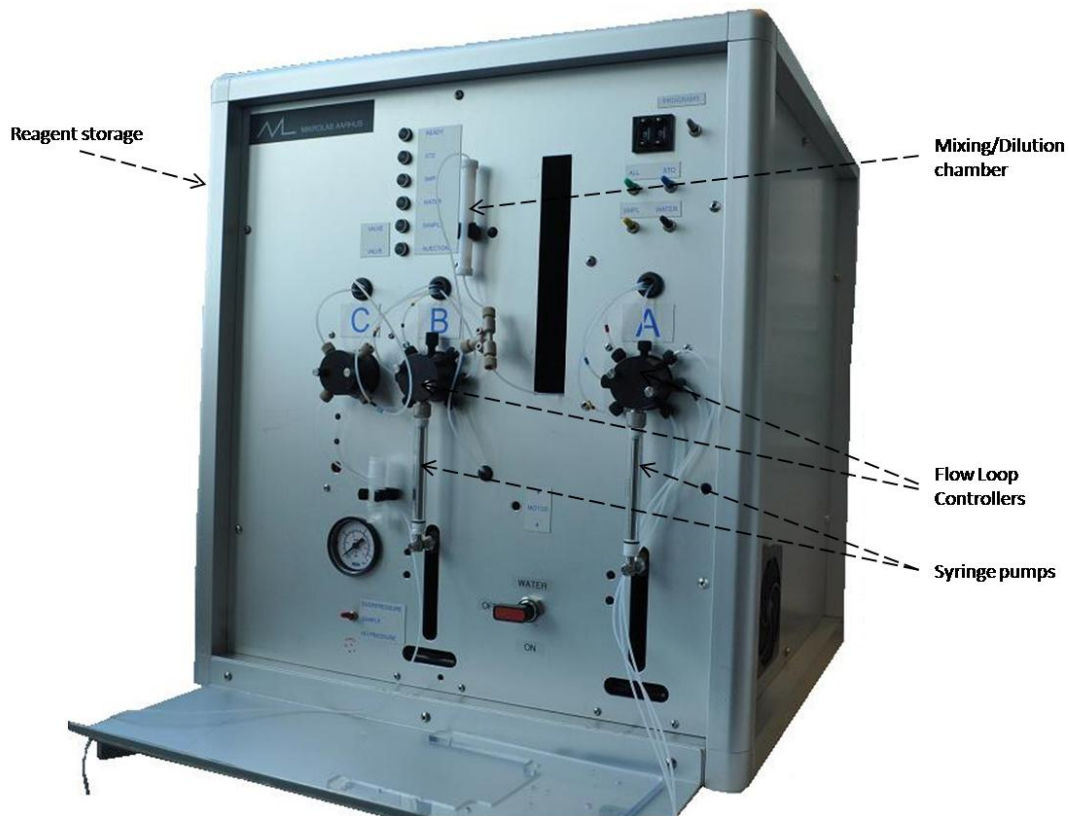


Figure 6.2: The sampling unit.

Since the existing prototype does not interact with the interface unit to receive field samples directly, further work needs to be conducted in this regard. This is mentioned in Section 7.3.1 of Chapter 7.

## 6.6. Conclusion

This chapter discussed the overall achievements of this project with respect to the goals of the project. It also introduced the need for further improvement and enhancement of the ABIS prototype. Chapter 7 focuses on these aspects.



# Chapter 7

## Conclusions and Outlook

---

### 7.1. Project achievements

As described in this thesis, the ABIS prototype was implemented through the following milestones:

- a) The traditional lab-based ELISA was transferred into a continuous, in-line monitoring system (Chapter 2).
- b) A microfluidic platform with an inbuilt FIA was designed (Chapter 3 and Chapter 4).
- c) The miniaturized sensor unit was automated using LEGO® Mindstorms® NXT bricks (Chapter 5).
- d) Regeneration of the immunosurface was achieved and tested with both optical and electrochemical detection schemes (Chapter 4 and Chapter 5).
- e) The functioning prototype was tested and a typical sigmoidal dose response curve was generated for calibration purposes (Chapter 5).

### 7.2. Recap of thesis contributions

The following contributions have been described in detail in the thesis.

#### 7.2.1 A unique approach to optimizing the BAM immunoassay

Usually, optimization of heterogeneous immunoassays aimed at surface regeneration, focuses on changing the antibo. This comes at the cost of assay sensitivity. In this study, by keeping the antibody unchanged and modifying the immobilized haptens, antibody-surface interactions were tuned in favour of regeneration.

#### 7.2.2 Synthesis of new BAM haptens

A library of structurally different BAM haptens was synthesized in order to modify the original immunoreaction to one that offered greater possibilities of surface regeneration. Of these, hapt D was chosen because it showed better regeneration possibilities with a reasonable signal to noise ratio.

### **7.2.3 Isolation of new dichlobenil haptens**

By improvising the synthesis strategy, it was possible to create nitrile derivatives of BAM haptens which were never isolated prior to this project. These haptens have the potential to be used as dichlobenil haptens for immunization and subsequent antibody development. This will enable development of antibodies for the parent herbicide itself. (Chapter 2)

### **7.2.4 Novel design of in-built standalone $\mu$ FIA**

The  $\mu$ FIA, which facilitates the detection scheme on the microfluidic platform, is a significant contribution as can be seen through the details presented in the earlier chapters. The entire microfluidic environment itself has a modular design and presents the potential of being used in various new application areas through suitable rearrangement/redesign of its constituent modules.

## **7.3. Scope for future work**

### **7.3.1 Interacting with the macro-world**

As described and discussed so far, the immunosensor prototype functions well in a laboratory environment. However, the system is yet to be completed. In an ideal operating environment, this system is intended to function as an on-site, in-line monitoring device. Further work needs to be done to investigate and implement a suitable interconnection between the current  $\mu$ FIA-based prototype and the existing sample and pre-treatment chamber as described in Section 0. Following this, field tests can be performed and the results can be validated with the current conventional techniques.

### **7.3.2 Alternatives to PDMS**

As detailed in Section 6.4, though PDMS is used predominantly in prototype systems it has significant drawbacks that make it not very suitable for use in the actual system. New materials that can replace PDMS need to be investigated. Like PDMS, a suitable material needs to be elastic and at the same time more durable.

### **7.3.3 Managing air bubbles**

The efficiency of the prototype systems is affected by the occurrence of air bubbles in the channels of the microfluidic BAM immunosensor device. Design reconsiderations need to be made to introduce structures such as valves which can effectively remove air bubbles from the channels without significantly disrupting the pump/device operation.

### **7.3.4 Making the system real-time**

Section 6.4 also discussed briefly about how enzymatic reactions with long incubation time affects the desired real-time function of the system. To improve the real-time performance of the prototype, some design changes affecting the flow of reagents and reaction times need to be considered. In order to address these, structural changes to the microfluidic platform need to be considered. This may be in the form of modification of the stop flow mechanism to one using back and forth movement of the reagents in the immunochannel to introduce forced convection dynamics (within a limited boundary). In addition, the scope for introducing parallelization in the system needs to be further investigated. There are also other techniques that could be suitable alternatives such as improved control of reaction times through the introduction of an end point analysis scheme that is analogous to the one applied on the ELISA plates.

### **7.3.5 Multiplexing with multiple residues**

The current BAM immunosensor design can be applied for only one pesticide residue analysis. A second generation of the amperometric immunosensors could possibly include the analysis of more than one pesticide residues. This requires a careful design of the microfluidics which allows parallelization of immunochannels. Such a system may also support the combinatorial analysis with different antibodies.

## **7.4. Final remarks**

Most of the goals envisaged at the start of this project have been achieved over the course of the last three years. The course work pursued over the duration of this PhD project was useful at the various stages of development of this prototype. Results of the studies published in the earlier chapters detail a largely successful prototype

implementation and the evolution of a  $\mu$ FIA design with immense potentials. The modular approach adopted for the microfluidic platform fabrication along with the  $\mu$ FIA function can be possibly used for similar applications in environmental as well as biological analysis.

## References

- [1] W.J. Cosgrove, F.R. Rijsberman, *The Use of Water Today*, World Water Vision, World Water Council, UK, 2000, p. 6.
- [2] W.U.J.M. Programme, *Millenium Development Goal (MDG) Assessment Report - Progress on Drinking Water and Sanitation*, WHO/UNICEF Joint Monitoring Programme for Water Supply and Sanitation, UNICEF/WHO, 2008.
- [3] W.J. Cosgrove, F.R. Rijsberman, *Water Futures*, World Water Vision, World Water Council, UK, 2000, p. 23.
- [4] N.L.M. Berger, *Nanotechnology and Water Treatment*, 2008.
- [5] B.C.M.o. *Agriculture, Environmental Fate*, 2011.
- [6] C. Martínez Navarrete, J. Grima Olmedo, J. Durán Valsero, J. Gómez Gómez, J. Luque Espinar, J. de la Orden Gómez, *Environmental Geology*, 54 (2008) 537.
- [7] J. Stockmarr, *Geological Survey of Denmark and Greenland Bulletin* 7(2005) 33
- [8] K.W. Oh, C.H. Ahn, *Journal of Micromechanics and Microengineering*, 16 (2006) R13
- [9] F.J. Santos, M.T. Galceran, *Journal of Chromatography A*, 1000 (2003) 125.
- [10] E. Porazzi, M. Pardo Martinez, R. Fanelli, E. Benfenati, *Talanta*, 68 (2005) 146.
- [11] G.G. Jensen, E. Björklund, A. Simonsen, B. Halling-Sørensen, *Journal of Chromatography A*, 1216 (2009) 5199.
- [12] A. Ghanem, P. Bados, F. Perreau, R. Benabdallah, C. Plagellat, L.F.d. Alencastro, J. Einhorn, *Analytical and Bioanalytical Chemistry*, 391 (2008).
- [13] Y. Picó, C. Blasco, G. Font, *Mass Spectrometry Reviews*, 23 (2004) 45.
- [14] L. Baraud, D. Tessier, J.-J. Aaron, J.-P. Quisefit, J. Pinart, *Analytical and Bioanalytical Chemistry*, 377 (2003) 1148.
- [15] J. Hernández-Borges, S. Frías-García, A. Cifuentes, M.A. Rodríguez-Delgado, *Journal of Separation Science* 27 (2004) 947
- [16] R.L. Searcy, J. V. P. Carroll, J.S. Carlucci, L.M.B. quist, *Clinical Chemistry*, 8 (1962) 166
- [17] B.C.D. Villano, S. Brennan, P. Brock, C. Bucher, V. Liu, M. McClure, B. Rake, S. Space, B. Westrick, H. Schoemaker, J. V R Zurawski, *Clinical Chemistry*, 29 (1983) 549.
- [18] S.R. Nussbaum, R.J. Zahradnik, J.R. Lavigne, G.L. Brennan, K. Nozawa-Ung, L.Y. Kim, H.T. Keutmann, C.A. Wang, J. J T Potts, G.V. Segre, *Clinical Chemistry*, 33 (1987) 1364.
- [19] R.S. Yalow, S.A. Berson, *The Journal of Clinical Investigation*, 39 (1960) 1157.
- [20] B.D. Hammock, R.O. Mumma, *Pesticide Analytical Methodology*, ACS Symposium Series, Edited by John Harvey, Jr. and Gunter Zweig, 136 (1980) 321
- [21] F. Jung, S.J. Gee, R.O. Harrison, M.H. Goodrow, A.E. karu, A.L. Braun, Q.X. Li, B.D. Hammock, *Pesticide Science*, 26 (1989) 303
- [22] C.D. Ercegovich, *Pesticides Identification at the Residue Level*, *Advances in Chemistry*, ACS Publication, 104 (1971) 162
- [23] G. Jay, B. Svetlana, *Analysis of Pesticides in Food and Environmental Samples*, CRC Press, 2008.
- [24] V.S. Morozova, A.I. Levashova, S.A. Eremin, *Journal of Analytical Chemistry*, 60 (2005) 202.



- [25] R.L.T. Churchill, C. Sheedy, K.Y.F. Yau, J.C. Hall, *Analytica Chimica Acta*, 468 (2002) 185.
- [26] E. Mallat, D. Barceló, C. Barzen, G. Gauglitz, R. Abuknesha, *TrAC Trends in Analytical Chemistry*, 20 (2001) 124.
- [27] J.A. Gabaldón, A. Maquieira, R. Puchades, *Critical Reviews in Food Science and Nutrition*, 39 (1999) 519.
- [28] M.-C. Hennion, D. Barcelo, *Analytica Chimica Acta*, 362 (1998) 3.
- [29] C. Raman Suri, R. Boro, Y. Nangia, S. Gandhi, P. Sharma, N. Wangoo, K. Rajesh, G.S. Shekhawat, *TrAC Trends in Analytical Chemistry*, 28 (2009) 29.
- [30] E.P. Meulenbergh, W.H. Mulder, P.G. Stoks, *Environmental Science & Technology*, 29 (1995) 553.
- [31] M. Vanderlaan, B.E. Watkins, L. Stanker, *Environmental Science & Technology*, 22 (1988) 247.
- [32] M. Schwalbe-Fehl, *International Journal of Environmental Analytical Chemistry*, 26 (1986) 295
- [33] A.S. Khan, C.J. Cao, R.G. Thompson, J.J. Valdes, *Molecular and Cellular Probes*, 17 (2003) 125.
- [34] J. Svitel, I. Surugiu, A. Dzgoev, K. Ramanathan, B. Danielsson, *Journal of Materials Science: Materials in Medicine*, 12 (2001) 1075.
- [35] G.B. Wisdom, *Clinical Chemistry*, 22 (1976) 1243
- [36] J. Svitel, A. Dzgoev, K. Ramanathan, B. Danielsson, *Biosensors and Bioelectronics*, 15 (2000) 411.
- [37] C.D. Ercegovich, R.P. Vallejo, R.R. Gettig, L. Woods, E.R. Bogus, R.O. Mumma, *Journal of Agricultural and Food Chemistry*, 29 (1981) 559.
- [38] J. Svitel, A. Dzgoev, K. Ramanathan, B. Danielsson, *Biosensors and Bioelectronics*, 15 (2000) 411.
- [39] R.G. Heideman, R.P.H. Kooyman, J. Greve, *Sensors and Actuators B: Chemical*, 4 (1991) 297.
- [40] S. Rodriguez-Mozaz, M.L. de Alda, D. Barceló, *Water Research*, 39 (2005) 5071.
- [41] J. Ngeh-Ngwainbi, P.H. Foley, S.S. Kuan, G.G. Guilbault, *Journal of the American Chemical Society*, 108 (1986) 5444.
- [42] C. Steegborn, P. Skládalt, *Biosensors and Bioelectronics*, 12 (1997) 19.
- [43] B.B. Dzantiev, A.V. Zherdev, M.F. Yulaev, R.A. Sitdikov, N.M. Dmitrieva, I.Y. Moreva, *Biosensors and Bioelectronics*, 11 (1996) 179.
- [44] A.J. Bäumner, R.D. Schmid, *Biosensors and Bioelectronics*, 13 (1998) 519.
- [45] G.F. Blackburn, D.B. Talley, P.M. Booth, C.N. Durfor, M.T. Martin, A.D. Napper, A.R. Rees, *Analytical Chemistry*, 62 (1990) 2211.
- [46] C.R. Suri, J. Kaur, S. Gandhi, G.S. Shekhawat, *Nanotechnology*, 19 (2008) 235502.
- [47] R. Raiteri, G. Nelles, H.-J. Butt, *Sensors and Actuators B: Chemical*, 61 (1999) 213.
- [48] L. Bruun, C. Koch, M.H. Jakobsen, J. Aamand, *Analytica Chimica Acta*, 423 (2000) 205.
- [49] L. Bruun, C. Koch, B. Pedersen, M.H. Jakobsen, J. Aamand, *Journal of Immunological Methods*, 240 (2000) 133.
- [50] M.S. Holtze, H.C.B. Hansen, R.K. Juhler, J. Sørensen, J. Aamand, *Environmental Pollution*, 148 (2007) 343.

- [51] E. Bjorklund, B. Styrishave, G.G. Anskjaer, M. Hansen, B. Halling-Soerensen, *Science of The Total Environment*, 409 (2011) 3732.
- [52] E. Bjorklund, G.G. Anskjaer, M. Hansen, B. Styrishave, B. Halling-Soerensen, *Science of The Total Environment*, 409 (2011) 2343.
- [53] E.H. Gendloff, W.L. Casale, B.P. Ram, J.H. Tai, J.J. Pestka, L.P. Hart, *Journal of Immunological Methods*, 92 (1986) 15.
- [54] J.-M.A. Schlaeppli, A. Kessler, W. Foery, *Journal of Agricultural and Food Chemistry*, 42 (1994) 1914.
- [55] P. Schneider, B.D. Hammock, *Journal of Agricultural and Food Chemistry*, 40 (1992) 525.
- [56] S.I. Wie, B.D. Hammock, *Journal of Agricultural and Food Chemistry*, 32 (1984) 1294.
- [57] M.H. Goodrow, R.O. Harrison, B.D. Hammock, *Journal of Agricultural and Food Chemistry*, 38 (1990) 990.
- [58] R.O. Harrison, M.H. Goodrow, B.D. Hammock, *Journal of Agricultural and Food Chemistry*, 39 (1991) 122.
- [59] E.J. Sundberg, *Epitope Mapping Protocols*, 2009, p. 23.
- [60] N.S. Lipman, L.R. Jackson, L.J. Trudel, F. Weis-Garcia, *ILAR Journal*, 46 (2005) 258.
- [61] J.D. Beatty, B.G. Beatty, W.G. Vlahos, *Journal of Immunological Methods*, 100 (1987) 173.
- [62] N.L. Benoiton, *Chemistry of Peptide Synthesis*, CRC Press, 2005, p. 25.
- [63] R.V. Hoffman, *Jonh Wiley and Sons INC., Publication, Second Edition (2004)*.
- [64] J.L. Greene, R.E. Clark, *United States Patent*, 3686307 (1972).
- [65] K.J. Merchant, *Tetrahedron Letters*, 41 (2000).
- [66] E.D. Laganis, B.L. Chenard, *Tetrahedron Letters*, 25 (1984) 5831.
- [67] M.-P. Marco, S. Gee, B.D. Hammock, *TrAC Trends in Analytical Chemistry*, 14 (1995) 415.
- [68] S.J. Gee, T. Miyamoto, M.H. Goodrow, D. Buster, B.D. Hammock, *Journal of Agricultural and Food Chemistry*, 36 (1988) 863.
- [69] A.S. Hill, D.P. McAdam, S.L. Edward, J.H. Skerritt, *Journal of Agricultural and Food Chemistry*, 41 (1993) 2011.
- [70] C.-W. Tsao, D. DeVoe, *Microfluidics and Nanofluidics*, 6 (2009) 1.
- [71] H. Becker, C. Gärtner, *Analytical and Bioanalytical Chemistry*, 390 (2008) 89.
- [72] J.S. Kuo, D.T. Chiu, *Lab on a Chip*, 11 (2011) 2656.
- [73] Y. Chen, L. Zhang, G. Chen, *Electrophoresis*, 29 (2008) 1801.
- [74] R. Truckenmüller, P. Henzi, D. Herrmann, V. Saile, W.K. Schomburg, *Microsystem Technologies*, 10 (2004) 372.
- [75] S. Shoji, M. Esashi, *Journal of Micromechanics and Microengineering*, 4 (1994) 157
- [76] D.J. Laser, J.G. Santiago, *Journal of Micromechanics and Microengineering*, 14 (2004) R35
- [77] P. Skaft-Pedersen, D. Sabourin, M. Dufva, D. Snakenborg, *Lab on a Chip*, 9 (2009) 3003.
- [78] D. Sabourin, D. Snakenborg, M. Dufva, *Journal of Micromechanics and Microengineering*, 19 (2009) 035021.
- [79] A.J. Conde, D. Sabourin, P. Skaft-Pedersen, M. Dufva, *15th International Conference on Miniaturized Systems for Chemistry and Life Sciences*, October 2-6, 2011, Seattle, Washington, USA (2011) 978.
- [80] Dropsens, *Screen Printed Carbon Electrode*, Llaneras, Spain, 2012.

- [81] D. Sabourin, D. Snakenborg, M. Dufva, *Microfluid Nanofluid*, 9 (2010) 87
- [82] A.A.S. Bhagat, P. Jothimuthu, A. Pais, I. Papautsky, *Journal of Micromechanics and Microengineering*, 17 (2007) 42
- [83] W. Zhang, S. Lin, C. Wang, J. Hu, C. Li, Z. Zhuang, Y. Zhou, R.A. Mathies, C.J. Yang, *Lab on a Chip*, 9 (2009) 3088.
- [84] W.K.T. Coltro, S.M. Lunte, E. Carrilho, *Electrophoresis*, 29 (2008) 4928
- [85] B. Huang, H. Wu, S. Kim, R.N. Zare, *Lab on a Chip*, 5 (2005) 1005
- [86] J. Ruzicka, E.H. Hansen, *Flow Injection Analysis (Second Edition)*, A Wiley-Interscience publication, New York, 1998.
- [87] B. Leca-Bouvier, L.J. Blum, *Analytical Letters*, 38 (2005) 1491.
- [88] S.M. Borisov, O.S. Wolfbeis, *Chemical Reviews*, 108 (2008) 423
- [89] P.D. Josephy, T. Eling, R.P. Mason, *The Journal of Biological Chemistry*, 257 (1982) 3669
- [90] P. Fanjul-Bolado, M.B. González-García, A. Costa-García, *Analytical and Bioanalytical Chemistry*, 382 (2005) 297.
- [91] G.A.E. Mostafa, *The Open Electrochemistry Journal*, 2 (2010) 22
- [92] M. Badihi-Mossberg, V. Buchner, J. Rishpon, *Electroanalysis*, 19 (2007) 2015.
- [93] M. Mehrvar, M. Abdi, *Analytical Sciences*, 20 (2004) 1113.
- [94] W.R. Everett, G.A. Rechnitz, *Analytical Letters*, 32 (1999) 1.
- [95] S. Sole, A. Merkoci, S. Alegret, *Critical Reviews in Analytical Chemistry*, 33 (2003) 89.
- [96] S. Sole, A. Merkoci, S. Alegret, *Critical Reviews in Analytical Chemistry*, 33 (2003) 127.
- [97] M. Trojanowicz, M.L. Hitchman, *TrAC Trends in Analytical Chemistry*, 15 (1996) 38.
- [98] O.A. Sadik, E. Jeanette Van, *Biosensors and Bioelectronics*, 11 (1996) i
- [99] E.S. Bos, A.A. van der Doelen, N.v. Rooy, A.H.W.M. Schuurs, *Journal of Immunoassay*, 2 (1981) 187.
- [100] G. Volpe, D. Compagnone, R. Draisci, G. Palleschi, *The Analyst*, 123 (1998) 1303
- [101] G. Liu, S.L. Riechers, C. Timchalk, Y. Lin, *Electrochemistry Communications*, 7 (2005) 1463
- [102] Y.-n. He, H.-y. Chen, J.-j. Zheng, G.-y. Zhang, Z.-L. Chen, *Talanta*, 44 (1997) 823.
- [103] E. Niranjana, B.E. Kumara Swamy, R. Raghavendra Naik, B.S. Sherigara, H. Jayadevappa, *Journal of Electroanalytical Chemistry*, 631 (2009) 1.
- [104] S. Daunert, L.G. Bachas, G.S. Ashcom, M.E. Meyerhoff, *Analytical Chemistry*, 62 (1990) 314.
- [105] R. Puchades, A. Maquieira, J. Atienza, *Critical Reviews in Analytical Chemistry*, 23 (1992) 301
- [106] W.U. De Alwis, B.S. Hill, B.I. Meiklejohn, G.S. Wilson, *Analytical Chemistry*, 59 (1987) 2688.
- [107] D.A. Palmer, T.E. Edmonds, N.J. Seare, *Analyst*, 117 (1992) 1679.
- [108] M. Stiene, U. Bilitewski, *Analyst*, 122 (1997) 155.
- [109] A.L. Ghindilis, P. Atanasov, M. Wilkins, E. Wilkins, *Biosensors and Bioelectronics*, 13 (1998) 113.
- [110] M.D. Carlo, M. Mascini, *Analytica Chimica Acta*, 336 (1996) 167
- [111] J.M. Fernández Romero, M. Stiene, R. Kast, M.D. Luque de Castro, U. Bilitewski, *Biosensors and Bioelectronics*, 13 (1998) 1107.
- [112] B. Lu, M.R. Smyth, R. O'Kennedy, *Analytica Chimica Acta*, 331 (1996) 97.

- [113] M.A. Gonzales-Martinez, R. Puchades, A. Maquieira, *TrAC Trends in Analytical Chemistry*, 18 (1999) 204
- [114] M.A. Gonzalez-Martinez, R. Puchades, A. Maquieira, *Food Technology and Biotechnology*, 35 (1997) 193
- [115] B. Uthuppu, N. Kostesha, S.M. Kiersgaard, J. Aamand, C. Jorgensen, M.H. Jakobsen, Optimization of immunochemistry for sensing techniques to detect pesticide residues in water, *IEEE Sensors Applications Symposium*, San Antonio, TX, USA, 2011.
- [116] T. Koseki, N. Kitabatake, E. Doi, *Journal of Biochemistry*, 103 (1988) 425



# Appendix I

## **Optimization of immunochemistry for sensing techniques to detect pesticide residues in water**

Basil Uthuppu, Natalie Kostesha, Jens Aamand, Claus Jørgensen, Spire M. Kiersgaard, Mogens Havsteen Jakobsen

Part of: Sensors Applications Symposium (ISBN: 978-1-4244-8063-0), 2011, Wiley-IEEE press,

Type: - Article in refereed conference proceedings

Presented at: IEEE Sensors Applications Symposium 2011, San Antonio, TX, USA



# Optimization of Immunochemistry for Sensing Techniques to Detect Pesticide Residues in Water

Basil Uthuppu, Natalie Kostesha, Mogens Havsteen

Jakobsen

Dept. of Micro- and Nanotechnology  
Technical University of Denmark (DTU)  
DK – 2800 Kgs Lyngby, Denmark  
basil.uthuppu@nanotech.dtu.dk

Spire M. Kiersgaard, Jens Aamand

Dept. of Geochemistry  
Geological Survey of Denmark and Greenland (GEUS)  
Østervoldgade 10  
DK-1350 Copenhagen K, Denmark

Claus Jørgensen

Dept. of Environmental Riskassessment, DHI  
Agern Alle 5  
DK – 2970 Hørsholm, Denmark

**Abstract** - We are working on the development of a real-time electrochemical sensor based on an immunoassay detection system to detect and quantify the presence of pesticide residues in ground water. Highly selective and sensitive immuno-reactions are being investigated to be optimised in order to bring them into the level of real-time in-line sensors. In this project a competitive immunoassay between surface immobilized 2,6-dichlorobenzamide (BAM) haptens and BAM present in the water sample using an anti-BAM monoclonal antibody is being described. 2,6-Dichlorobenzamide (BAM) is a degradation product of the herbicide, dichlobenil which has been used extensively in the past and it is among the most frequently found pesticide residues in European ground water. BAM is highly resistant to further degradation and is fairly soluble in water. We have synthesized and immobilized a small library of BAM haptens and compared the affinity constants of the antibody towards this library. Furthermore, since regeneration of the BAM-hapten surface is a prerequisite for the development of a real-time electrochemical sensor with immunoassay-based detection, studies on regeneration of surfaces, modified with the newly synthesized BAM-haptens has been preformed and compared and correlated to the measured affinity constants. By using conventional ELISA we were able to indicate that one of the immobilized BAM haptens with an intermediate affinity towards the anti-BAM antibody was better in terms of regeneration. Design and fabrication of a fully automated microfluidic based on this immunoassay and electrochemical detection are in progress.

**Key words:** 2,6-Dichlorobenzamide (BAM), BAM-haptens, anti-BAM monoclonal antibody, ELISA, electrochemistry, real-time sensor, surface modification.

## INTRODUCTION

During the last few decades, the use of pesticides increased tremendously all over the world. Studies show that pesticides and related chemicals can destroy the delicate balance in the ecosystem. Water bodies are the most vulnerable media to be polluted by pesticides since the pesticides or their residues

originating from human activity or agriculture farming are directly or indirectly discharged into the receiving waters. Thus, monitoring the extent of pollution of the water body demands important attentions in terms of social health issues. The European Union has set the limit for individual pesticide content in drinking water to 0.1 µg/L and a total of 0.5 µg/L for the total pesticide content.

Until recently, traditional chromatographic and spectroscopic methods were employed for the detection and quantification of pesticides in water and other sources [10, 11, 14]. Immunological methods for measuring the pesticide content in drinking water poses several advantages in price, speed and in being sensitive enough not to require any pre-concentration of the water sample. We have developed monoclonal antibodies to a variety of pesticides belonging to the group of s-triazines [48] and the degradation product of the pesticide Dichlobenil, 2,6-dichlorobenzamide (BAM) [49] (Fig. 1). The latter monoclonal antibody has very low cross-reactivity towards structurally related compounds, and a quantitative enzyme-linked immunosorbent assay (ELISA) was developed based on competitive binding of the antibody

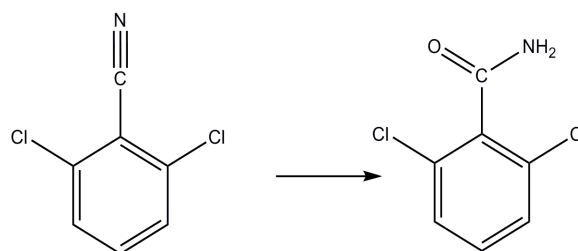


Figure 1. Chemical structures of the pesticide Dichlobenil and the degradation product 2,6-dichlorobenzamide (BAM).

between BAM in solution and BAM hapten immobilized in the



micro-wells. The assay is now validated and run as a routine analysis in Denmark.

As an alternative to conventional coating of micro-plates, the assay is based on direct covalent immobilization of the hapten in the micro-wells. We achieved a surface which requires a very short time for immobilization, very low CV and long time stability (several years) when stored dry.

Fully automated immuno sensing in combination with microfluidics and miniaturized transduction methods holds a great promise for in-line, on-site control of drinking water quality. Unlike the ELISA technology, which enables the analysis of many samples in parallel with internal calibration, the miniaturized system runs each analytical cycle in a sequential manner more like a chromatographic system. Being a heterogeneous assay this means that the surface must be regenerated between each analytical cycle, allowing for blanks and standards to be injected. The covalent nature of the above described BAM assay makes it an attractive candidate for an in-line immuno sensor system, but also a good model system and a potential indicator for water contamination by other pesticides and their degradation products.

The regeneration between each analytical cycle requires the right balance between binding of the antibody to the immobilized hapten and the ability to be removed again under relatively mild conditions. In the original ELISA assay, the same hapten was used for immunization as well as for immobilization. Design of suitable haptens is critical, not only for immunization, but also for the subsequent assay performance in terms of regeneration. We therefore decided to synthesize a small hapten library with structural variations compared to the original hapten with the purpose of optimizing assay performance, especially by measuring the affinity constants of the monoclonal antibody towards these immobilized haptens, and the influence of affinity constants on regeneration of the hapten surfaces.

### I. HAPTEN LIBRARY

The new haptens together with the original BAM hapten that used for immunization and generation of the monoclonal antibody are shown in Fig. 2. Besides the BAM haptens, also the nitrile precursors were synthesized and tested (nitrile instead of the simple amide in BAM, like in dichlobenil). In our original paper, the nitrile precursor was not purified and characterized. All haptens were covalently immobilized in micro wells by conjugating the haptens to the carrier protein ovalbumin followed by second conjugation to the photo probe anthraquinone and tested as described in [49]

### II. OPTIMIZATION OF THE IMMUNOASSAY –AFFINITY CONSTANTS

Affinity constants ( $K_{aff}$ ) for new structurally different BAM-hapten molecules were measured in order to quantify and compare the interaction of anti-BAM monoclonal antibody with them, on ELISA plates as described by Beatty et al. [61] with two-fold serial dilution of antibody and two different concentrations of each immobilized BAM-hapten.. To keep standard assay conditions, concentrations of all the BAM-haptens were estimated by UV-Vis spectroscopy and adjusted to approximately 0.8 mg/mL. The antibody concentration was determined by performing Bradford protein assay using bovine serum albumin (BSA) as the standard and was found to be 1.0 mg/mL.

The interaction between anti-BAM antibody and each BAM-hapten were treated as sigmoidal dose-response curves; the data was fitted to the four-parameter logistic equation using GraphPad Prism software (version 4.03 for windows, GraphPad Prism, San Diego, CA, USA). A non-linear regression was performed to obtain effective concentration ( $EC_{50}$ ) values. Using  $EC_{50}$  values,  $K_{aff}$  of anti-BAM monoclonal antibody to each BAM-hapten molecules were calculated according to the equation described in [61] and presented in Table 1. The affinity of anti-BAM antibody towards the various BAM-haptens was found to be different. It has lower affinities towards the newly synthesised BAM-haptens than the original one due to the structural difference (Fig. 2). We were not able to calculate  $K_{aff}$  to BAM-hapten 02 probably, due to the low affinity of anti-BAM antibody towards the hapten.

Though antibodies are capable of binding an antigen with high degree of affinity and specificity, it is not uncommon that they show cross-reactivity with structurally similar, yet distinct, antigenic molecules [59]. Relatively minor changes in antigen structure can bring about considerable changes in the strength of interaction, because a relatively smaller component of an antigen is being recognised by the antibody and hence they can cross-react with similar epitopes on such antigens, but with less affinity [60]. This means cross-reaction of anti-BAM antibody with the newly synthesized BAM-haptens is probable if they keep some of the antigenic epitopes in their structures. Similar to original BAM-hapten, all the new BAM-haptens retain the amide group on the ring. They differ from the original BAM-hapten structure in the length of the tail linker (BAM-hapten 02), in number of chlorine atoms on the ring (BAM-hapten 03 and 04) or the position of linker attached to the ring (BAM-hapten 04) (Fig. 2).

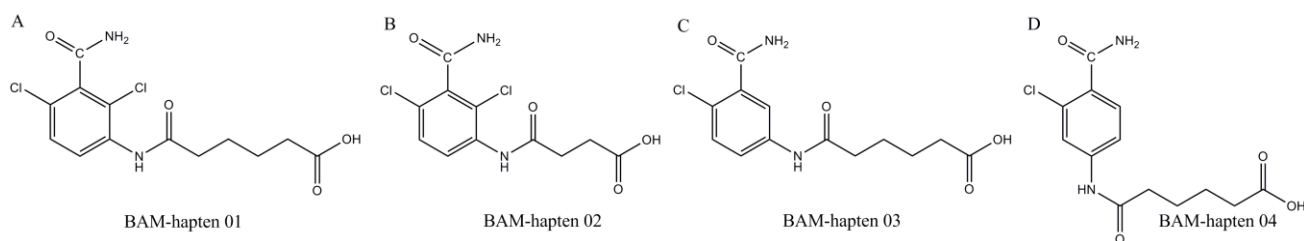


Figure 2. Chemical structures of original BAM hapten (BAM-hapten 01) and the three new analogues. Compared to BAM-hapten 01, BAM-hapten 02 has a shorter linker, BAM-hapten 03 has the same linker but one of the chlorine atoms is missing on the ring, and BAM-hapten 04 has the same linker, but the position is moved from ortho- to para-position relative to the amide functionality and missing one chlorine atom on the ring.

Haptens	$K_{aff}$ (1/nM)
BAM-hapten 01	0.5836
BAM-hapten 02	NA
BAM-hapten 03	0.2176
BAM-hapten 04	0.3081

From the results, it is evident that the amide group on the ring is the primary epitope for the antibody. This is also supported by the fact that anti-BAM antibody which is raised against BAM-hapten 01 binds strongly with the analyte BAM molecules in water sample. Since the electronegativity of the two chlorine atoms on the ring has a prominent role in anti-BAM antibody – BAM-hapten original interaction [49], losing one of these chlorine atoms can impart a considerable change in the interaction and affinity which is evident from the reduced anti-BAM antibody – BAM-hapten 03 and 04 interaction. In the case of BAM-hapten 04, the loss of one of the chlorine atoms is compensated by the change in orientation of the antigenic sites due to the para position of the linker relative to the most important epitope motifs. In the case of BAM-hapten 02, though it has retained all the major epitope motifs, reduction of the linker length almost totally inhibits binding. Our conclusion is that the amide bond is the primary epitope, followed by the chlorine atoms while the spacer do not participate in the motif, but only serves to present the epitopes in the right way. Although we only have tested a small hapten library, it still gives insight to how changes in the hapten structure can affect on antibody/hapten interactions.

### III. OPTIMIZATION OF THE IMMUNOASSAY – REGENERATION

To test and optimize regeneration conditions, microtitre plates were prepared as described in [49], keeping the immobilized BAM-haptens concentration the same. Preliminary investigations showed that a 100 mM glycine.HCl buffer of pH 1.8 was close to the optimum. Figure 3 shows a

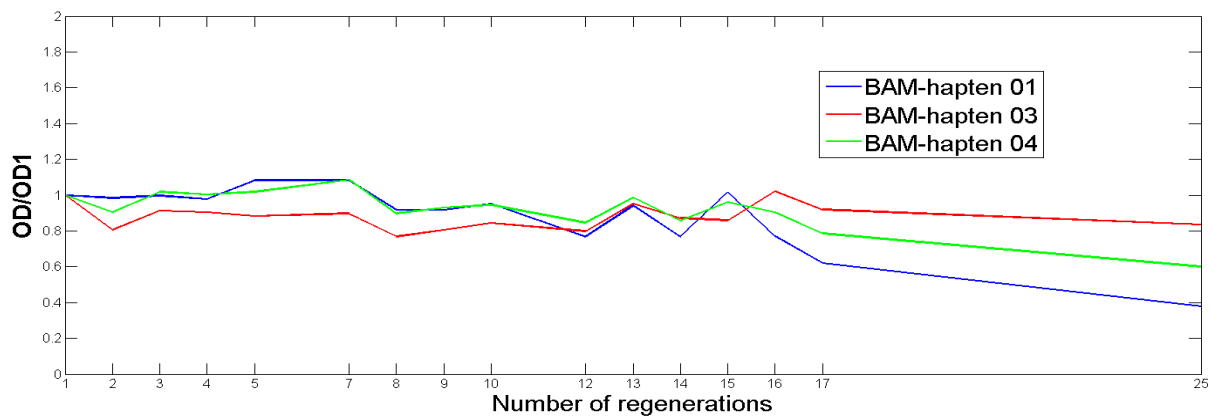


Figure 3. Regeneration results of 3 different immobilized BAM-haptens. In this experiment a 96-well polysorp microtitre plate was immobilized with the same concentration of all BAM-haptens. In each cycle, same concentration of anti-BAM antibody was added to all the wells and incubated for 1 hour. After washing, TMB substrate solution was added and the OD values were read after 15 minutes. After washing, 100 mM glycine.HCl buffer of pH 1.8 was added for 10 min. to remove antibody. A new TMB substrate reaction was performed to confirm complete removal of the antibody. This analytical cycle was repeated until 17th cycle. After 17th cycle, eight more hybridization and stripping were performed without substrate reaction until the full cycle was repeated at the 25th cycle. All data are plotted relative to the signal intensity of the first cycle.

typical result after 25 analytical cycles.

On the basis of results presented in Table I, we were able to find the correlation in interactions between anti-BAM antibody and various BAM-haptens, this knowledge can tremendously prove the regeneration step. From the obtained results we can conclude that BAM-hapten 03-hapten binds the antibody too weakly to keep a good signal to noise ratio, but at the same time is best regarding regeneration. BAM-hapten 01 has higher affinity and hence the best signal to noise ratio but at the same time faces the most difficulties in maintaining the surface activity. BAM-hapten 04 with the intermediate affinity towards the antibody and with a reasonable signal to noise ratio is a promising candidate when this assay is moved to a fully automated immuno sensing system in combination with microfluidics and miniaturized transduction methods.

### IV. OUTLOOK

Moving the optimized immuno sensing assay to a fully automated microfluidic set-up, several miniaturized transducer principles can be applied. Immunosensors can broadly be classified into micromechanical, optical, piezoelectrical and electrochemical. We will use an electrochemical approach, in which the oxidized substrate solution will be passed by screen printed carbon paste electrode. The carbon paste electrode will act as the working electrode reducing the oxidized substrate where the current will be measured by a potentiostat. Initial experiments (data not shown) have shown an excellent quantitative correlation between the amount of oxidized substrate and the obtained current peaks with sensitivity in the same order as the conventional ELISA. The immunosensor is schematically depicted in Fig. 4, with an insert of the screen printed carbon paste electrode.

Other factors required for unattended on-site operation is the long term stability of the antibody and TMB substrate solutions. Preliminary results suggest that unattended operation for at least one month can be achieved.

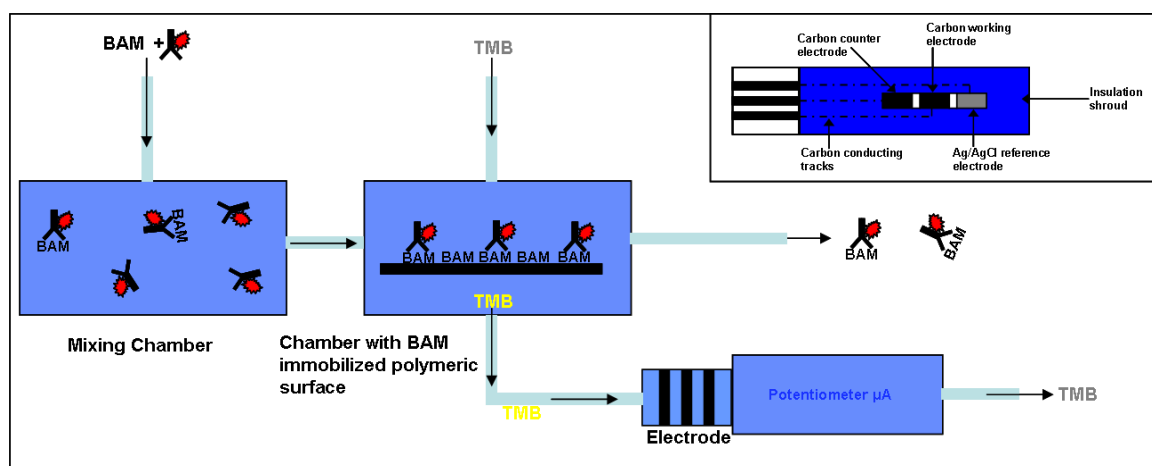


Figure 4. Schematic diagram of the biosensor. Antibody and sample is injected into a mixing chamber. After a short incubation, the mixture is transferred to the solid support containing immobilized BAM-haptens. After a short incubation time unbound antibody is washed out and TMB substrate solution added. Finally the oxidized substrate solution is passed by the electrode and the current peak recorded. After regeneration and washing, the analytical cycle can be repeated. The inserted picture shows the screen printed electrode in detail.

## V. CONCLUSION

An existing immunoassay between anti-BAM monoclonal antibody and BAM-hapten entity immobilized on polymeric surface has been optimized and feasibility of using this well-established immunoassay as the sensing technique of a real-time, in-line sensor has been investigated. We were able to perform effective surface modifications using new BAM-haptens and it was found that BAM-hapten 04 is a better candidate in terms of regeneration aspects. However, in the future it would be interesting to perform a combinatorial analysis of a sequence of light and heavy variable chains of anti-BAM monoclonal antibodies and a library of hapten molecules. Such studies may help us to understand more about interactions between anti-BAM monoclonal antibodies and BAM-haptens and thus to improve the sensor properties.

By combining the optimised BAM ELISA with an electrochemical detection system, a real-time biosensor can be achieved for quantification of the pesticide residue BAM in ground water. A second generation of sensors which can quantify multiple analytes at the same time is a future goal of this project. By combining sensing technology, fluorescent and electrochemical detections we can improve not only the sensor sensitivity but also data reliability.

## ACKNOWLEDGEMENT

This work was supported by the Danish Council for Strategic Research (grant no 2104-06-0006) and Copenhagen Energy.

## REFERENCES

- <sup>1</sup> Jensen, G.G., et al., Determination of 2,6-dichlorobenzamide and its degradation products in water samples using solid-phase extraction followed by liquid chromatography-tandem mass spectrometry. *Journal of Chromatography A*, 2009. 1216(27): p. 5199-5206.
- <sup>2</sup> Baraud, L., et al., A multi-residue method for characterization and determination of atmospheric pesticides measured at two French urban and

rural sampling sites. *Analytical and Bioanalytical Chemistry*, 2003. 377(7): p. 1148-1152.

<sup>3</sup> Porazzi, E., et al., GC-MS analysis of dichlobenil and its metabolites in groundwater. *Talanta*, 2005. 68(1): p. 146-154.

<sup>4</sup> Bruun, L., et al., New monoclonal antibody for the sensitive detection of hydroxy-s-triazines in water by enzyme-linked immunosorbent assay. *Analytica Chimica Acta*, 2000. 423(2): p. 205-213.

<sup>5</sup> Bruun, L., et al., A quantitative enzyme-linked immunoassay for the detection of 2,6-dichlorobenzamide (BAM), a degradation product of the herbicide dichlobenil. *Journal of Immunological Methods*, 2000. 240(1-2): p. 133-142.

<sup>6</sup> Beatty, J.D., B.G. Beatty, and W.G. Vlahos, Measurement of monoclonal antibody affinity by non-competitive enzyme immunoassay. *Journal of Immunological Methods*, 1987. 100: p. 173-179.

<sup>7</sup> Sundberg, E.J., *Structural Basis of Antibody-Antigen Interactions*, in *Epitope Mapping Protocols*. 2009. p. 23-36.

<sup>8</sup> Lipman, N.S., et al., *Monoclonal Versus Polyclonal Antibodies: Distinguishing Characteristics, Applications, and Information Resources*. *ILAR Journal*, 2005. 46(3): p. 258-268.

## Appendix II

### **Optimization of an immunoassay of 2,6-dichlorobenzamide (BAM) and development of regenerative surfaces by surface modification with newly synthesised BAM hapten library**

Basil Uthuppu, Jens Aamand, Claus Jørgensen, Spire M. Kiersgaard,  
Natalie Kotesha, Mogens Havsteen Jakobsen

Type: - Full Paper, submitted to Analytica Chimica Acta on 2 November 2011  
Status on 8 December 2011: Under review



1 Optimization of an immunoassay of 2,6-dichlorobenzamide (BAM) and  
2 development of regenerative surfaces by surface modification with newly  
3 synthesised BAM hapten library

4  
5 Basil Uthuppu<sup>a\*</sup>, Jens Aamand<sup>b</sup>, Claus Jørgensen<sup>c</sup>, Spire M. Kiersgaard<sup>b</sup>,  
6 Natalie Kostesha<sup>a</sup>, Mogens Havsteen Jakobsen<sup>a</sup>

7  
8 <sup>a</sup>*Dept. of Micro-and Nanotechnology, Technical University of Denmark (DTU), Produktionstorvet 423/220, DK – 2800 Kgs*  
9 *Lyngby, Denmark*

10 <sup>b</sup>*Dept. of Geochemistry, Geological Survey of Denmark and Greenland (GEUS), Østervoldgade 10, DK-1350 Copenhagen K,*  
11 *Denmark*

12 <sup>c</sup>*Dept. of Environmental Riskassessment, DHI, Agern Alle 5, DK – 2970 Hørsholm, Denmark*

13  
14 **Abstract**

15 Dichlobenil is an extensively used herbicide worldwide which is transformed to the mobile 2,6-  
16 dichlorobenzamide (BAM) in soil. BAM has been found in many European groundwater resources that  
17 are exploited for drinking water. Currently, immunoassay based monitoring technique is being  
18 employed to quantitatively detect BAM in water samples. In this work, as a starting step of moving this  
19 heterogeneous assay from ELISA plates to an in-line real-time sensor, the immunoassay is optimized in  
20 terms of surface (polymer) regeneration. We have synthesized and immobilized on surfaces a small  
21 library of BAM haptens which are slightly different in chemical structure and compared the affinity  
22 constants of the monoclonal antibody HYB 273 towards this library. By using ELISA technology, we  
23 also have checked the regeneration potentials of the haptens, correlated these results to the affinity  
24 constants and found that BAM hapten with an intermediate affinity has better regeneration potential.

25  
26 *Key words:* 2,6-Dichlorobenzamide; BAM; dichlobenil, BAM-haptens; anti-BAM monoclonal antibody; ELISA;  
27 electrochemistry; real-time sensor; in-line sensor; surface modification; surface regeneration.

28  
29 *Abbreviations:* BAM: 2,6-dichlorobenzamide; ELISA: Enzyme linked immuno sorbent assay; HYB 273: anti-BAM monoclonal  
30 antibody; RB flask: Round bottomed flask; TLC-Thin layer chromatography; UV: ultraviolet radiation; hapt: hapten; OA:

31 ovalbumin; EQ 0028: photoactive anthraquinone entity; UV-Vis: ultraviolet-visible spectroscopy; HRP: horseradish peroxidase  
32 enzyme; TMB: 3,3',5,5'-tetramethylbenzidine dihydrochloride (substrate for HRP); [Ag]: concentration of hapten conjugate;  
33 OD: optical density (absorption values from UV-Vis analysis); RT: room temperature.

34

35 \*Corresponding author. Tel.: +4545258143; fax: +4545887762

36 E- mail address: [basil.uthuppu@nanotech.dtu.dk](mailto:basil.uthuppu@nanotech.dtu.dk)

37

## 38 **1. Introduction**

39 Lack of safe-drinking water raises many troubles to the mankind. Reports say that one billion of  
40 the world's population do not have access to clean and safe water[12, 90]. Monitoring the quality of  
41 drinking water thus becomes as important as its preservation. A rapid, reliable and continuous  
42 monitoring is also highly demanded for homeland security reasons to protect drinking water from  
43 intentional contaminations. Pollution by pesticides poses a real threat to the availability of clean water.  
44 Water bodies are the most vulnerable media to be polluted by pesticides since the pesticides or their  
45 residues originating from human activity or agriculture farming are directly or indirectly discharged  
46 into the receiving waters. The European Union has set the limit for individual pesticide in drinking  
47 water to 0.1 µg/L[29, 30] and a total of 0.5 µg/L for all pesticides. Detection and quantification of such  
48 low concentrations require highly sensitive analytical techniques. Normally, traditional methods like  
49 gas chromatography (GC), high-pressure liquid chromatography (HPLC), capillary electrophoresis  
50 (CE) and mass spectrometry (MS) are being employed[10-12, 117].

51 Use of immunological methods for environmental pesticide analysis [29, 30, 118] offers several  
52 advantages in terms of price, speed of analysis and due to their high sensitivity, no sample pre-  
53 treatments like purification, concentration or derivatization required. We have developed monoclonal  
54 antibodies recognising a variety of pesticides including the s-triazine group[119], their degradation  
55 products[49] and 2,6-dichlorobenzamide (BAM) [49]. BAM (Fig. 1B), a degradation residue of  
56 dichlobenil (Fig. 1A) is highly resistant to further degradation and is fairly soluble in water. The anti-  
57 BAM monoclonal antibody has very low cross-reactivity towards structurally related compounds, and a  
58 quantitative enzyme-linked immunosorbent assay (ELISA) was developed based on competitive  
59 binding of the antibody to BAM in solution and BAM haptens immobilized on micro-wells. In the  
60 present work the BAM immunoassay is chosen as a model system to investigate the possibility of  
61 bringing current state of the art immunological methods into a fully automated in-line immunosensor in  
62 combination with microfluidics and miniaturized electrochemical transduction method.

63 A detailed description of the BAM immunoassay is reported by Bruun *et al.*[49]. In this assay, the  
64 BAM hapten was covalently immobilized on the micro-wells and thereby achieved a surface that  
65 requires a very short time for immobilization (30 minutes of UV exposure), low coefficient of variation  
66 (CV) and long shelf life (several years) when stored dry.

67 Unlike the ELISA technology, which enables analysis of many samples in parallel with internal  
68 calibration, the miniaturized in-line immunosensing system runs each analytical cycle in a sequential  
69 manner. Being a heterogeneous assay, this means that the surface must be regenerated between each  
70 analytical cycle, allowing for blanks and standards to be injected. The regeneration requires the right  
71 balance between binding of the antibody to the surface immobilized hapten and then its removal under  
72 mild regeneration conditions before next analysis. In the original assay, the same hapten (hapt A) (Fig.  
73 1C) was used for immunization as well as for immobilization. Preliminary attempts to regenerate hapt  
74 A immobilised surfaces resulted in a significant lowering of the signal after a few cycles (8 cycles). We  
75 hypothesised that lowering the antibody-hapten interaction by redesigning the haptens may improve the  
76 potential for regeneration of the surfaces. It is not uncommon that antibodies show cross-reactivity to  
77 structurally similar, yet distinct, antigenic molecules[59]. Relatively minor changes in an antigen  
78 structure may lead to considerable changes in the strength of the antibody-hapten interaction, because a  
79 relatively smaller component of an antigen is being recognised by the antibody and hence the same  
80 antibody can interact with structurally different antigens, but with lower affinity[60].

81 In the present research we have synthesised three new haptens (Fig. 2) and compared the affinity  
82 of the anti-BAM antibody (HYB 273) to these haptens. It is shown that the surface activity towards  
83 HYB 273 can be changed in a way improving regeneration of the active surface of a micro-well. Like  
84 the original hapten, the new haptens retain the amide group on the ring, but they differ in the length of  
85 the linker (hapt B), in number of chlorine atoms on the ring (hapt C and D) or the position of linker  
86 attached to the ring (hapt D).

87

## 88 2. Experimental

### 89 2.1. Reagents, buffers and materials

90 2,6-dichloro-3-nitrobenzotrile (98%) [5866-98-8] was from Alfa Aesar, Germany, 4-amino-2-  
91 chloro-benzotrile (99%) [20925-27-3] was from Aldrich, Switzerland, 2-chloro-5-nitrobenzotrile  
92 (99%) [16588-02-6], methyl 4-chloro-4-oxobutanoate (methyl succinyl chloride, 97%) [1490-25-1] and



93 potassium trimethylsilanolate ( $\text{KOSi}(\text{CH}_3)_3$ , 90%) [10519-96-7] were from Aldrich, USA, methyl  
94 adipoylchloride (97%) [35444-44-1] was from Aldrich, UK, lithium hydroxide monohydrate  
95 ( $\text{LiOH}\cdot\text{H}_2\text{O}$ , 98%) [1310-66-3] and acetic acid were from Sigma-Aldrich, USA., hydrochloric acid,  
96 petroleum ether, dichloromethane and ethanol were from Sigma-Aldrich, Germany, tetrahydrofuran  
97 (THF) was from Sigma-Aldrich, UK, ethylacetate was from Fluka, Mexico, iron powder (Fe), silica gel  
98 60 (0.04-0.063) were from Merck, Germany and Sodiumcarbonate ( $\text{Na}_2\text{CO}_3$ ) was from Sigma, USA.  
99 Benzotriazol-1-yloxy-tris(dimethylamino)phosphonium hexafluorophosphate (BOP) was from Nova  
100 biochem, Germany. *N*-ethyl-diisopropylamine (DIEA), dimethylsulfoxide (DMSO) and sulphuric acid  
101 ( $\text{H}_2\text{SO}_4$ ) were from Fluka, Germany, TMB-Plus substrate (3,3',5,5'-tetramethylbenzidine  
102 dihydrochloride) was from KEM EN TEC, Denmark, ovalbumin was from Sigma, USA., Brad-ford  
103 reagent was from Sigma-Aldrich, USA, BAM monoclonal antibodies (Bruun et al., 2000) provided by  
104 Statens Serum Institut, Denmark, phosphate buffered saline (PBS) powder in pouches was from Sigma,  
105 USA, PBS with Tween<sup>®</sup> 20 (PBST) tablets were from Fluka, Sweden. Sodiumbicarbonate ( $\text{NaHCO}_3$ )  
106 was from Fluka, Germany. Glycin hydrochloride and BSA (Bovine Serum Albumin) were from Sigma,  
107 USA.

108 PBS buffer of pH 7.4 (1 M) was prepared by dissolving one packet of buffer powder in 1000 mL  
109 of milli-Q water. PBST buffer of pH 7.4 (1 M) was made by dissolving one PBST tablet in 1000 mL of  
110 milli-Q water. Conjugation buffer was made by dissolving 1.68 g of sodium hydrogen carbonate in 200  
111 mL of Milli-Q water (100 mM) and the pH was adjusted to 8.1. Regeneration buffer was made by  
112 dissolving 1.12g of glycine hydrochloride in 100 mL of Milli-Q water (100 mM) and the pH was  
113 adjusted to 2.

114 Polysorp microtitre plates were from Nunc<sup>®</sup>, Denmark. Milli-Q water purifier was from Millipore,  
115 USA and TLC aluminium sheets coated with silica gel 60 F<sub>254</sub> with layer thickness 0.2 mm was from  
116 Merck, Germany.

117

## 118 2.2. Instruments

119 The Hot air oven was a BINDER with temperature and time control (Max. temperature: 250°C).  
120 UV reaction chamber was UV Stratalinker 2400 from Stratagene. The UV spectrometer was Shimadzu  
121 UV – 1800 (range: 190 – 1100) and the spectra were analysed by UVProbe 2.33 software. The  
122 microtitre plate reader was Thermomax with the software SOFTmax<sup>®</sup> from Molecular Devices, USA.

123 The Plate washing instrument was Wellwash Ascent from Labsystems (Beverly MA, USA). The NMR  
124 was Varian Mercury 300 MHz and the software used to analyse the spectra was MestReNova.

125

### 126 2.3. Synthesis of Haptens

127 Synthesis of hapten library was achieved by modifying the three stage synthesis route described  
128 by Bruun *et al.* [49]. The modified scheme (Fig. 3A) made it possible to obtain nitrile derivatives of  
129 each of the new haptens (Fig. 3B) giving altogether eight haptens named hapt A, hapt B, hapt C, hapt  
130 D, hapt E, hapt F, hapt G and hapt H. Final products and intermediates were identified using <sup>1</sup>H NMR  
131 and the purity of the compounds was checked by Thin Layer Chromatography (TLC).

132

#### 133 2.3.1. Synthesis of hapt A

##### 134 2.3.1.1. 3-amino-2,6-dichlorobenzonitrile

135 3-nitro-2,6-dichlorobenzonitrile (10 g, 46.1 mmol) and iron powder (7.7 g, 138.1 mmol) were  
136 swirled in absolute ethanol (200 mL) in a round bottomed flask (R.B. flask) fitted with a water  
137 condenser and a dropping funnel in a nitrogen atmosphere. Acetic acid (15.8 mL, 276.6 mmol) was  
138 added dropwise to avoid vigorous reactions. The mixture was heated to reflux and followed by TLC  
139 and finally completed by the addition of conc. HCl (2 mL) after 1 hr of boiling. Milli Q water (750 mL)  
140 was added to precipitate the crude product. The crude product was then centrifuged and dried at 50°C.  
141 The product was extracted from the crude by the Soxhlet method using ethylacetate as solvent followed  
142 by purification by flash chromatography (eluent: ethylacetate / petroleum ether 1:1) and used in the  
143 next step. Yield: 97%. <sup>1</sup>H NMR (CDCl<sub>3</sub>) δ : 7.19 (d, 1H), 6.83 (d, 1H), 4.22 (s, 2H). *R<sub>f</sub>*: 0.38  
144 (Ethylacetate / petroleum ether 1:1).

145

##### 146 2.3.1.2. methyl 6-(2,4-dichloro-3-cyanophenylamino)-6-oxohexanoate

147 Purified 3-amino-2,6-dichlorobenzonitrile (1.53 g, 10 mmol) was dissolved in CH<sub>2</sub>Cl<sub>2</sub> (50 mL) in  
148 an R.B. flask. 5% w/v Na<sub>2</sub>CO<sub>3</sub> (125 mL) was added followed by drop wise addition of Methyl 6-  
149 chloro-6-oxohexanoate (methyl adipoylchloride, 7.2 mL, 30 mmol) dissolved in dichloromethane (25  
150 mL). The reaction mixture was stirred at room temperature till completion indicated by TLC. On  
151 completion, the mixture was transferred to a separatory funnel and the organic layer was washed with  
152 5% w/v Na<sub>2</sub>CO<sub>3</sub> solution three times. The product was then isolated from the organic layer by  
153 evaporating CH<sub>2</sub>Cl<sub>2</sub> after drying over MgSO<sub>4</sub>. Yield: 99.5%. <sup>1</sup>H NMR (CDCl<sub>3</sub>) δ : 8.61 (d, 1H), 7.69 (s,

154 1H), 7.41 (d, 1H), 3.67 (s, 3H), 2.49 (t, 2H), 2.37 (m, 2H), 1.72 (m, 4H).  $R_f$ : 0.32 (Ethylacetate /  
155 petroleum ether 1:1).

156

157 2.3.1.3. 6-(3-carbamoyl-2,4-dichlorophenylamino)-6-oxohexanoic acid (hapt A)

158 Methyl 6-(4-chloro-3-cyanophenylamino)-6-oxohexanoate (0.33 g, 1 mmol) and potassium  
159 trimethylsilanolate (0.8 g, 6 mmol) were dissolved in tetrahydrofuran (5 mL) and heated to reflux  
160 overnight in a nitrogen atmosphere. The brown precipitate formed was completely dissolved in Milli Q  
161 water and the aqueous layer acidified with 1 M HCl. The final product was extracted with ethylacetate,  
162 and the product obtained by evaporating the solvent after drying over  $MgSO_4$ . Yield: 60%. Off-white  
163 powder obtained was shown to be pure by TLC.  $R_f$ : 0.45 (Ethylacetate / acetic acid 95:5).  $^1H$  NMR  
164 (DMSO- $d_6$ )  $\delta$ : 12.1 (s, 1H), 7.88 (s, 1H), 7.75 (d, 1H), 7.51 (d, 1H), 2.47 (t, 2H), 2.3 (m, 2H), 1.64 (m,  
165 2H), 1.56 (m, 2H).

166

167 2.3.2. Synthesis of hapt B

168 2.3.2.1. methyl 4-(2,4-dichloro-3-cyanophenylamino)-4-oxobutanoate

169 Purified 3-amino-2,6-dichlorobenzonitrile from 2.3.1.1 (7.5 g, 4 mmol) was dissolved in  $CH_2Cl_2$   
170 (40 mL) in an R.B. flask. 5% w/v  $Na_2CO_3$  (80 mL) was added into it. Methyl 4-chloro-4-oxobutanoate  
171 (methyl succinyl chloride, 1.5 mL, 12 mmol) dissolved in  $CH_2Cl_2$  (15 mL) was added drop-wise. The  
172 reaction was then carried out as described in Section 2.3.1.2. Yield: 99.3%.  $^1H$  NMR ( $CDCl_3$ )  $\delta$ : 8.6 (d,  
173 1H), 8.04 (s, 1H), 7.4 (d, 1H), 3.72 (s, 3H), 2.77 (m, 4H).  $R_f$ : 0.42 (Ethylacetate / petroleum ether 1:1).

174

175 2.3.2.2. 4-(3-carbamoyl-2,4-dichlorophenylamino)-4-oxobutanoic acid (hapt B)

176 The same procedure as in Section 2.3.1.3 was done for methyl 4-(2,4-dichloro-3-  
177 cyanophenylamino)-4-oxobutanoate (1.040 g, 3.5 mmol) with potassium trimethylsilanolate (2.7 g, 21  
178 mmol) in THF (15 mL) to get hapt B. Yield: 60%.  $^1H$  NMR (DMSO- $d_6$ )  $\delta$ : 12.15 (s, 1H), 8.08 (s, 2H),  
179 7.8 (s, 1H), 7.69 (d, 1H), 7.42 (d, 1H), 2.63 (t, 2H), 2.49 (m, 2H).  $R_f$ : 0.28 (ethylacetate / acetic acid  
180 95:5).

181

182

183

184 2.3.3. Synthesis of hapt C

185 2.3.3.1. 5-amino-2-chlorobenzonitrile

186 2-chloro-5-nitrobenzonitrile (8.4 g, 46.1 mmol) was reduced with Fe powder (7.7g, 138.1 mmol),  
187 acetic acid (15.8 mL) and conc. HCl (2 mL) to 5-amino-2-chlorobenzonitrile as explained in Section  
188 2.3.1.1. Yield: 85%.  $^1\text{H NMR}$  ( $\text{CDCl}_3$ )  $\delta$ : 7.24 (d, 1H), 6.91 (d, 1H), 6.8 (dd, 1H), 3.91 (s, 2H).  $R_f$ : 0.35  
189 (ethylacetate / petroleum ether 1:1).

190

191 2.3.3.2. methyl 6-(4-chloro-3-cyanophenylamino)-6-oxohexanoate

192 Purified 5-amino-2-chlorobenzonitrile (1.53 g, 10 mmol) was coupled with methyl 6-chloro-6-  
193 oxohexanoate (methyl adipoylchloride, 7.2 mL, 30 mmol) as explained in Section 2.3.1.2. Yield: 99%.  
194  $^1\text{H NMR}$  ( $\text{CDCl}_3$ )  $\delta$ : 8.12 (d, 1H), 7.77 (dd, 1H), 7.55 (d, 1H), 4.91 (s, 1H), 3.65 (s, 3H), 2.36 (m, 4H),  
195 1.67 (m, 4H).  $R_f$ : 0.23 (ethylacetate / petroleum ether 1:1).

196

197 2.3.3.3. 6-(3-carbamoyl-4-chlorophenylamino)-6-oxohexanoic acid (hapt C)

198 Hydrolysis of methyl 6-(4-chloro-3-cyanophenylamino)-6-oxohexanoate (0.3 g, 1 mmol) by  
199 potassium trimethylsilanolate (0.8 g, 6 mmol) was done as described in Section 2.4.1.3. to obtain hapt  
200 C. Yield: 70%.  $^1\text{H NMR}$  ( $\text{DMSO-d}_6$ )  $\delta$ : 10.22 (s, 1H), 7.88 (d, 1H), 7.71 (d, 1H), 7.62 (dd, 1H), 7.56  
201 (s, 2H), 7.34 (s, 1H), 2.31 (t, 2H), 2.20 (m, 2H), 1.50 (m, 4H).  $R_f$ : 0.51 (ethylacetate / acetic acid 95:5).

202

203 2.3.4. Synthesis of hapt D

204 2.3.4.1. methyl 6-(3-chloro-4-cyanophenylamino)-6-oxohexanoate

205 4-amino-2-chlorobenzonitrile (commercially available, 1.5 g, 10 mmol) is coupled with methyl 6-  
206 chloro-6-oxohexanoate (methyl adipoylchloride, 7.2 mL, 30 mmol) as described in Section 2.3.1.2.  
207 Yield: 78%.  $^1\text{H NMR}$  ( $\text{CDCl}_3$ )  $\delta$ : 8.14 (s, 1H), 7.95 (d, 1H), 7.58 (dd, 1H), 7.38 (d, 1H), 3.7 (s, 3H),  
208 2.42 (m, 4H), 1.74 (m, 4H).  $R_f$ : 0.26 (ethylacetate / petroleum ether 1:1).

209

210 2.3.4.2. 6-(4-carbamoyl-3-chlorophenylamino)-6-oxohexanoic acid (hapt D)

211 Hydrolysis of methyl 6-(3-chloro-4-cyanophenylamino)-6-oxohexanoate (0.3 g, 1 mmol) by  
212 potassium trimethylsilanolate (0.8 g, 6 mmol) was done as described in 2.3.1.3. to obtain hapt D. Yield:

213 75%. <sup>1</sup>H NMR (DMSO-d<sub>6</sub>) δ : 10.62 (s, 1H), 8.17 (s, 1H), 7.95 (d, 1H), 7.70 (d, 1H), 7.52 (s, 2H), 7.28  
214 (s, 1H), 2.41 (t, 2H), 2.35 (m, 2H), 1.65 (m, 4H). *R<sub>f</sub>*: 0.54 (ethylacetate / acetic acid 95:5).

215

216 2.3.5. Synthesis of nitrile derivatives of BAM haptens (hapt E, hapt F, hapt G, and hapt H - potential  
217 dichlobenil haptens)

218 Hapt E, hapt F, hapt G and hapt H were synthesised by a mild hydrolysis of corresponding stage 2  
219 products with LiOH.H<sub>2</sub>O. 10 mmol of each Stage 2 products were dissolved in THF (40 mL).

220 LiOH.H<sub>2</sub>O (60 mL of 0.5 M solution, 30 mmol) was added to it and stirred at room temperature for two  
221 hours. THF was boiled off and 10 mL of 1 M HCl was then added to precipitate corresponding nitrile  
222 haptens. The precipitates were dried in oven at 50°C overnight.

223

224 2.3.5.1. 6-(2,4-dichloro-3-cyanophenylamino)-6-oxohexanoic acid (Hapt E)

225 Yield: 90%. <sup>1</sup>H NMR (DMSO-d<sub>6</sub>) δ : 12 (s, 1H), 9.86 (s, 1H), 8.02 (d, 1H), 7.7 (d, 1H), 2.45 (m,  
226 2H), 2.22 (t, 2H), 1.56 (m, 4H) . *R<sub>f</sub>*: 0.61 (ethylacetate/acetic acid 95:5).

227

228 2.3.5.2. 4-(2,4-dichloro-3-cyanophenylamino)-4-oxobutanoic acid (Hapt F)

229 Yield: 95%. <sup>1</sup>H NMR (DMSO-d<sub>6</sub>) δ : 12.18 (s, 1H), 9.98 (s, 1H), 8.05 (d, 1H), 7.7 (d, 1H), 2.68 (t,  
230 2H), 2.48 (m, 2H). *R<sub>f</sub>*: 0.56 (ethylacetate/acetic acid 95:5).

231

232 2.3.5.3. 6-(4-chloro-3-cyanophenylamino)-6-oxohexanoic acid (Hapt G)

233 Yield: 92%. <sup>1</sup>H NMR (DMSO-d<sub>6</sub>) δ : 12.03 (s, 1H), 10.55 (s, 1H), 8.2 (d, 1H), 7.83 (s, 1H), 7.64  
234 (d, 1H), 2.34 (t, 2H), 2.21 (t, 2H), 1.54 (m, 4H). *R<sub>f</sub>*: 0.56 (ethylacetate/acetic acid 95:5).

235

236 2.3.5.4. 6-(3-chloro-4-cyanophenylamino)-6-oxohexanoic acid (Hapt H)

237 Yield: 87%. <sup>1</sup>H NMR (DMSO-d<sub>6</sub>) δ : 12.03 (s, 1H), 10.63 (s, 1H), 8.05 (d, 1H), 7.61 (d, 1H), 2.36  
238 (t, 2H), 2.21 (t, 2H), 1.53 (m, 4H). *R<sub>f</sub>*: 0.59 (ethylacetate/acetic acid 95:5).

239

240 2.4. Synthesis and characterisation of different conjugates

241 To immobilize haptens on microtitre plates, the newly synthesised haptens (5 mole equivalents)  
242 were conjugated to 1 mL of 1 mg mL<sup>-1</sup> ovalbumin (OA). To attain a photo-catalysed covalent

243 immobilization, rather than a normal physical absorption, an anthraquinone entity (EQ 0028, 10 mole  
244 equivalents) is conjugated to the hapten-ovalbumin conjugate. This conjugation process and the  
245 synthesis of EQ 0028 were described by Bruun *et al.*[49]. The molar equivalence ratio during synthesis  
246 of hapten-OA-EQ 0028 conjugates was kept as 5:1:10. All conjugates were finally dialyzed against 1x  
247 PBS and stored at 4°C.

248 The antibody-Horse Radish Peroxidase (HYB 273 - HRP) conjugate concentration was determined  
249 by performing Bradford protein assay using bovine serum albumin (BSA) as the standard and was  
250 found to be 1.0 mg mL<sup>-1</sup>. Concentrations of all the haptens-OA-EQ 0028 conjugates were estimated by  
251 UV-Vis spectroscopy. From the UV-Vis data, it was able to calculate the number of anthraquinone  
252 entity per OA. Concentrations of OA and EQ 0028 are directly calculated from the UV-Vis data as they  
253 are photoactive (Eq. 1 and 2). Molar extinction coefficients of OA and EQ 0028 at 260nm and 280 nm  
254 in PBS are found by measuring absorbances of a series of solutions with known concentrations.

$$255 \quad A_{conjugate}^{280} = \epsilon_{OA}^{280} C_{OA} + \epsilon_{EQ}^{280} C_{EQ} \quad (1)$$

$$256 \quad A_{conjugate}^{260} = \epsilon_{OA}^{260} C_{OA} + \epsilon_{EQ}^{260} C_{EQ} \quad (2)$$

257

## 258 2.5. Assay method

259 Immobilization of hapt-OA-EQ 0028 conjugates on Polysorp<sup>®</sup> microtitre plates was always carried  
260 out by filling the wells with (100 µL/well) hapten-conjugate solutions of appropriate concentrations in  
261 0.1x PBS. The plates were then irradiated with UV light (300 – 400 nm) at 34°C for 30 min, washed  
262 with 1x PBST four times and used for the assay immediately or sealed with a taped lid and stored at  
263 room temperature in darkness until use. During the competitive assays, the total volume of antibody or  
264 antibody with samples or standards in wells was always kept at 100 µL, because of the assumption that  
265 the surface provided by the 100 µL volume of hapten-conjugate solution was available for antibody-  
266 antigen interaction (hybridization). The plates were incubated for 1 hr and then washed with 1x PBST  
267 four times. The TMB substrate volume was kept as 200µL/well to make the reaction kinetically  
268 independent of the substrate concentration. All assays except the regeneration experiments were  
269 conducted as end-point analysis by stopping the substrate reaction at a point of time by adding 1 M  
270 H<sub>2</sub>SO<sub>4</sub> (50 µL/well) and the absorbances were measured at 450 nm.

271

272

## 273 2.6. Affinity constants

274 Affinity constants ( $K_{aff}$ ) of structurally different new hapten molecules were measured in order to  
275 quantify and compare the interaction of HYB 273 with them, on ELISA plates as described by Beatty  
276 et al. [61] with two-fold serial dilution of antibody and two different concentrations of each  
277 immobilized hapten conjugates. Accordingly, each plate was divided into two halves of 4 rows and 12  
278 columns. The upper half was immobilized with hapten-conjugate of concentration  $[Ag]$  and lower part  
279 with  $[Ag]/2$ . A 2-fold serial dilution of HYB 273 was done in the direction of rows. The interaction  
280 between the antibody and each BAM-hapten were treated as sigmoidal dose-response curves; the data  
281 was fitted to the four-parameter logistic equation using GraphPad Prism software (version 4.03 for  
282 windows, GraphPad Prism, San Diego, CA, USA). A non-linear regression was performed to obtain  
283 effective concentration ( $EC_{50}$ ) values. Using  $EC_{50}$  values,  $K_{aff}$  of anti-BAM monoclonal antibody to  
284 each BAM-hapten molecules were calculated according to the equation described in [61].

285

## 286 2.7. Regeneration cycles

287 To test and optimize regeneration conditions, microtitre plates were prepared as described in Assay  
288 method, keeping the immobilized hapten conjugate concentration the same. Preliminary investigations  
289 showed that a 100 mM glycine.HCl buffer of pH 2 was close to the optimal regeneration agent. In  
290 regeneration experiments, no stop solution was used and the colour obtained by the substrate reaction  
291 was directly measured at 650 nm. After the first cycle of hybridization and substrate reaction, the  
292 coloured substrate was discarded and the plates were washed with  $1\times$  PBST four times. 100 mM  
293 glycin.HCl solution (pH~2) was added to each well (100 $\mu$ L/well) and incubated for 10 min at room  
294 temperature in a shaker at 200 rpm. The plates were again washed and used for next cycle of  
295 hybridization and substrate reaction. These processes were continued many times to check the ability of  
296 the surface to retain its capacity for further hybridizations. In order to bring the assay into an in-line  
297 sensor platform, this regeneration of surfaces is critical.

298

## 299 3. Results

300 Careful selection of commercially available starting chemicals with small structural variations  
301 and linkers of different chain lengths made it possible to synthesise new haptens with new available  
302 motifs for binding pockets of HYB 273 which in turn resulted in reduction of hapten-HYB 273

303 interactions. This was evident from the inhibition assays performed with all 8 haptens and HYB 273.  
304 HYB 273 could bind with only three of them-hapt A, hapt C and hapt D. No nitrile derivative did bind  
305 to the antibody, since they lack the prime epitop, the amide group.

306 The results obtained from UV-Vis analysis of hapten-OA-EQ0028 conjugates are given in Table  
307 1. The concentration of OA was found to vary in a very small range in all of the conjugates (0.9 – 1.1  
308 mg mL<sup>-1</sup>). To keep standard assay conditions, the concentrations of conjugates were adjusted to 0.9 mg  
309 mL<sup>-1</sup>. The number of photoreactive anthraquinone entities per OA was found to be 4 in hapt G-OA-EQ  
310 0028 and it was 2 for all other conjugates.

311 Since haptens B, E, F, G and H did not show any binding with HYB 273, we decided to consider  
312 only the active haptens (hapt A, C and D) for further analysis. Standard curves were generated by  
313 inhibition assays with active hapten conjugates on surfaces and BAM standards ranging from 0.0008  
314 µg L<sup>-1</sup> to 62.5 µg L<sup>-1</sup> in solutions. Direct OD values are plotted on the Y axis against the logarithmic  
315 concentrations of the BAM standards (Fig. 5). Concentrations of hapten conjugates immobilized on  
316 microplates were the same. As expected, the original BAM hapten conjugate (hapt A-OA-EQ0028) had  
317 higher response to the antibody than the other two chemically modified new conjugates at all  
318 concentrations of BAM standards in solution. The reliable detection range is retained in new haptens as  
319 well (indicated by blue dotted lines).

320 Table 2 presents the affinity constants ( $K_{aff}$ ) of HYB 273 towards the active hapten conjugates. The  
321 antibody (HYB 273) showed lower affinities towards the newly synthesised haptens than the original  
322 hapt A. These results are in good agreement with the standard curves shown in figure 5. We were not  
323 able to calculate  $K_{aff}$  to hapt B and nitrile derivatives (hapt E, F, G and H), due to the low affinity of  
324 anti-BAM antibody towards these haptens.

325 Figure 6 shows the signal following up to 25 analytical cycles with regeneration step between each  
326 cycle. Original hapten (hapt A) conjugate showed a steeper signal drop (blue line in fig. 6) though it  
327 had a good signal to noise ratio. After 25 cycles, the OD value reduced to approximately 40%. Among  
328 the three active conjugates, hapt C conjugate was the best in terms of regeneration (red line in fig.6);  
329 but it showed a poor signal to noise ratio. However, hapt D conjugate showed an intermediate  
330 performance in both signal strength and regeneration capability. Combining these results with the  
331 affinity constants given in table 2, hapt D seems to be the optional choice with respect to a signal-to-



332 noise, regeneration capability and detection limit for surface immobilization when this assay is used in  
333 real-time sensor applications.

334

#### 335 4. Discussion

336 As mentioned earlier, in this work the original synthesis route reported by Bruun *et. al.*[49] has  
337 been modified, keeping the same reaction sequence, but by improving the process in terms of reaction  
338 time, yield and purity at each step. As shown in Figure 3A, three different stages were involved in the  
339 overall synthesis and product purity at each stage was crucial in the success of next stage reaction. In  
340 the reduction of nitro compounds to the corresponding amines (Stage 1), the yield and reaction time  
341 were improved by adding a catalytic amount of conc.HCl into the reaction mixture. Purification of the  
342 resulting amines by flash chromatography technique improved the efficiency of next stage reaction. In  
343 the linker coupling reactions (Stage 2), instead of activating and coupling a dicarboxylic acid with a  
344 number of chemicals as descscribed by Bruun et al., 2000, we used the acid chloride derivatives of the  
345 corresponding di-acids with the other end protected by methyl ester group. The reaction was carried out  
346 in a two-phase medium consisting of aqueous  $\text{Na}_2\text{CO}_3$  and  $\text{CH}_2\text{Cl}_2$ [120]. This two-phase reaction  
347 avoided the possibilities of formation of undesirable biproducts and dimer of the expecting product as  
348 impurities. Aqueous  $\text{Na}_2\text{CO}_3$  acted as proton acceptor and hydrolysing agent for the excess reagent. Use  
349 of one side protected acid chlorides of diacids in this stage eventually helped in obtaining nitrile  
350 derivatives of haptens (stage 3b). It should be noted that esters resulted from stage 2 and nitrile haptens  
351 obtained by stage 3b were pure solid compounds rather than oily adduct reported by Bruun et al., 2000.  
352 Use of mild hydrolysing agent  $\text{LiOH} \cdot 2\text{H}_2\text{O}$  in THF helped to make the process simple in terms of  
353 hydrolysing only the ester group (with out affecting the nitrile group on the ring) and effective in terms  
354 of increased solubility of ester in aqueous THF with respect to the traditional saponification by an  
355 aqueous alkali[63]. At room temperature, an aromatic nitrile hardly hydrolysed by LiOH and thus we  
356 obtained nitrile derivatives of haptens[121](Figure 4). These compounds have a potential value as  
357 dichlobenil haptens for immunization and development of useful immunochemistry for the herbicide  
358 itself.

359 In the new reaction scheme, both hydration of nitrile group (on the ring) and hydrolysis of the ester  
360 group (at the linker end) could be achieved in a single step by an anhydrous hydrolysis with  $\text{KOSiMe}_3$   
361 in THF (stage 3a). It was reported that on refluxing  $\text{KOSiMe}_3$  with a ntrile in THF, the intermediate salt

362 gets precipitated (Figure 7)[65]. This means that the reaction can be controlled by stopping at the amide  
363 stage with out going into carboxylic stage and any impurities can be washed off as the salt is insoluble  
364 in THF. Finally free amide can be obtained by a simple aqueous workup. At the same time KOSiMe<sub>3</sub> in  
365 THF also functions as hydrolysing agent for the methyl ester at the linker end. The appreciable  
366 solubility of KOSiMe<sub>3</sub> in THF and the easily cleavable silicon-oxygen bond made it capable of  
367 functioning as an organic soluble equivalent of O<sup>2-</sup> and thus converting ester directly to its anhydrous  
368 salt[122]. The free acid is subsequently liberated by acidification.

369 Interaction of HYB 273 with new haptens indicates clearly the importance of various epitope  
370 motifs in the binding process and how they can be tuned to manipulate the interaction in terms of  
371 regeneration aspects. The fact, none of the nitrile haptens bind to HYB 273 whereas free BAM  
372 molecules in samples and standards bind strongly to HYB 273 indicates that the amide group on the  
373 ring is the primary epitope for the antibody and the linker does not participate in the binding process at  
374 all. The next important motifs are the chlorine atoms on the ring. The role of their electronegativity in  
375 the binding mechanism is proved by the reduced  $K_{aff}$  values of hapt C and hapt D as compared to hapt  
376 A (Table 2). Thus losing one of these chlorine atoms can impart a considerable change in the  
377 interaction and affinity. The next important factor that affects the interaction is the steric hindrances  
378 exhibited by different haptens while the antibody molecules approach for binding. In the case of hapt  
379 D, the loss of one chlorine atom is compensated to some extent by the relieved steric effect by a change  
380 in orientation of the antigenic sites due to the para position of the linker relative to the most important  
381 epitope motifs. This is evident from the difference in  $K_{aff}$  values of hapt C and hapt D (Table 2). In hapt  
382 B, though it has retained all the major epitope motifs, reduction of the linker length almost totally  
383 inhibits binding. This explains the need of a spacer with a considerably long hydrophobic chain to  
384 present the main epitop motifs for effective binding when the antibody and haptens are in aqueous  
385 solutions. It should also be noted that the haptens are conjugated to ovalbumin molecules which are  
386 huge in size as compared to hapten molecules. A reduction in length of the spacer arm between the  
387 epitopes and OA would increase the steric factor for an effective binding with HYB 273. In  
388 heterogeneous assays, diffusion of antibody molecules and ease of availability of antigenic epitopes  
389 determine the extent of interaction. We manipulated the latter factor and tuned the interaction of HYB  
390 273 with surfaces immobilized with various haptens. After considering all these factors, it is interesting  
391 to assume that a hypothetical hapten molecule with the main epitops ie., amide group and both the

392 chlorine atoms on the ring and a linker of six membered chain at para position with respect to the amide  
393 would have a higher affinity than even hapt A for HYB 273. Above findings are summarised in Table 3  
394 along with the structure of hypothetical hapten molecule. Our conclusion is that the amide group is the  
395 primary epitope, followed by the chlorine atoms while the spacer do not participate in the motif, but  
396 only serves to present the epitopes in the right way. Although we only have tested a small hapten  
397 library, it still gives insight to how changes in the hapten structure can affect on antibody/hapten  
398 interactions. Among the active heptens (hapt A, C and D), thus hapt D seemed to be a promising  
399 candidate for surface immobilisation as the immunochemistry shifts from ELISA to a flow system of  
400 an inline sensor.

401 Through this study, we have experienced that state of the art ELISA can not be transferred as such  
402 into a flow system, since it is an end-point analysis with internal calibration. In fluidic systems, where  
403 different steps are in a sequential manner, reactivation of the surface is required for repeated reliable  
404 measurements and calibrations. Relatively mild conditions are appreciable for reactivation of surfaces  
405 in a microfluidic flow system. This demands a proper balance between the interaction and the ease of  
406 removal of bound antibodies from the surface. On the basis of results presented, we were able to find  
407 the correlation in interactions between HYB 273 and various haptens, this knowledge can tremendously  
408 prove the regeneration step. From the obtained results we can conclude that hapt C binds the antibody  
409 too weakly to keep a good signal to noise ratio, but at the same time is best regarding regeneration.  
410 Hapt A has higher affinity and hence the best signal to noise ratio but at the same time faces the most  
411 difficulties in maintaining the surface activity. Hapt D with the intermediate affinity towards the  
412 antibody and with a reasonable signal to noise ratio is a promising candidate when this assay is moved  
413 to a fully automated immuno sensing system in combination with microfluidics and miniaturized  
414 transduction methods. Regeneration experiments carried out on micro-titre plates were in good  
415 agreement with the affinity results.

416 Moving the optimized immuno sensing assay to a fully automated microfluidic set-up, several  
417 miniaturized transducer principles can be applied. Immunosensors can broadly be classified into  
418 micromechanical, optical, piezoelectrical and electrochemical. We will use an electrochemical approach,  
419 in which the oxidized substrate solution will be passed by screen printed carbon paste electrode. A  
420 carbon paste electrode will act as the working electrode reducing the oxidized substrate where the  
421 current will be measured by a potentiostat. Initial experiments (data not shown) have shown an excellent

422 quantitative correlation between the amount of oxidized substrate and the obtained current peaks with  
423 sensitivity in the same order as the conventional ELISA.

424 Other factors required for unattended on-site operation is the long term stability of the antibody and  
425 TMB substrate solutions. Preliminary results suggest that unattended operation for at least one month  
426 can be achieved.

427

## 428 **5. Conclusion**

429 An existing immunoassay between anti-BAM monoclonal antibody (HYB 273) and 2,6-  
430 dichlorobenzamide (BAM) on ELISA has been optimized and feasibility of using this well-established  
431 immunoassay as the sensing technique of a real-time, in-line sensor has been investigated. As a part of  
432 attaining reusable surface, a library of new haptens was synthesized. Interaction of HYB 273 with new  
433 haptens was investigated in detail and we were able to pick one of the new haptens (hapt D) with two  
434 changes in its chemical structure from the original hapten (hapt A), as a better surface for flow systems.  
435 However, in the future it would be interesting to perform a combinatorial analysis of a sequence of light  
436 and heavy variable chains of anti-BAM monoclonal antibodies and a library of hapten molecules. Such  
437 studies may help us to understand more about interactions between anti-BAM monoclonal antibodies  
438 and BAM-haptens and thus to improve the sensor properties.

439 By combining the optimised BAM ELISA with an electrochemical detection system, a real-time  
440 biosensor can be achieved for quantification of the pesticide residue BAM in ground water. A second  
441 generation of sensors which can quantify multiple analytes at the same time is a future goal of this  
442 project. By combining sensing technology, fluorescent and electrochemical detections we can improve  
443 not only the sensor sensitivity but also data reliability.

444

## 445 **Acknowledgement**

446 This work was supported by the Danish Council for Strategic Research (grant no 2104-06-0006) and  
447 Copenhagen Energy.

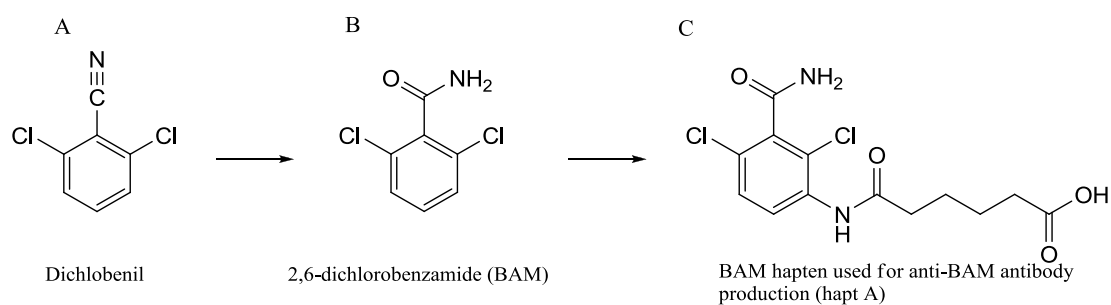
448

449

450 **References**

- 451 [1] WHO/UNICEF Joint Monitoring Programme for Water Supply and Sanitation,  
452 ISBN 92 4 156293 5 (2005).
- 453 [2] WHO/UNICEF Joint Monitoring Programme for Water Supply and Sanitation, ISBN 978 92  
454 806 4313 8, 978 92 4 156293 5 (2008).
- 455 [3] E.P. Meulenber, W.H. Mulder, P.G. Stoks, *Environmental Science & Technology*, 29 (1995)  
456 553.
- 457 [4] C. Raman Suri, R. Boro, Y. Nangia, S. Gandhi, P. Sharma, N. Wangoo, K. Rajesh, G.S.  
458 Shekhawat, *TrAC Trends in Analytical Chemistry*, 28 (2009) 29.
- 459 [5] G.G. Jensen, E. Björklund, A. Simonsen, B. Halling-Sørensen, *Journal of Chromatography A*,  
460 1216 (2009) 5199.
- 461 [6] E. Porazzi, M. Pardo Martinez, R. Fanelli, E. Benfenati, *Talanta*, 68 (2005) 146.
- 462 [7] A. Ghanem, P. Bados, F. Perreau, R. Benabdallah, C. Plagellat, L.F.d. Alencastro, J. Einhorn,  
463 *Analytical and Bioanalytical Chemistry*, 391 (2008).
- 464 [8] J. Hernández-Borges, S. Frías-García, A. Cifuentes, M.A. Rodríguez-Delgado, *Journal of*  
465 *Separation Science*, 27 (2004) 947.
- 466 [9] J.M. Van Emon, *Journal of AOAC INTERNATIONAL*, 84 (2001).
- 467 [10] L. Bruun, C. Koch, M.H. Jakobsen, J. Aamand, *Food & Agricultural Immunology*, 12 (2000)  
468 253.
- 469 [11] L. Bruun, C. Koch, M.H. Jakobsen, J. Aamand, *Analytica Chimica Acta*, 423 (2000) 205.
- 470 [12] L. Bruun, C. Koch, B. Pedersen, M.H. Jakobsen, J. Aamand, *Journal of Immunological*  
471 *Methods*, 240 (2000) 133.
- 472 [13] E.J. Sundberg, *Epitope Mapping Protocols*, 2009, p. 23.
- 473 [14] N.S. Lipman, L.R. Jackson, L.J. Trudel, F. Weis-Garcia, *ILAR Journal*, 46 (2005) 258.
- 474 [15] J.D. Beatty, B.G. Beatty, W.G. Vlahos, *Journal of Immunological Methods*, 100 (1987) 173.
- 475 [16] N.L. Benoiton, CRC Press (2006) 43.
- 476 [17] R.V. Hoffman, *Jonh Wiley and Sons INC., Publication, Second Edition (2004)*.
- 477 [18] J.L. Greene, R.E. Clark, *United States Patent*, 3686307 (1972).
- 478 [19] K.J. Merchant, *Tetrahedron Letters*, 41 (2000).
- 479 [20] E.D. Laganis, B.L. Chenard, *Tetrahedron Letters*, 25 (1984) 5831.

480 **Figures**

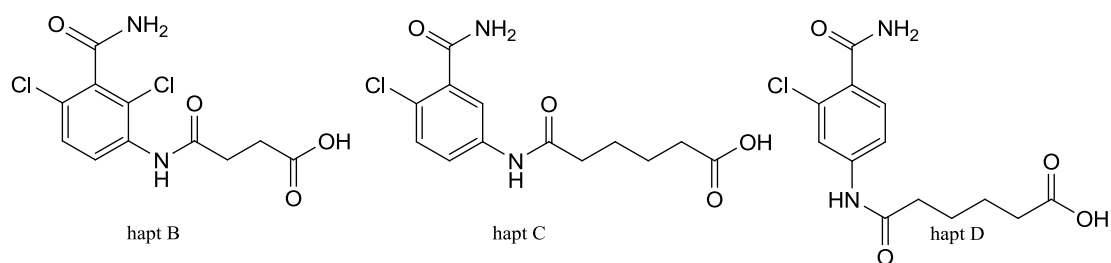


481

482 Fig. 1. Chemical structures of the herbicide Dichlobenil (A), the degradation product 2,6-dichlorobenzamide (BAM) (B) and the  
483 synthesised BAM hapten (C) to immunise animals for the production of anti-BAM antibody (HYB 273)

484

485

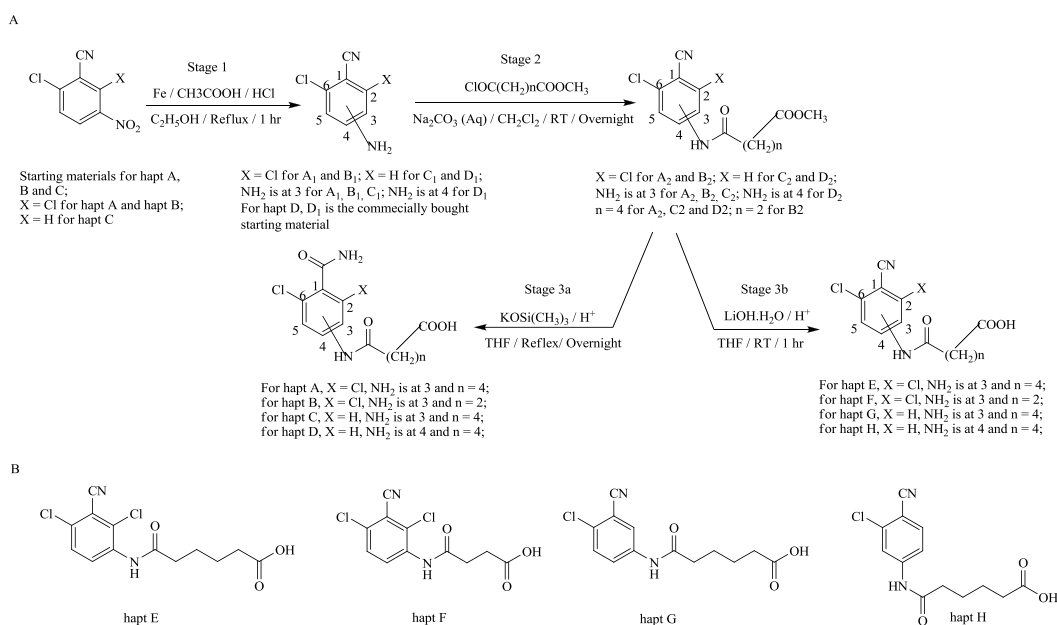


486

487 Fig. 2. Chemical structures of three newly synthesised BAM haptens (hapt B, hapt C and hapt D). Compared to hapt A, hapt B  
488 has a shorter linker, hapt C has the same linker but one of the chlorine atoms is missing on the ring, and hapt D has the same  
489 linker, but the position is moved from ortho to para relative to the amide functionality and missing one chlorine atom.

490

491

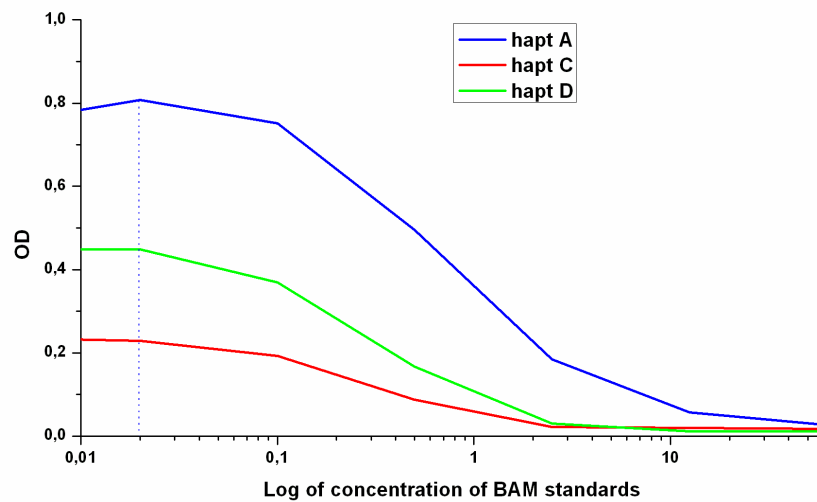


492

493 Fig. 3. A. Overall reaction route of hapten library synthesis; B. Nitrile-derivatives of BAM-haptens

494

495



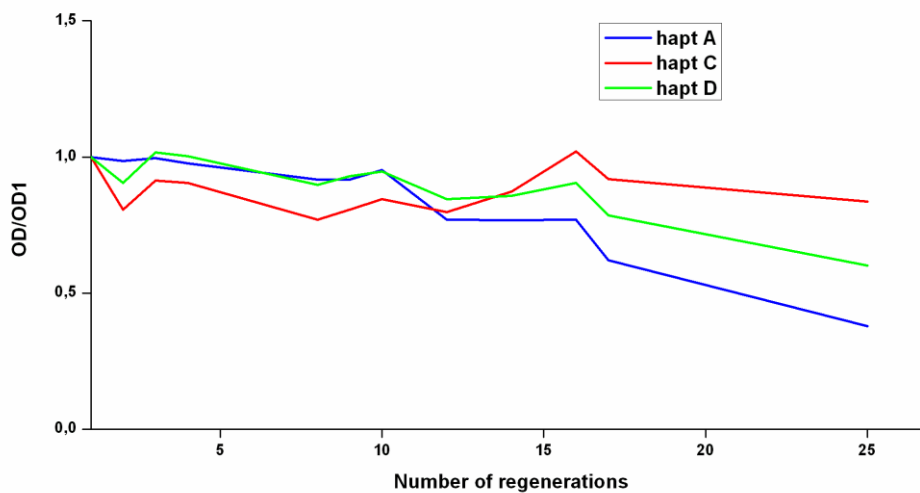
496

497

Fig. 4. Standard curves generated by active hapten surfaces (hapt A, C and D; none other than these did bind with HYB 273) with BAM-standards on micro-titre plates. Each OD value plotted is an average of 10 repeats.

499

500



501

502

503

504

505

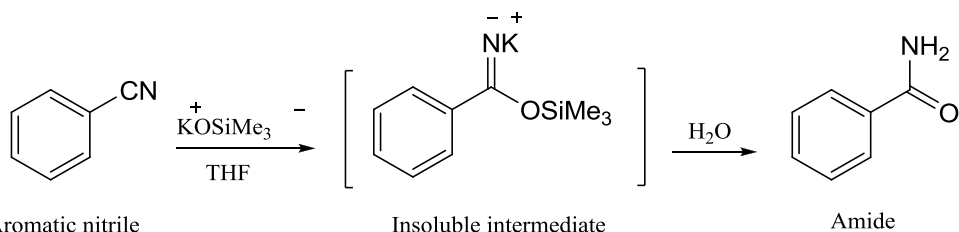
506

Fig. 5. Regeneration results of 3 different immobilized hapten conjugates. In this experiment a 96-well polysorp microtitre plate was immobilized with the same concentration of the three hapten conjugates. In each cycle, same concentration of anti-BAM antibody was added to all the wells and incubated for 1 hour. After washing, TMB substrate solution was added and the OD values were read after 15 minutes. After washing, 100 mM glycine.HCl buffer of pH 2 was added for 10 min. to remove antibody. A new TMB substrate reaction was performed to confirm complete removal of the antibody. This analytical cycle was

507 repeated until 17th cycle. After 17th cycle, eight more hybridization and stripping were performed without substrate reaction  
 508 until the full cycle was repeated at the 25th cycle. All data are plotted relative to the signal intensity of the first cycle.

509

510



511

512 Figure 6: Hydrolysis of nitrile group into amide by KOSiMe<sub>3</sub> in THF via an intermediate salt which is insoluble in THF

513

### 514 Tables

515 Table 1

516 Characterization of hapt-OA-EQ 0028<sup>a</sup> conjugates by UV-Vis spectroscopy

Conjugates	Concentration (mg mL <sup>-1</sup> )	No. of EQ 0028 per OA
hapt A-OA-EQ 0028	0.9	2
hapt B-OA-EQ 0028	1.0	2
hapt C-OA-EQ 0028	1.0	2
hapt D-OA-EQ 0028	0.9	2
hapt E-OA-EQ 0028	1.1	2
hapt F-OA-EQ 0028	0.9	2
hapt G-OA-EQ 0028	1.0	4
hapt H-OA-EQ 0028	1.0	2

517 <sup>a</sup>hapt: hapten; OA: ovalbumin; EQ 0028: photoactive anthraquinone entity.

518

519 Table 2

520 Affinity constants ( $K_{aff}$ ) of HYB 273 towards the active haptens

Haptens	$K_{aff}$ , nm <sup>-1</sup>
hapt A	0.5836
hapt C	0.2176
hapt D	0.3081

521

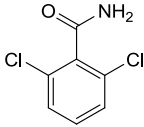
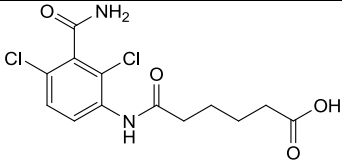
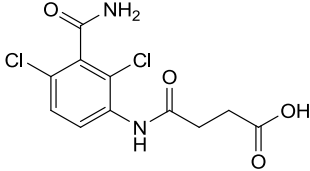
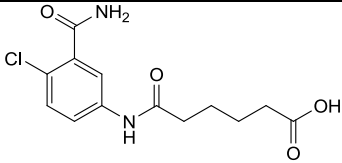
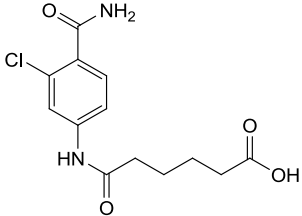
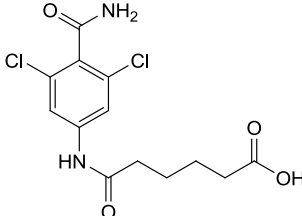


522

Table 3

523

The dependence of structural aspects on the nature of interactions between BAM haptens and HYB 273

Species	Structure	Nature of bonding with HYB 273	Comments
Free BAM		Very strong	All epitopes are present No steric effect
Hapt A		Strong	All epitopes are present. Steric effect due to meta positioned linker chain.
Hapt B		No binding	All epitopes are present. Linker is not long enough to present the epitopes for effective binding.
Hapt C		Weak	One of the epitope is missing. Meta positioned linker contributes considerable steric effect.
Hapt D		Intermediate	One of the epitope is missing. Para positioned linker relieves steric effect to compensate the missing chlorine to some extent.
Nitrile haptens	(Fig. 3B)	No binding	The primary epitope is missing.
Hypothetical		Assumed to be as strong as free BAM	All epitopes are present. Steric factor is minimum. Linker is long enough to present the epitopes as if free BAM in aqueous solution.

524

## Appendix III

**An amperometric immunosensor with an in-built micro flow-injection analysis ( $\mu$ FIA) system for quantitative determination of 2,6- dichlorobenzamide (BAM) herbicide residue in ground water**

Basil Uthuppu, Arto Heiskanen, Ida Thygesen, Claus Jørgensen, Jens Aamand, Mogens Havsteen Jakobsen

Type: - Full Paper, ready to submit



# **An amperometric immunosensor with an in-built micro flow-injection analysis ( $\mu$ FIA) system for quantitative determination of 2,6- dichlorobenzamide (BAM) herbicide residue in ground water**

## ***Abstract***

As a part of developing new systems for monitoring the presence of pesticides in ground water continuously over a long period of time, a prototype of an in-line amperometric immunosensor is developed. A herbicide residue, 2,6- dichlorobenzamide (BAM) is chosen as a model system for the prototype. The optimized BAM immunoassay is transferred to a microfluidic platform in order to attain a miniaturized, portable, easy to automate device that can be readily integrated with amperometric detection technique. The modular microfluidic platform has a novel feature of in-built micro flow-injection analysis ( $\mu$ FIA) system which makes the device prototype unique and extremely sensitive and cost effective. The regeneration of the immunosurface is evaluated in the sensor prototype. A standard curve generated with known concentrations of BAM in solution shows a good agreement with the ELISA based BAM immunoassay in terms of detection limit ( $12.5 \mu\text{g L}^{-1} - 0.02 \mu\text{g L}^{-1}$ ) and the  $\text{IC}_{50}$  value ( $0.19 \mu\text{g L}^{-1}$ ).

## **1. Introduction**

Immunoassays have been widely used in clinical chemistry<sup>1,2</sup> and endocrinology<sup>3</sup> since their appearance in the form of an analytical tool<sup>4</sup> in 1960. In 1971, Ercegovich *et al.* presented immunoassays for DDT, malathion and aminotriazole providing the first strong suggestion to the environmental chemists to consider immunoassays as an analytical method for environmental monitoring<sup>5</sup>. Since then, immunoassays as an analytical technique have found a greater acceptance in environmental analysis indicated by the growing number of publications in the field<sup>6-10</sup>. These methods pose many advantages over the existing chromatographic methods in terms of cost, speed, simplicity and number of simultaneous analyses. However, as a part of setting up new systems based on immunochemistry to monitor the presence of an analyte continuously over a long period of time, the idea of automated immunosensors emerged. Along with expensive and complex centrifugal analyzers and air-segmented continuous flow system<sup>11</sup>, flow- injection immunoanalysis (FIIA) systems are pioneers in this area by joining batch immunoassay principles with simple flow-injection analysis (FIA) methodology described by Ruzicka and Hansen in 1975<sup>12</sup>. The strength of FIA lies in its ability of making a controlled and reproducible dispersion of a sample zone when it is introduced into an unsegmented, continuously-

flowing carrier stream. A comprehensive review on the FIA application in various immunoanalysis techniques is found in literature <sup>13</sup>. Most of the reported amperometric FIA applications rely on the use of a reaction column to carry out the immunoreaction and/or the marker reaction where the detection is performed by coupling a separate amperometric detector with commercially available FIA instrumentations <sup>14-17</sup>. This paper reports the development and fabrication of an automated amperometric immunosensor that employs a simple and unique approach with a modular microfluidic (chip-based) flow-injection analysis ( $\mu$ FIA) system. Such a system has the obvious benefit of being cost-effective as well as being largely designed and developed in-house. It is built into the microfluidic platform which is developed for incorporating the well established immunoassay of 2,6-dichlorobenzamide (BAM), a herbicide residue <sup>18</sup> and amperometric detection scheme for constructing a continuous in-line monitoring system.

BAM is a principle metabolite of a widely used herbicide, dichlobenil <sup>19</sup> (Figure 3(a)). It is more persistent, more mobile and has higher water solubility than dichlobenil and hence it may reach natural water resources. The toxicity studies of BAM indicate that consumption of a few hundred mg/kg of BAM can cause acute toxicity in mammals <sup>20</sup>. In Denmark where the drinking water supply is totally based on ground water <sup>21</sup>, studies conducted by the Danish ground water monitoring programme revealed that 25% of water supply wells have BAM) and 10% have concentrations above the maximum admissible concentration (MAC) value of 0.1  $\mu$ g/L <sup>22</sup>. The immunological method described by Bruun *et al.* <sup>18</sup> for BAM analysis in water employs a heterogeneous labelled competitive immunoassay (Figure 3(b)). It is highly specific and sensitive as well as much simpler and cost-effective than conventional chromatography based techniques <sup>23</sup> in terms of the necessary sample pre-treatment and instrumentation. In the competitive format, the free BAM in water sample inhibits the binding of the horseradish peroxidase (HRP) labelled anti-BAM monoclonal antibody (HYB 273) on to the immunosurface which is immobilized with BAM hapten. The surface bound antibody concentration (inversely proportional to the concentration of BAM in a sample) is then detected by peroxidase reaction of 3,3',5,5'- tetramethylbenzidine (TMB) substrate which is both optically and electrochemically active <sup>24,25</sup>. However, the regeneration of the immunosurface is a key issue for the development of an immunosensor based on this immunoassay. The

assay is optimized in terms of regenerations which is described elsewhere<sup>26</sup>. By incorporating this heterogeneous enzyme-labelled immunoassay in  $\mu$ FIA and amperometric detection, the system explores the advantages of a flow system, selectivity of the immunoreactions as well as sensitivity of enzyme reaction and amperometric detection.

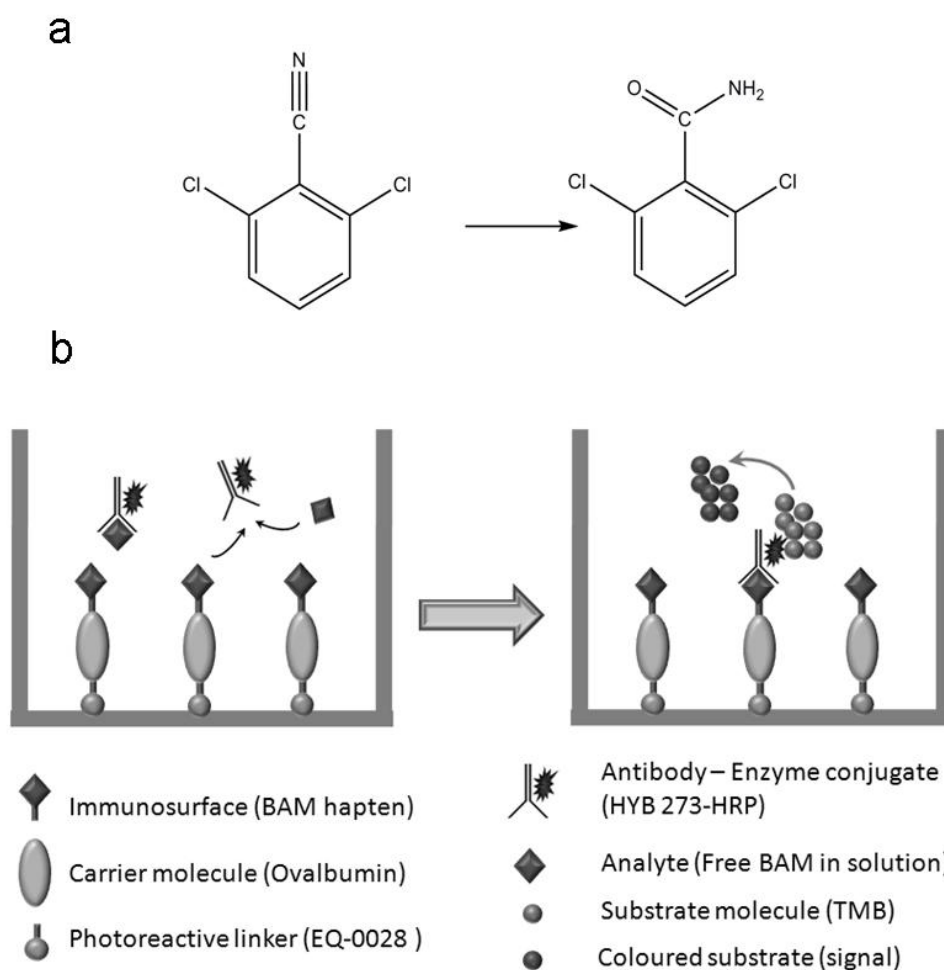


**Figure 3 a) Chemical structures of dichlobenil and its residue 2,6- dichlorobenzamide and b) a schematic representation of the heterogeneous enzyme labelled BAM immunoassay.**

## 2. Experimental

### a. Materials, chemicals and instruments

Poly(methyl methacrylate) (PMMA) (Röchling Technische Teile KG, Mainburg, Germany), Polycarbonate (PC) (Bayer MaterialScience AG, Leverkusen, Germany),

and polydimethylsiloxane (PDMS) made of Sylgard<sup>®</sup> 184 silicone elastomer kit (Dow Corning, Wiesbaden, Germany) were used for fabrication and interfacing of microfluidic components.

Anti-BAM monoclonal antibodies (HYB 273) (Bruun et al., 2000) were provided by Statens Serum Institut, Copenhagen, Denmark. Horseradish peroxidase (HRP) (EZ-Link<sup>®</sup> Plus Activated Peroxidase) was purchased from Pierce, Rockford, IL, USA and conjugated with HYB 273 at pH 7.2 according to the procedure given by the supplier. Ready-to-use TMB-Plus substrate (3,3',5,5'-tetramethylbenzidine) was from KEM EN TEC, Taastrup, Denmark. 2,6-dichlorobenzamide (10 mg mL<sup>-1</sup> in acetonitrile) reference material was purchased from Dr. Ehrenstorfer GmbH, Augsburg, Germany. Phosphate buffered saline (PBS) powder in pouches, potassium chloride (KCl), glycine hydrochloride, PBS with Tween<sup>®</sup> 20 (PBST) tablets, potassium hexacyanoferrate (III) (K<sub>3</sub>Fe(CN)<sub>6</sub>) were from Sigma-Aldrich Corporation (St. Louis, MO, USA).

All solutions were prepared using ultra pure water (resistivity 18.2 MΩ·cm) from a Milli-Q<sup>®</sup> water purification system (Millipore Corporation, Billerica, MA, USA). Dissolving one pouch of PBS buffer powder in 1 L of milli-Q water yielded 0.01 M PBS (containing 0.14 M NaCl and 0.0027 M KCl) of pH 7.4. This was used in the baseline buffer flow (BBF). Dissolving one tablet of PBS with Tween<sup>®</sup> 20 in 500 mL of milli-Q water yielded 0.01 M PBS containing 0.05% Tween<sup>®</sup> 20 (containing 0.14 M NaCl and 0.0027 M KCl) of pH 7.4. This was used as the assay buffer. The regeneration buffer was prepared by dissolving 1.12g of glycine hydrochloride in 100 mL of Milli-Q water (100 mM) and the pH was adjusted to 2. BAM standard solutions in a 5-fold dilution series with concentrations 62.5 µg mL<sup>-1</sup>, 12.5 µg mL<sup>-1</sup>, 2.5 µg mL<sup>-1</sup>, 0.5 µg mL<sup>-1</sup>, 0.1 µg mL<sup>-1</sup>, 0.02 µg mL<sup>-1</sup>, 0.004 µg mL<sup>-1</sup> and 0.0008 µg mL<sup>-1</sup> were prepared in Milli-Q<sup>®</sup> water by diluting the standard reference 10 mg mL<sup>-1</sup> BAM in acetonitrile.

UV reaction chamber used for hapten immobilization in microchannels was UV Stratalinker<sup>®</sup> 2400 from Stratagene, La Jolla, CA, USA. All parts of the microfluidic system were fabricated using Computer Numerical Control (CNC) micromilling machine (Folken, Glendale, California) and a Mini-Mill/3Pro software system (Minitech Machinery Corporation, Norcross, GA, USA) which executes G-code

generated by EZ-CAM15 Express software (EZCAM Solutions, Inc., New York, NY, USA). UV-activated thermal bonding of the microfluidic chips was done using 5000-EC Series UV Curing Flood Lamp System (Dymax Corporation, Torrington, CT, USA) and a PW10 hydraulic press (Paul-Otto Weber GmbH, Remshalden, Germany). Screen printed carbon electrodes used in the electrochemical detection unit were purchased from Dropsens (Llanera, Spain). Cyclic voltammetric and amperometric experiments were performed by using a computer controlled 8-channel CHI1010A potentiostat (CH Instruments, Inc., Austin, TX, USA). Miniaturized pump and valves pumps were operated with Lego<sup>®</sup> Interactive Servo Motors (Lego System A/S, Billund, Denmark) that were controlled by an NXT Intelligent Brick (Lego System A/S, Billund, Denmark) executing a LabView-based script. Mettler-Toledo SevenEasy pH meter S 20 (Mettler-Toledo AG, Schwerzenbach, Switzerland) was used to measure pH of different solutions. Generation of sigmoidal dose-response curve and data analysis were done using GraphPad Prism software (version 4.03 for windows, GraphPad Prism, San Diego, CA, USA).

#### **b. Fabrication of $\mu$ FIA based amperometric immunosensor**

The microfluidic platform for developing the amperometric BAM immunosensor was fabricated using a modular approach (the different modules responsible for different operations such as pumping, valving, detection etc. were fabricated and then integrated into the complete system), The structure and fabrication of the different modules that were used to construct the complete system and their functions are briefly described below.

##### **i. Immunochip (IC)**

The most important module of the BAM immunosensor, the immunochip (IC) consists of two simple microchannels that were micromilled on a 3 mm thick PMMA substrate. This channel plate was bonded to a 1.5 mm thick lid made of PMMA with inlet and outlet holes in a pattern that complements the channel plate. **Figure 4(a)** shows a bonded immunochip. The curved channel in which the immunosurface is created by immobilizing BAM hapten (immunochannel) has the dimensions of 150 mm x 0.5 mm x 0.4 mm (L x W x D) with a volume capacity of 30  $\mu$ L. The immunochannel is connected to the seven of the eight inlets allowing the sequential loading of different



reagents required for the BAM immunoassay. The other channel with the same width and depth as the immunochannel is connected to the eighth inlet to have an independent and continuous flow of baseline buffer to the detection module. Two of the three outlets are interconnected and used to dispose the flow from the immunochannel either to the waste or to the detector, whereas the third outlet carries the uninterrupted baseline buffer flow to the detector.

The most important module of the BAM immunosensor, the immunochip (IC) consists of two simple microchannels of dimensions 150 mm x 0.5 mm x 0.4 mm (L x W x D) with an approximate volume capacity of 30  $\mu$ L and was micromilled on a 3 mm thick PMMA substrate. This channel plate is bonded to a 1.5 mm thick lid made of PMMA with inlet and outlet holes in a pattern that complements the channel plate. **Figure 4(a)** shows a bonded immunochip. Seven of eight inlets are interconnected to the immunochannel for the sequential loading of different reagents which is controlled by Valve-1. The eighth inlet allows a channel of the same width and depth as the immunochannel to keep an independent and continuous flow of baseline buffer to the detection module. Switching between two of the three active outlets of the IC is controlled by Valve-2 to direct the flow from the immunochannel to either the waste channel or detector. The third active outlet leads the baseline buffer flow to the detector.

## ii. Mixing chip (MC)

The mixing chip (MC) (a part of the electrochemical detection module), fabricated in the same way as the immunochip, has a different channel shape as shown in **Figure 4(b)**. It has three active inlets and receives the flow from the immunochip. The undisturbed baseline buffer flow enters into one of the inlets and continues to the detector. The other two inlets of MC receive the flow from the immunochannel of IC and direct it, either to the waste channel or to be mixed with the baseline buffer channel and flowed to the detector for signal recording..

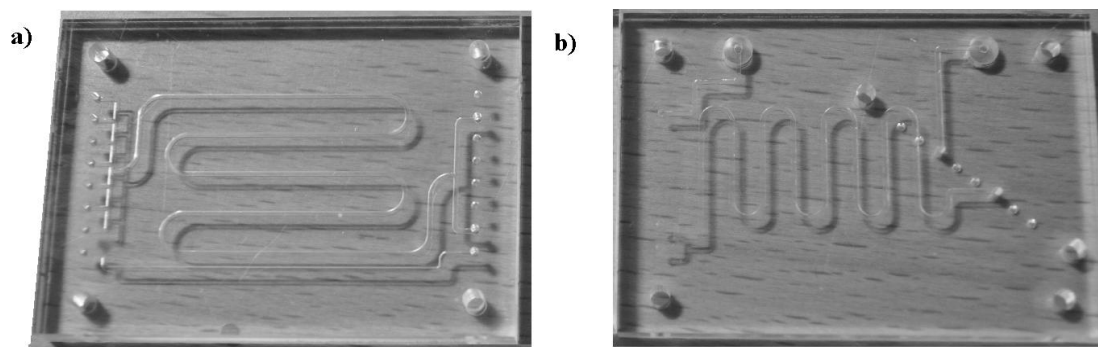


**Figure 4: A bonded a) immunochip and b) mixing chip.**

### iii. Electrode chamber (EC)

The main part of the detection module is the electrode chamber (EC), which is fabricated of PMMA as two pieces as shown in **Figure 5**. The lower half, made of five mm thick PMMA substrate has a 1.5 mm deep rectangular ‘pocket’ to place the screen printed ceramic electrode chip (L: 34mm; W: 10 mm; T: 0.5 mm), which has a circular carbon working electrode (4 mm in diameter), carbon counter electrode and Ag/AgCl reference electrode. The upper part of the electrode unit has a 0.7 mm high counter-projection with a 0.8 mm deep circular chamber with 8.5-mm radius. When pressing the two parts together, a space is provided for the 0.5 mm thick electrode chip. While screwing the two halves together, a 0.5 mm thick PDMS gasket with a hole of diameter 8.5 mm (aligned over the circular chamber) is placed on top of the electrode in the lower part to ensure the assembly is perfectly leak-proof. The upper surface of the upper half has the provision to connect the MC with the assembled EC using a specially designed double-sided interconnection block with eight channels. Two diametrically opposite channels are activated as inlet and outlet for the circular chamber to minimize the chances of air bubbles. Three holes (2 mm in diameter) on the upper half provide the provision for three spring-loaded contacts (soldered onto a Printed Circuit Board (PCB)) to be aligned and connected with the electrode contact pads when the parts are screwed together.

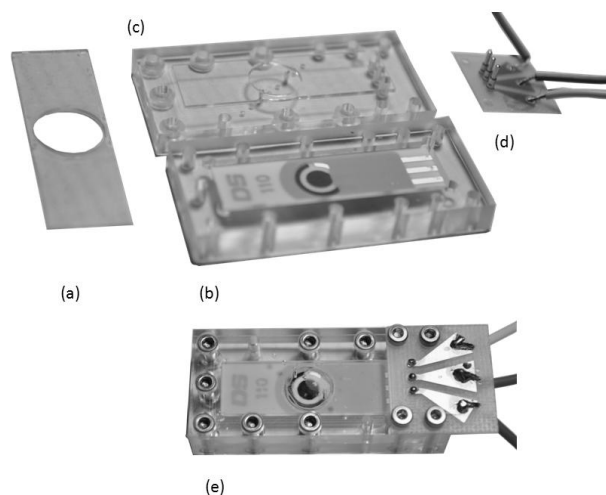


**Figure 5:** The components of the electrochemical detection chamber: (a) a PDMS gasket used to tighten the two halves together, (b) a lower half with a SPCE in a 1.5 mm deep pocket, (c) an upper half with a 0.7 mm deep counter protrusion and a 0.8 mm deep circular well, (d) a PCB with soldered spring loaded contact pins, and (e) an assembled electrochemical detection chamber.

#### iv. Reservoir modules

The reservoir module also consists of two parts. The upper part is made of 10 mm thick PC and has eight elliptical holes (each having 3 mL volume capacity when closed). The lower part is essentially a microfluidic chip made of a channel plate bonded with a lid (both are made of 2 mm thick PMMA). The channel plate has eight individual micromilled channels of width 0.5 mm and depth 0.4 mm. The upper part is screwed onto the chip. In order to make the reservoir leak-proof, a PDMS gasket is inserted between the two parts. The upper surface of the lid has elliptical grooves to accommodate the PDMS gasket. These grooves and the gasket are of the same shape as the elliptical holes of the upper part. The eight channels end at a specific 8-hole interconnection junction. **Figure 6** shows an assembled reservoir module and its parts.

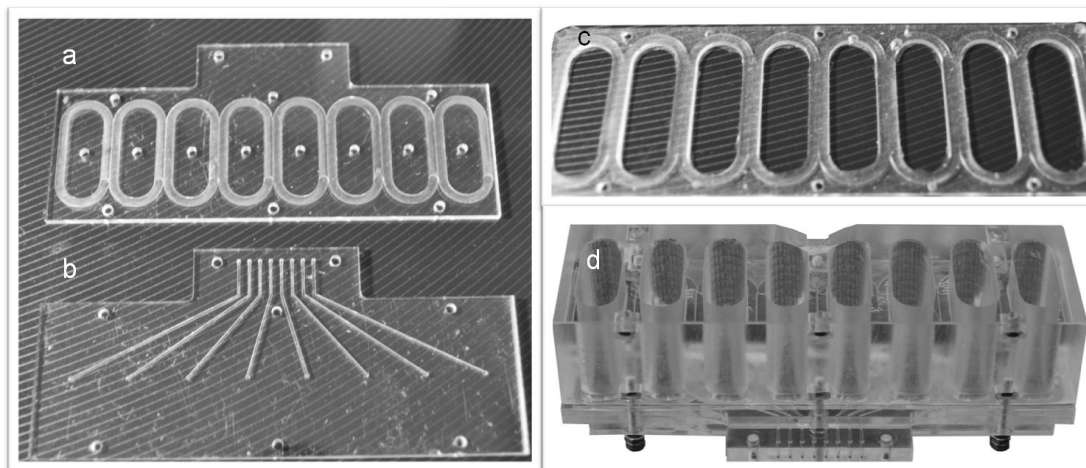


**Figure 6: Components of a reservoir module..a) A channel plate of the lower part, b) a lid of the channel plate with grooves to hold a PDMS gasket and the upper part, c) a PDMS gasket, and d) an assembled reservoir module**

#### v. Miniaturized pump and valves

The microfluidic device described in this paper uses an 8-channel version of the miniaturized peristaltic pump reported by Skafto-Pedersen *et al.*<sup>27</sup> for the effective pumping of various reagents used in the BAM immunoassay. It comprises of three main components: i) a multi-roller, ii) a pumping inlay made of PDMS with embedded eight channels, and iii) a rigid rotor bed made of polycarbonate. The fabrication details of these components are given in the supplementary material of<sup>27</sup>.

The sequential addition of different reagents into the IC and the subsequent flow of these liquids into the MC are well controlled and guided by two miniaturized valve modules which was originally designed and published by Conde *et al.*<sup>28</sup>. The valve modules also consist of three components: i) a valve inlay made of PDMS, ii) two blocks of rigid supports, and iii) a brass shaft stacked with eight asymmetric discs which are aligned and screwed together. These valves can control the flow in 8 channels independently.

**Figure 7** shows the completely assembled electrochemical BAM immunosensor prototype. This was achieved by fixing the various modules described above onto a base plate using 2-mm screws and nuts. The modules are interconnected by using specially designed features called ball joint interconnection blocks (BJIBs) reported by Sabourin *et al.*<sup>29</sup> and complementary planar structures with eight holes of diameter

of 0.8 mm (separated by a distance of 2.25 mm from centre to centre) which is flanked by two 2-mm holes (with a distance 25 mm from centre to centre) as shown in **Figure 7**

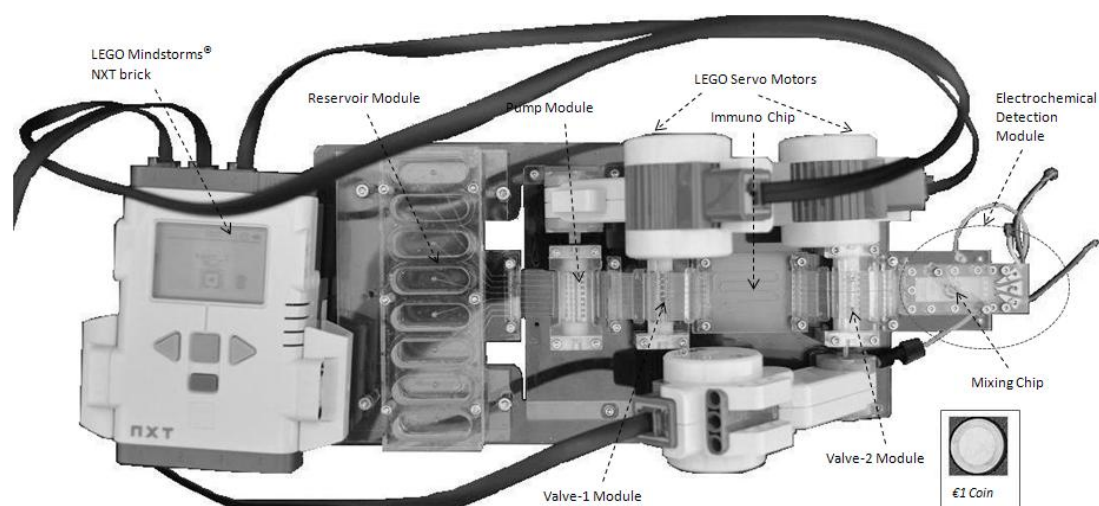


**Figure 7: A completely integrated amperometric Bam immunosensor prototype**

### c. Pump calibration

Leak pressure testing of the ball joint interconnection blocks, flow pattern of the miniaturized peristaltic pump and validation of the miniaturized valve for mixing and routing are described elsewhere<sup>27-29</sup>. After assembling the different modules, except the detection chamber, onto a base plate, the miniaturized peristaltic pump was calibrated by flowing Milli Q<sup>®</sup> water through each channel. The Lego<sup>®</sup> servo motor that drives the pump was run for five minutes at four different speeds expressed in % power (40%, 50%, 60% and 75%). Flow rate of each channel was estimated in  $\mu\text{L min}^{-1}$  with three repetitions.

### d. Characterization of $\mu\text{FIA}$ system

The characterization of the in-built  $\mu\text{FIA}$  system was done by amperometric detection of 2.5 mM solution of  $\text{K}_3[\text{Fe}(\text{CN})_6]$  in 0.1 M KCl. The Lego<sup>®</sup> servo motors that operate the micropump and valves were controlled by a programmed script to facilitate filling of the immunochannel with the  $\text{K}_3[\text{Fe}(\text{CN})_6]$  solution from one of the reservoirs and elution by 0.1 M KCl from another reservoir into the baseline

electrolyte (0.1 M KCl) that continuously flows from a third reservoir to the detection module. This was repeated four times at an interval of 5 min. The working electrode was poised at -200 mV with respect to the Ag/AgCl reference electrode. The reduction current was recorded as a function of time and the current-time traces were integrated to obtain the charge. The relative standard deviation was calculated. In a second experiment, six different standard solutions (3 mM, 1.5 mM, 0.75 mM, 0.375 mM, 0.1875 mM, 0.09375 mM) of  $K_3[Fe(CN)_6]$  prepared in 0.1 M KCl. were used to characterise the system. The calculated charge from three repetitions for each concentration was plotted as a function of time to obtain a calibration curve. The error bars represent +/- standard error of mean (SEM). All these experiments were performed at room temperature. Characterization of amperometric  $\mu$ FIA based BAM immunosensor

Cyclic voltammograms (CV) of commercially available ready-to-use TMB substrate and its oxidized (by HRP) product, TMB(ox), were recorded to determine the appropriate potential for the amperometric detection of the oxidized species. Both solutions were prepared by mixing with baseline buffer (0.01 M PBS) in 1:1 ratio (as counter electrolyte). The CV of TMB(ox) was recorded 40 min after addition of HRP in TMB solution (final HRP concentration 125 pM).

Repeated BAM immunoassays were performed in the inhibition format to characterize the immunosensor. The oxidized substrate, TMB(ox), was detected amperometrically on the working electrode poised at -100 mV with respect to Ag/AgCl reference electrode (deduced based on the recorded CVs) as an indicator of the indirect inhibition BAM immunoassay. The regeneration capability of the immunochannel with immobilized BAM hapten (hapt D, described in <sup>26</sup>) was examined by inhibition assays using zero BAM according to the protocol given below. Each i-t curve recorded after a regeneration cycle was integrated and the relative standard deviation of the charge associated with 15 cycles was determined. A standard curve with different known concentrations of BAM in solution was obtained by following the regeneration protocol with an incubation period of 40 min for the enzymatic reaction. The sigmoidal standard curve (charge vs. concentration on logarithmic scale) was fitted to the four-parameter logistic equation using non-linear regression to obtain the effective concentration at 50% inhibition ( $EC_{50}$ ). The linear

working range was determined from standard curve. The determined values were compared with those obtained by using ELISA based determination.

#### Protocol

1. Immobilization of BAM hapten in the immunochip: The immuno(micro)channel of the immunochip was filled with 30  $\mu\text{L}$  of Hapt D (<sup>26</sup>) which was diluted 10 times with 0.01 M PBS. Both sides of the chip were then irradiated in the UV chamber for 30 min to facilitate the photo-reactive covalent immobilization. After the completed immobilization, the chip was inserted into the microfluidic system.
2. Using Valve 1 and 2, the immunochannel was opened to the waste to allow washing of the unbound Hapt D for 5 min with 0.01 M PBST.
3. The immunochannel was filled with HYB-273 solution (1:1000 dilution with 0.01 M PBS containing 0.05% Tween<sup>®</sup> 20).
4. The system was kept under stop-flow for 15 min to allow complete binding of the antibody to the immobilized hapten in the immunochannel.
5. The immunochannel was washed as described in step 2.
6. The immunochannel loop was filled with TMB solution (substrate).
7. The immunochannel was kept under stop-flow for 15 min to allow complete oxidation of the substrate.
8. The plug of reacted substrate was eluted into the detector with the base-line buffer (0.01x PBS).
9. The immunochannel was washed as described in step 2.
10. The immunochannel was filled with Glycine.HCl buffer.
11. The immunochannel was kept under stop-flow for 3 min to allow complete removal of the bound antibody.
12. The immunochannel was washed as described in step 2.

13. Steps 3 to 12 were repeated several times to establish the regeneration capacity of the hapt D immobilized surface and to obtain a standard curve using different BAM concentrations.

### **3. Results and discussions**

#### **a. Fabrication of $\mu$ FIA based amperometric immunosensor**

Attempts to fabricate a microfluidic platform for amperometric BAM immunosensor with cheap polymeric materials such as PMMA, PDMS and PC has resulted in the development of a simple, cost-effective, well-functioning and easy to use prototype. Selection of such base materials also benefited in adoption of much simpler and easily accessible techniques such as micromilling and UV assisted thermal bonding as fabrication processes. PMMA was used as a base material for fabricating the important parts of the BAM immunosensor for many reasons such as its low cost, low hydrophobicity, amenability for fabrication and modification<sup>30</sup>. It is also compatible with the hapten immobilization and the reagents used in the BAM immunoassay. The well-known elasticity of PDMS<sup>31</sup> has been instrumental in achieving functional inlays of the pump and valves as well as tight sealing to flat surfaces and ability to function as O-rings when compressed at interconnections. At the same time, the known disadvantage of using PDMS, i.e., its ability to adsorb different molecules, especially protein molecules,<sup>32</sup> has been minimised in this application since the assay buffer contains the surfactant Tween<sup>®</sup>20.

The modular approach where the final system is an assembly of different modules capable of performing distinct operations to accomplish the desired functions yielded many advantages in terms of fabrication simplicity, interchangeability, high maintainability, easy integration and easy automation. Each module is composed of smaller structural units, which brings about fabrication simplicity into a level of making 3-dimensional structures based on 2-dimensional designs. The array order of the different modules is easily interchangeable depending on the intended application of the final microfluidic system. In other words, the same modules can be used to construct different systems for different applications. Issues related to changing PDMS inlays, removal of air-bubbles from the detection chamber, exchange of immunochips with different surfaces, replacement of electrodes etc. are handled very



easily to ensure high level of maintainability. All these require disassembling and reassembling of the concerned modules by merely using a few screws. By maintaining the common features for interconnections on each module, easy integration is possible between different modules and assembly of the modules onto the base plate. The final microfluidic system under study was constructed by assembling the different interconnected modules onto a base plate using 2-mm screws. The automation of the prototype was achieved by connecting the mechanically actuated modules of the device (miniaturized pump and valves) with the Lego<sup>®</sup> servomotors. These motors are controlled by the Mindstorms<sup>®</sup> NXT brick using LabView based program.

The ‘plug-and-socket’ combination of BJIBs present at both ends of the PDMS inlays and the characteristic planar 8-holes structures present at interfaces of each module made the prototype integration easy, tight and leak-proof. Figure xxx shows the schematic representation of the assembled prototype.

The most important feature of the microfluidic system reported in this paper is the in-built flow-injection analysis (FIA) system. A close look at the design of the immunochip (**Figure 4**) and its function along with the mixing chip reveals the built-in FIA function in microfluidic format ( $\mu$ FIA). The immunochannel itself behaves as the loop of this FIA system. The bypassed baseline buffer provides the background signal as it flows to the detector continuously. As shown in the schematic diagram of the microfluidic system with built-in FIA function (**Figure 8**) Valve 2 module controls the injection of reacted substrate into the baseline buffer by a carrier stream which is the same as the baseline buffer, but originates from a different reservoir in this design. Diffusive mixing of the reacted substrate with the baseline buffer plug is facilitated by the narrow long mixing channel. Unlike the conventional FIA system, the  $\mu$ FIA of the BAM immunosensor has a separate baseline buffer flow to record the background signal prior to the injection of the reactive sample plug from the loop by the carrier stream. This introduces a dilution factor in the detected signal. However, the obtained output signal depends on the concentration of the electroactive substance in the loop. Another advantage of the design is that the employed reagents and washing solutions as part of the immunoassay are bypassed to the waste using  $V_{21}$  (**Figure 8**). This keeps

the electrode surface clean and thereby eliminating the effect of electrode fouling on the recorded signal.

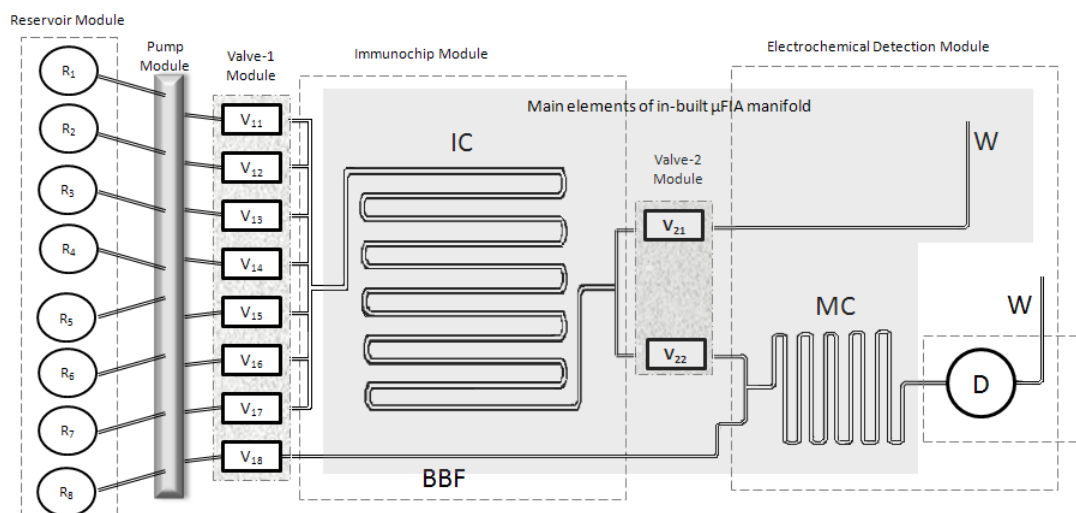


**Figure 8:** A schematic representation of the electrochemical BAM Immunosensor. The in-built  $\mu$ FIA elements are shown in the shaded portion

### b. Pump calibration

**Figure 9** shows the results of pump calibration. The flow rate of the channels increases linearly with the applied power to the LEGO servomotor. As the error bars (+/- standard error of mean) indicate, disparity in flow rates is slightly higher at higher applied power. Ideally, all the channels are expected to behave in the same manner at a particular level of motor speed. However, the middle channels are found to be more consistent in this regard compared to the channels at the sides of the PDMS inlays. In this project, the speed of the LEGO<sup>®</sup> motor was set to be 50%, at which the channels showed a flow rate of  $31.06 (+/-0.24) \mu\text{L min}^{-1}$  with At this speed the pump inlay also showed a better durability. This also simplified the automation of the protocol since the volume capacity of the immunochannel is approximately  $30 \mu\text{L}$ .

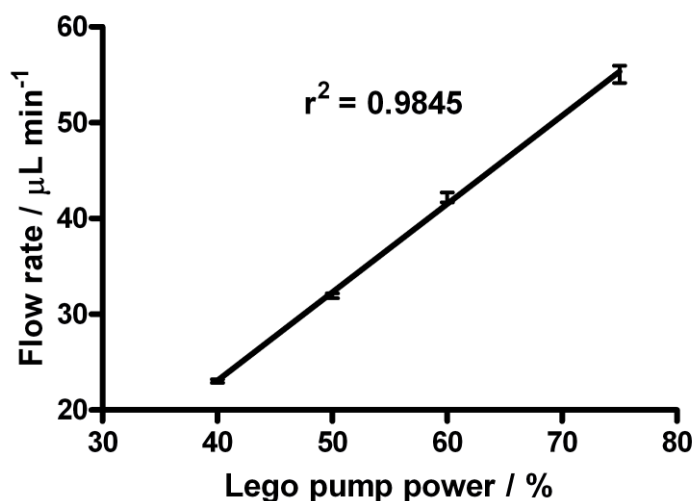


**Figure 9: Pump calibration - Flow rate dependence on the applied power to the LEGO servomotor.**

### c. Characterization of $\mu\text{FIA}$

The reduction current of  $\text{K}_3[\text{Fe}(\text{CN})_6]$  is monitored in  $\mu\text{FIA}$  using amperometric detection. The area covered by each amperometric peak (the total charge associated with the reduction process) is proportional to the concentration of the electrochemically active substance giving rise to the recorded current of the peak. In the first case, when the immunochannel (the injection loop of the  $\mu\text{FIA}$  system) was filled with 2.5 mM  $\text{K}_3[\text{Fe}(\text{CN})_6]$  solution and eluted to the detector a number of times, identical peaks (not shown) were obtained with a variation in peak area less than 1%. In the second case of detector calibration, the peak area (charge) varied linearly with respect to the concentration of  $\text{K}_3[\text{Fe}(\text{CN})_6]$ . The mean of peak area of three trials for each concentration with standard error of mean is plotted as a function of concentration (**Figure 9**) indicating a good linear fit ( $R^2 = 0.9969$ ). In each case, the variation in peak area was less than 5%. The well defined peaks of  $\text{K}_3[\text{Fe}(\text{CN})_6]$  reduction demonstrate that the  $\mu\text{FIA}$  system functions perfectly in terms of delivering a constant flow rate and switching between the loading and injection mode using the valves. The low variations found in both experiments indicate the effectiveness of the built-in  $\mu\text{FIA}$  and a relatively low dead-volume in the detection chamber at the applied flow rate. Furthermore, the result also shows that the diffusive mixing facilitated by the narrow channels and the sufficiently long path the two solutions

(baseline buffer and electroactive substance) travel together on the mixing chip is complete.

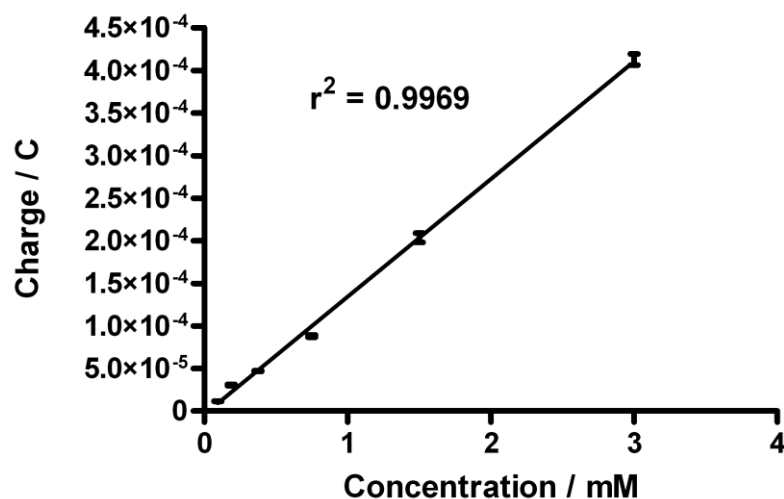


**Figure 10:** The linear relationship between the amperometric peak areas and concentration of the electroactive substance in the loop of the  $\mu$ FIA system injected into the detection chamber. Three values of each concentration are plotted with standard error of mean as error bars.

#### d. Characterization of BAM immunosensor

From the cyclic voltammograms shown in **Figure 11**, a potential of -100 mV was chosen for the amperometric detection of TMB(ox) for BAM immunoassay cycles in both regeneration experiment and standard curve generation. At this point there is sufficient cathodic over potential for the reduction of TMB(ox) and at the same time no anodic interfering reactions. In an immunoassay, the area of the obtained amperometric peaks is directly proportional to the concentration of TMB(ox) formed during the immunoassay cycles, which in turn is inversely proportional to the concentration of the analyte that competes for the antibody (HYB 273) with the surface immobilized BAM hapten (hapt D).

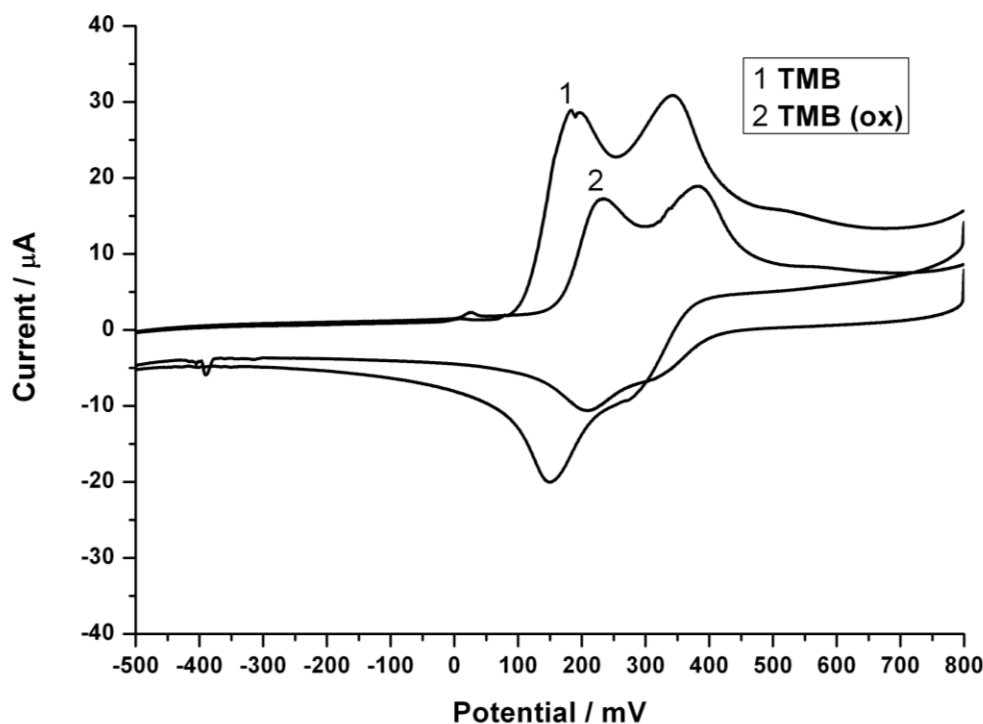


**Figure 11: Cyclic voltammograms of TMB and oxidised TMB (TMB (ox)). 0.01 M PBS was added as counter electrolyte and the scan rate was  $50 \text{ mV s}^{-1}$ .**

In the regeneration experiment where the BAM immunoassay was repeated in the inhibition format without added BAM (zero BAM) in the solution (to evaluate the maximum signal) at the same reaction conditions resulted in amperometric peaks with a RSD of peak area of 20 (for 15 cycles). However, the signal observed with the 15th cycle retained almost 95% of the intensity of the signal produced by the first cycle. The high %RSD value may be attributed to the choice of enzyme-substrate incubation period of 15 min applied to each cycle. From the kinetic curve of HRP – TMB reaction (curve not shown) the incubation period of 15 min is at the rising part of the slope of the curve. At this point of time, a tiny operational error may result in significant variations in the signal. The regeneration experiment primarily aimed to establish the feasibility of performing BAM immunoassay for a number of times without losing the immunosurface activity. This is considered to be a very important prerequisite in the development of an in-line monitoring system based on immunoassay. The result obtained in this experiment is supported by the findings described in <sup>26</sup> which showed the possibility of regenerating hapt D immobilized surface for a number of times (25 cycles of BAM inhibition assay with zero BAM in solution) without significant signal reduction on ELISA plates In each cycle an

incubation time of 15 min was given with 100 mM glycine HCl buffer (pH 2). Compared to this, hapt D immobilized immunochannel was regenerated under relatively mild conditions (incubation with 100 mM glycine HCl buffer at pH 2 for 3 min) by exploring the advantages of a microfluidic flow system. The increased surface to volume ratio available in the microfluidic immunochannel enhances the interaction of the immunosurface with the liquid reagents filled in it. Such a situation is equally beneficial for both formation and desorption of antibody – surface antigen complex and therefore results in better signal and stripping interactions for repeated BAM immunoassay cycles.

The standard curve obtained in electrochemical BAM immunosensor prototype is shown in **Figure 12**. To allow the enzymatic reaction of each standard solution to be complete, an incubation time of 40 min was applied. The area of the amperometric peaks obtained for each standard (ranging from  $62.5 \mu\text{g L}^{-1}$  to  $0.0008 \mu\text{g L}^{-1}$ ) was plotted as a sigmoidal dose-response curve. An  $\text{IC}_{50}$  (the concentration at which 50% inhibition is obtained) value of  $0.1924 \mu\text{g L}^{-1}$  and a linear working range from  $12.5 \mu\text{g L}^{-1}$  to  $0.02 \mu\text{g L}^{-1}$  were obtained. These values are exactly the same as the ones reported for the plate based ELISA experiments <sup>18</sup>.

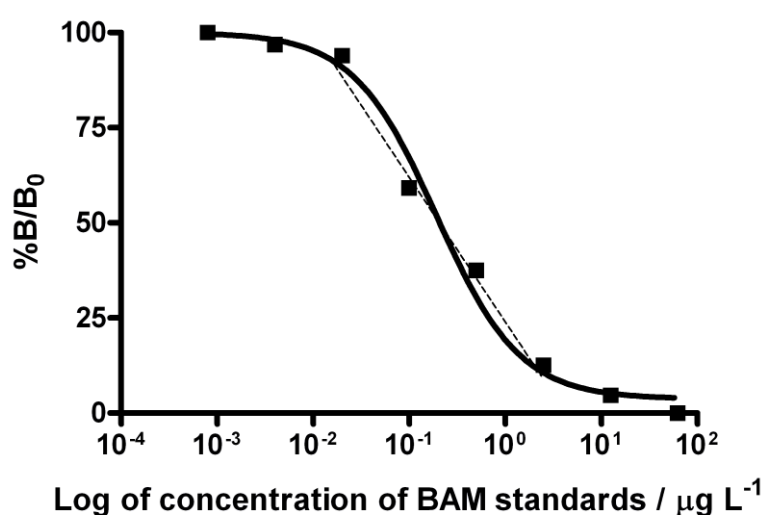


**Figure 12:** A sigmoidal standard dose response curve generated with 8 BAM standards. An  $\text{IC}_{50}$  value of  $0.1924 \mu\text{g L}^{-1}$  is obtained and the linear working range of the curve is shown as a dotted line.

The current design of the reservoir module does not provide separate chambers for different (premixed) antibody-BAM standard solutions. The use of a single reservoir for all the standards required prolonged washing steps to avoid foot prints of each analytical cycle. Such situations resulted in greater difficulty to obtain reproducible data. Though the reproducibility of the curve is not shown, the experiment provides the proof of concept achieved by the BAM immunosensor prototype.

This is a clear evidence for the fact that, in the heterogeneous BAM immunoassay, the reduced affinity of HYB 273 towards the immobilized hapten (hapt D which is chosen for surface immobilization after the optimization of BAM immunochemistry described in <sup>26</sup>) is compensated by the increased surface area to volume ratio of microchannels. At the same time, use of the same antibody (HYB 273) helped to retain the analyte-antibody affinity. In short, by utilizing the advantages of microfluidic platform, the modified heterogeneous BAM immunoassay is successfully shifted from ELISA plates to continuous flow analysis system.

#### **4. Conclusion**

A prototype of a microfluidic amperometric immunosensor with a novel built-in micro flow-injection analysis ( $\mu$ FIA) function was developed for 2,6-dichlorobenzamide (BAM) analysis in ground water. The setup has a modular structure, which makes it simple and cost effective to construct as well as easy to automate and maintain. Reagent consumption is significantly reduced in comparison with ELISA based assays. The immunosensor explores the advantages of a microfluidic system, selectivity of the immunoassay and sensitivity of the amperometric detection. The regeneration experiment confirmed the reusability of the immunosurface. The standard curve experiment proved that using the same antibody and a suitably modified hapten (modified to improve reusability of the surface by decreasing hapten-antibody affinity) the sensitivity and the detection limit (from  $12.5 \mu\text{g L}^{-1}$  to  $0.02 \mu\text{g L}^{-1}$ ) of the ELISA-based BAM immunoassay are retained when performed in a flow system. This result emphasizes the immense potential of the prototype and also validates the proof-of-concept on which this research project is based. Although this prototype was used to detect a single pesticide residue (BAM), it can be easily tailored for many different applications. Modularity of the microfluidic platform used in the BAM immunosensor offers the possibility of constructing

different systems for different applications by merely interchanging the array order of various modules. Having an automated in-built flow injection analysis system in a microfluidic environment ( $\mu$ FIA) makes the system unique and facilitates easy integration with sensitive detection schemes

## 5. References

1. R. L. Searcy, J. V. P. Carroll, J. S. Carlucci and L. M. B. quist, *Clinical Chemistry*, 1962, **8**, 166 - 171.
2. B. C. D. Villano, S. Brennan, P. Brock, C. Bucher, V. Liu, M. McClure, B. Rake, S. Space, B. Westrick, H. Schoemaker and J. V R Zurawski, *Clinical Chemistry*, 1983, **29**, 549-552.
3. S. R. Nussbaum, R. J. Zahradnik, J. R. Lavigne, G. L. Brennan, K. Nozawa-Ung, L. Y. Kim, H. T. Keutmann, C. A. Wang, J. J T Potts and G. V. Segre, *Clinical Chemistry*, 1987, **33**, 1364-1367.
4. R. S. Yalow and S. A. Berson, *The Journal of Clinical Investigation*, 1960, **39**, 1157-1175.
5. C. D. Ercegovich, *Pesticides Identification at the Residue Level, Advances in Chemistry, ACS Publication*, 1971, **104**, 162 - 178.
6. R. L. T. Churchill, C. Sheedy, K. Y. F. Yau and J. C. Hall, *Analytica Chimica Acta*, 2002, **468**, 185-197.
7. M.-C. Hennion and D. Barcelo, *Analytica Chimica Acta*, 1998, **362**, 3-34.
8. G. Jay and B. Svetlana, in *Analysis of Pesticides in Food and Environmental Samples*, CRC Press, 2008.
9. E. P. Meulenberg, W. H. Mulder and P. G. Stoks, *Environmental Science & Technology*, 1995, **29**, 553-561.
10. V. S. Morozova, A. I. Levashova and S. A. Eremin, *Journal of Analytical Chemistry*, 2005, **60**, 202-217.
11. S. Daunert, L. G. Bachas, G. S. Ashcom and M. E. Meyerhoff, *Analytical Chemistry*, 1990, **62**, 314-318.
12. J. Ruzicka and E. H. Hansen, *Flow Injection Analysis (Second Edition)*, A Wiley-Interscience publication, New York, 1998.
13. R. Puchades, A. Maquieira and J. Atienza, *Critical Reviews in Analytical Chemistry*, 1992, **23**, 301 - 321.
14. W. U. De Alwis, B. S. Hill, B. I. Meiklejohn and G. S. Wilson, *Analytical Chemistry*, 1987, **59**, 2688-2691.
15. B. B. Dzantiev, A. V. Zherdev, M. F. Yulaev, R. A. Sitdikov, N. M. Dmitrieva and I. Y. Moreva, *Biosensors and Bioelectronics*, 1996, **11**, 179-185.
16. D. A. Palmer, T. E. Edmonds and N. J. Seare, *Analyst*, 1992, **117**, 1679-1682.
17. M. Stiene and U. Bilitewski, *Analyst*, 1997, **122**, 155-159.
18. L. Bruun, C. Koch, B. Pedersen, M. H. Jakobsen and J. Aamand, *Journal of Immunological Methods*, 2000, **240**, 133-142.
19. M. S. Holtze, H. C. B. Hansen, R. K. Juhler, J. Sørensen and J. Aamand, *Environmental Pollution*, 2007, **148**, 343-351.
20. E. Bjorklund, B. Styrihave, G. G. Anskjaer, M. Hansen and B. Halling-Soerensen, *Science of The Total Environment*, 2011, **409**, 3732-3739.



21. C. Martínez Navarrete, J. Grima Olmedo, J. Durán Valsero, J. Gómez Gómez, J. Luque Espinar and J. de la Orden Gómez, *Environmental Geology*, 2008, **54**, 537-549.
22. J. Stockmarr, *Geological Survey of Denmark and Greenland Bulletin* 2005, **7**, 33 - 36.
23. E. Bjorklund, G. G. Anskjaer, M. Hansen, B. Styrishave and B. Halling-Soerensen, *Science of The Total Environment*, 2011, **409**, 2343-2356.
24. P. Fanjul-Bolado, M. B. González-García and A. Costa-García, *Analytical and Bioanalytical Chemistry*, 2005, **382**, 297-302-302.
25. G. Liu, S. L. Riechers, C. Timchalk and Y. Lin, *Electrochemistry Communications*, 2005, **7**, 1463 - 1470.
26. B. Uthuppu, N. Kostesha, S. M. Kiersgaard, J. Aamand, C. Jorgensen and M. H. Jakobsen, in *IEEE Sensors Applications Symposium*, San Antonio, TX, USA, 2011.
27. P. Skaft-Pedersen, D. Sabourin, M. Dufva and D. Snakenborg, *Lab on a Chip*, 2009, **9**, 3003.
28. A. J. Conde, D. Sabourin, P. Skaft-Pedersen and M. Dufva, *15th International Conference on Miniaturized Systems for Chemistry and Life Sciences, October 2-6, 2011, Seattle, Washington, USA*, 2011, 978-970-9798064-9798064-9798065/ $\mu$ TAS 9792011/\$9798020©9798011CBMS-9790001.
29. D. Sabourin, D. Snakenborg and M. Dufva, *Microfluid Nanofluid*, 2010, **9**, 87 - 93.
30. Y. Chen, L. Zhang and G. Chen, *Electrophoresis*, 2008, **29**, 1801-1814.
31. W. K. T. Coltro, S. M. Lunte and E. Carrilho, *Electrophoresis*, 2008, **29**, 4928 - 4937.
32. B. Huang, H. Wu, S. Kim and R. N. Zare, *Lab on a Chip*, 2005, **5**, 1005 - 1007.